Surface modification and characterization of Carbon Black; UV-cured colored Epoxy Composites

A dissertation for the degree of Doctorate in Material Sciences

Muhammad Atif

DISAT, Politecnico di Torino, Italy

Supervisor:

Prof. Roberta Bongiovanni

List of Figures

List of Tables

Table of contents

OVERVIEW

This chapter has been divided into an introductory description and aim of work for both parts of dissertation, i.e. Carbon Black surface modification and UV-cured epoxy composites.

INTRODUCTION:

PART-I: Carbon Black Surface Modification

Carbon Black is inexpensive widely used industrial filler, but its dispersability in solvents/polymeric media has always been a critical point. As a result either surfactants or higher mechanical forces have been utilized to disperse it well in the media. First part of research was aimed at surface modification of CB to increase its dispersability in different solvents and epoxy that directly effects filler-medium interactions. Type and magnitude of this interaction differs with structure and surface chemistry of filler, and this determines the ultimate properties of the composites. For CB surface modification Thermal and photochemical procedures have been implemented. Excellent results regarding surface modification and dispersability have been achieved.

PART-II: UV-cured Epoxy Composite

Utilization of light, as a substitute of heat, for nanocomposite synthesis, has a foundation on photochemical reaction. Liquid monomers/oligomers are jumbled with a minute percent of photoinitiator, and then exposed to UV light. In a few

seconds, the products inks, coatings or adhesives solidify. UV curing of colored composites has always been challenging because of light attenuation problems through colored composite samples; this results in incomplete polymerization. Second part of research was connected with UV-curing of colored epoxy composites. Certain techniques have been utilized, to photo-cure colored epoxy composites either in micron sized thin layers or outsized thick samples. Implementation of a unique method "Smart Approach" to photo-cure thick colored epoxy composites has fabricated promising results regarding polymerization kinetics and thermal / mechanical properties.

AIM OF WORK:

PART-I: Carbon Black Surface Modification

To upsurge the surface chemistry and activity of CB, attempts have been made since ages. This dissertation contains two different approaches for CB functionalization: thermal and photochemical (UV). Keeping in mind the effect of functionalization, the main objective of this exertion was to enrich the surface of carbon black with diverse functional moieties, to develop filler particle with increased compatibility, enhanced dispersion and improved performance. Thermal functionalization was carried out using ionic reaction mechanism. Sidewise, photochemical method was employed aiming at its simplicity, robustness and versatility; it values in either sense of chemical or surface engineering. Chemically it is clean and easy method, requiring only photons for reaction. About surface engineering point; it is easily adoptable, externally controllable and applicable to a number of UV active modifiers

as well as to a big array of substrates. These approaches are not only easy and effective but also have improved physical characteristics of modified CB.

Aim of this work was to enhance surface chemistry of CB, thermally or photochemically, to increase CB dispersion in a variety of media. CB, as filler, promotes mechanical, electrical and optical properties, only if CB dispersion in external medium is uniform. In the past, several approaches have been made to achieve uniform distribution of fillers in polymer matrix, which mainly involved extensive mixing steps. But these approaches were of limited success. In present research a different way was tried to solve the issue. CB was modified by organo-alkoxysilanes for improved dispersion and distribution. It was observed positively in different solvents and Epoxy. Hence assumed that modified carbon black (m-CB) could be employed as such in the composite blends, helping to avoid additional mixing steps. Products of both approaches were analyzed with different instrumental techniques, for change in their properties against different parameters like surface chemistry, surface area, particle size and aggregate structure.

PART-II: UV-cured Epoxy Composite

UV curing delivers good performance, environmental compatibility and processing efficiency, and for these reasons it is replacing thermal curing. Even then it has certain limitations; for transparent films it works only up to a certain thickness and for colored composites it strictly works for extremely thin films. To crack the issues like curing at line of sight, light penetration in thick layers and colored additives, new strategies have always been grown.

This part of thesis contains a unique approach to photo-cure very thick and highly colored composite samples. This unique approach was comparatively analyzed against a conventional protocol, under similar conditions; and due to unusual procedure, unique approach has been found to be able of overcoming issues like, curing at line of sight, light penetration in thick layers and colored additives.

This unique approach has been implemented on different kinds of additives and found to work for all fillers including CB which absorbs all wavelengths as well as Titanium dioxide which reflects all. Other advantages of this approach include economical method, reproducability of results, manageable initiation rate profile and no thermal curing required. Estimated intensity of UV radiation for a specific time interval can intiate polymerization, hence photon bombardment is inesential, that makes it an economical approach. Reproduceability is quite significant for any technique. For unique approach, initatiation rate profile is easily controlable by various factors out of which most important one is photoinitiator concentration. Since light attenuation is not an issue for unique approach so sufficient photoinitiator concentration can be utilized.

Another side of this research was to overcome certain physical disadvantages related to thermal curing of composites, by switching to photo curing of composites. Thermal curing requires complementary air-drying facility, as well as it shows mass shrinkage by more than 50% and creates environmental pollution. In UV curing, there is no solvent to evaporate, no environmental pollutants, limited loss of coating thickness, and little loss of volume. This results in higher productivity in less time, with a reduction in waste, energy use and pollutant emissions. Along with that UV

curing shows some excellent mechanical properties such as admirable scratch and solvent resistance and superior bonding. A part of this research has been conducted to verify the effectiveness of "Smart method" against traditional UV curing method by comparative analysis.

LITERATURE SURVEY

In this chapter literature cited is appraised for both sections; Carbon Black surface modification and UV-cured Epoxy composite preparation.

PART-I: Carbon Black Surface Modification

Term "Carbon Black", refers to a prime group of products, which has received much scientific and technological attention because of its wide-ranging applications [1]; in rubber reinforcement they are irreplaceable filler [2], on the other hand they are fascinating objects in electrically conductive materials [3]. Carbon Black is elemental carbon in the form of a fluffy fine powder with a large surface area; refers to a prime group of products most widely used material with dimensions in nanometers (nm).

2.1. Carbon Black; Structure and applications

Carbon black (CB) comprises of fine carbon particles (90-99% elemental carbon), an outcome of incomplete combustion of ample and beefy petroleum artifacts. Carbon black at its smallest level consists of spherical primary particles, which quickly form aggregates. Primary carbon particles fuse together permanently, in a randomly branched chain like structure, which is known as Aggregate. The aggregate can have a small number or hundreds of primary spherical particles, as per method used to prepare. Thermal black aggregates consist of single spheres rather than chains. These chains like structures are used to grip fluids and reinforce materials. The aggregates can fix with each other through van der Waals forces to form feebly

joined agglomerates [4-5].
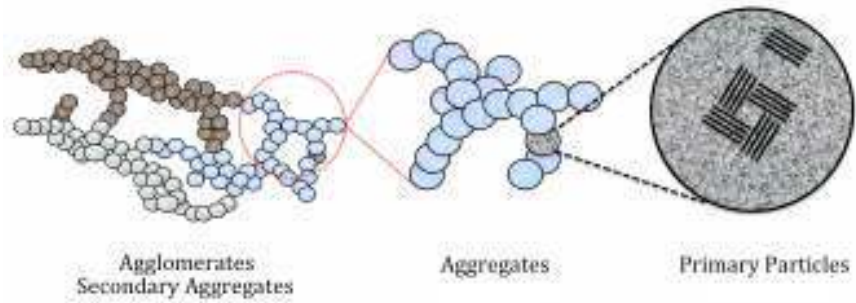
Figure 2.1: Carbon Black Primary and secondary structures

Summary information on dimensions of CB primary and secondary structures, is presented in Table 2.1 [6-7]:

Carbon black	Primary particle (nm)	Aggregate (nm)	Agglomerate size
Oil-furnace	10-400	50-400	Large (<2mm)
Thermal	120-500	400-600	Large (<2mm)
Channel	10-30	50-200	Large (<2mm)
Lampblack	60-200	300-600	Large (<2mm)
Acetylene Black	30-50	350-400	Pelletizes poorly

Table 2.1: Dimensions of CB particles, aggregates and agglomerates

Aggregates, in comparison to primary particles or agglomerates, contribute much for dispersion. For complete description of aggregates, two vital dimensions are:

1) Particle size: Diameter of sphere-shaped particles in the chain is defined as "Particle Size". It actually signifies "Thickness" [8] of the chain and is inversely proportional to the surface area. It profoundly affects blackness as well as dispersability of CB in resins and other medium [9].

2) Agglomeration: Capacity of aggregates to join each other is responsible for the formation of "Agglomerates", which actually represents size of rigid framework.

Like particle size, the size of secondary aggregate also affects tinting and dispersion [10]. Commonly dispersability improves with increase in secondary aggregate size but at the same time blackness reduces [11-12].

Despite these 2 dimensions, there is another property, known as "Structure", which consists of a long chain of spherical shaped primary particles. CBs with huge "Structure" show superb conductive behavior [13]. Another most important property of CB, irrelevant to dimension, is "Surface Chemistry", which explains amount or composition of functional groups on the surface of CB. All these properties have great influence on practical applications of CB.
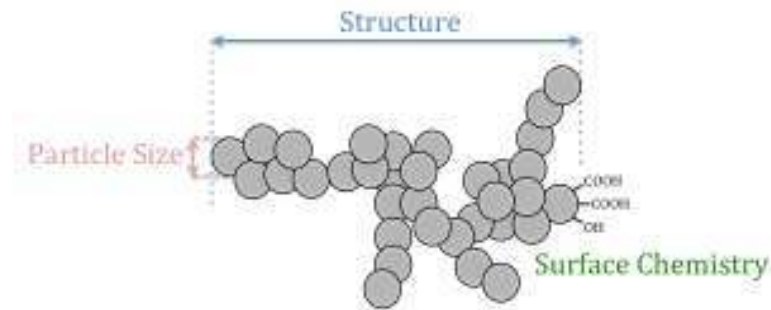
Figure 2.2: Basic properties of Carbon Black

Different procedures have evolved over the ages, generating CBs from different starting materials and procedures. All these CBs are named atop the process or source material used for preparation, e.g. Furnace black, Lampblack, Thermal Black, Acetylene Black, and Channel Black. All these CBs have different characteristics like particle size, structure and purity. A brief of different production methods along with distinguished characteristics is as follows:

Lampblack: This type of CB is obtained by collecting soot from fumes of burning oils

or pinewood. This is the oldest method, and is not appropriate for mass production. However, it delivers CB with precise color, proper for ink sticks.

Channel Black: This type of CB is modified version of Lampblack, produced by contacting, partially combusted natural gas with channel steel (H-shaped steel). This method has drawbacks of low yield and environmental issues. However, it provides numerous functional groups on CB surface, specific for painting applications.

Acetylene Black: This type of CB is obtained by thermally decomposing acetylene gas. This method provides CB with higher structures and higher crystallinity, good for electric conductive agents.

Furnace Black: This type of CB is produced by partially combusting petroleum/Coal oil into high-temperature gases. This method helps to control certain properties such as particle size or structure. Now a day, this is the most common method for CB manufacturing; and it yields distinctive quality of CB for numerous applications from rubber reinforcement to coloring.

Thermal Black: This type of CB is produced, by decomposing natural gas in the absence of oxygen. This method gives CB with largest particle size and lowest particle aggregation. Hence, its uses include applications in rubber, metallurgy, plastics, insulation, concrete and graphite. Drawbacks of the process include, high cost and limited implementation on gaseous or liquid hydrocarbons.

CB applications are progressively becoming diverse with time. Major applications include tire reinforcement, printing ink pigment and conductive agents.

Fillers are pretty imperative in industry since ages. Carbon black is vital economical filler in rubber industry as a reinforcing agent [14-15]. Rubber industry uses CB not

only to reinforce rubber, but also to increase resistance of rubber against abrasion, tear, fatigue and flexing. Likewise, CB develops the tensile strength of many elastomers (natural and synthetic). Global utilization of CB mainly depends on the rubber industry, which is normally responsible for 89– 91% of total consumption. A tyre, 20-40% by weight is typically CB. Alternative automotive uses of CB are tubes, wires, cables, belts, hoses, O-rings, insulation stripping, shock and motor mounts; and non-automotive uses include hoses, conveyor belts, roofing, covers for wire and cable, coated fabrics, gaskets, packaging, gloves, footwear, floor mats, tape, hard rubber products, pontoons and toys [16].

Major consumer of CB after rubber industry is printing ink industry, which consumes a huge amount of CB, with formulations having 5-22% CB content. Different varieties of CB are used in printing ink industry with different grades and concentrations to obtain the product with different type and quality of required factors including color, gloss and tone. Because of higher tinting strength of CB compared to iron black or organic pigments, it is commonly used as a pigment for coating[17], ink[18], inkjet[19] and toner applications[20]. Since ages, ancient Egyptians and Chinese culture had been known for using Carbon black as a pigment. Soot was employed for scripting letters on papyrus in ancient Egypt and on bamboo strips in ancient China. But as soon as paper production method established, CB production turned into industry. Then depending upon its features, CB found its uses in various industries, from black coloring pigment of inks to electric conductive agent in high-technology materials.

Other effective uses of CB include; ultraviolet light stabilizer [21], electrical conductivity controlling additive[22] and antistatic filler[23].

An array of CB applications in biological sciences is documented, after surface modifications [24-25].

2.2. Carbon Black Surface Modification

Reactivity of carbon black is due to its surface chemistry. Various commercial grade CBs, on their exterior, have oxygen complexes (i.e., phenolic, carboxylic, quinonic, lactonic groups and others) in diverging range [26-27], counted on the manufacturing status.
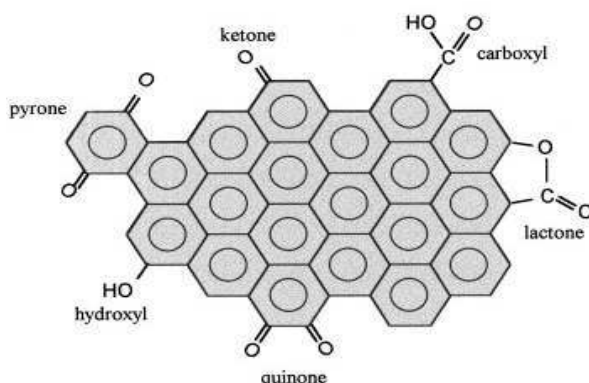
Figure 2.3: Surface Chemistry of Carbon Black

Eventually their concentration can be increased by simple oxidation reactions [28-30]. These groups provide support for reactions. CB surface modification has been carried out conventionally through thermal procedures, but modern era is trying to switch to UV modification, assuring interesting functionalities and architectures with controlled molecular weight and low polydispersities. CB due to its structural properties supports both thermal and UV modifications. Along with above-mentioned protocols, modification on the surface of CB has also been attempted by

plasma treatment [31].

Surface chemistry of CB plays important role for its dispersion in a medium. Change in surface chemistry ensues change in dispersion, as it effects "filler - filler" or "filler - medium" interactions, which mainly depend on surface energy [32]. CB, without modification, needs surfactants to be dispersed in water or polar media. These surfactants make a layer around CB with hydrophobic ends pointing towards CB and hydrophilic ends towards water / polar media. This arrangement makes sure disorganization of CB agglomerates by steric/static repulsion between CB aggregates. On the other side, CB after modification carries chemically bonded surface modifiers; which can provide higher dispersion stability and guarantee better performances.

2.3. Thermal Modification of CB

In general thermal modification of CB can be classified into; physisorption and chemisorption. Plentiful data on physisorbed surface alteration of CB have grown up in years [33-35]. Chemisorbed modification can further be subdivided into ionic [36-38] or radical [39-40] methods. Chemisorbed modifications usually graft polymers on CB Surface, either by anionic or free radical process [41]. A verity of functionalities has been utilized for graft polymerization on CB surface; some of them are: Azo[42], peroxyester [43], acylium perchlorate [44], potassium carboxylate groups [45]. Primary feature, of all these tracks, is formation of chemical bond between CB and the modifying agent.

Grafting functional molecules on CB surface improves its surface properties. A number of articles have verified that grafted CB not only disperses well in different solvents but also is more compatible in polymer matrices [46-49].

2.3.1. Oxidation of CB

Various scientists have implemented different methodologies to oxidize CB surface. P. E. Fanning *et. al.,* [50] has compared *in situ* oxidation of CB at 623K using Oxygen and Argon mixture, with CB oxidation in boiling Nitric Acid. *In situ* oxidation of CB was carried out after thermal treatment at 1230K under Argon or Hydrogen. Diffuse reflectance spectroscopy (DRIFTS) and FTIR studies proved the formation of cyclic ethers, which rearranged to form ether like structures in polyaromatic domains.

Y. Otake and R. G. Jenkins [51] has obtained promising results of CB oxidation by thermal treatment at 623K, which is one of the common approaches to form Oxygen containing functional groups on CB. M. A. Vannice *et. al.,* [52] has investigated that high temperature treatment, at 1223 K, which was principally intended to remove the Sulfur, also eliminates Oxygen containing surface functional groups.

2.3.2. Thiolation of Oxidized CB

The interaction of CB with Sulfur compounds is of practical interest, because of rubber industry. The reactions of sulfur or sulfur derivatives have been reported in the literature, either by ionic methods [38, 53-55] or by radical reactions [56-57].

Tendency of CB to fix sulfur on their surfaces is long since known [58-59]. Till that time, sulfur insertion was confused to be capillary condensation, physisorption or chemisorption. Afterward, Puri *et. al.* [60-61] discovered, sulfur is fixed on CB surface either by addition at unsaturated sites or by substitution with oxygen and

hydrogen-containing groups. Papirer *et. al.,* [62] studied formation of sulfur containing functional groups on CB surface by P_2S_5 reaction with CB in temperature range of 60-500°C and reaction time up to 4 hours.

2.3.3. Silanization of Oxidized CB

Silanization is another very popular method to improve dispersion. Silane coupling agents react with hydroxide-rich surfaces; moreover they are widely available with a large variety of end groups. Thus, by selecting the appropriate silane groups, the compatibility and interaction of the filler can be improved. Silane coupling agents have been applied to natural fibers[63], titanium oxide particles[64], clay nanoparticles[65], oxidized CNF [66] and oxidized CNT[67-68].

Silanization of CB has been studied [69], yet literature does not hold significant data on CB silanization. Where as various approaches have been tried time to time, to compare the effects of CB and silane on composite properties, with out any chemical connection between the two. Bokobza *et. al.,* [70] has studied in parallel the mechanical aspects of silanized or CB-natural rubber composites. Nugay *et. al.,* [71] has modified the approach by using dual filler system, containing both carbon black and silane agent, in different weight ratios.

2.4. Ultraviolet Modification of CB by Thiolation

Though utilization of UV for surface modification of fillers is a documented method [72-76], yet it is rather new for implanting CB surface with functional molecules. So, availability of literature, in the field, is not appreciably ample.

CB, owing to its polycondensed aromatic structures, is considered to be a strong radical scavenger [77-78]. Hence it is conceivable to have radical reactions on CB

surface by simply exploiting its radical scavenger nature. Free radical approach can effectively engage all kinds of CB without any severe pretreatment.

Reactions that break S–H bond of thiols, mostly add RS fragment into organic molecules. Such reactions are termed as sulfanylation (thiylation) reactions. Depending upon reaction conditions and thiol nature, S–H bond can homolytically dissociate, giving rise to sulfanyl radicals, providing the energy source is either thermal or photochemical. S. Oae [79] has reported photochemical generation of sulfanyl radical. P. M. Rao has documented photolyzed reactions of thiyl radicals [80].

PART-II: UV-cured Epoxy Composite

The description of nanocomposites is broadened appreciably. This phrase now covers a huge variety of systems combining one, two, three-dimensional materials merged at nanometric level. This is a quickly growing area with emphasis on discovering benefits with novel purposes. The core objective is to extend new functionalities with the pooled properties of every component and also with the morphology and interfacial characteristics of the two or three-dimensional network. The motivating mark is, the amalgamation of organic polymers and inorganic materials gives quite different properties then the properties of the pure components. The properties of nanocomposites are not simply the average properties of its components. In a composite, one component maybe enclosed by another component that forms a continuous phase, but it is also possible that the components form continuous phase resulting in interpenetrating networks.

Epoxy composites have different classes based upon different criteria. Some of them are discussed briefly as follows:

(a) Dispersed phase dimensions: Nanocomposites can be classified on the bases of dispersed phase having either one dimension or two dimensions or all three dimensions in nanometer scale (composites with fillers having particles, elongated or sheet like structures respectively).

(b) Interactions between the two phases: Nanocomposites can be classified into 2 categories, either having week bonds at interface or with strong chemical (covalent/ ionic) bonds.

(c) Synthetic process: polymer nanocomposites can be obtained either by a top-down or a bottom up approach. Bottom-up approach pursues to build huge assemblies from smaller components, by using their chemical properties to assemble them in useful configurations. While top-down approach pursues to design nano-scale devices by joining bigger fragments through cutting, milling and shaping into the desired shape and order.

Epoxy resins have prominent inspiration as per their wide-ranging material performance. Thanks to the excellent mechanical properties, the outstanding dimensional stability, the good adhesion and coating properties, and suitable corrosion resistance [81]. They have well known applications in various industries, like laminates, flooring, caulking and aerospace [82]. Epoxy composites with improved properties can be prepared by adding nanofillers (e.g., clay [83-85], colloidal silica [86-87] and carbon nanotubes [88-92]. Likewise, CB furnishes special properties in epoxy composites.

Epoxy polymerization is an exothermic curing process [93]. This process can be triggered by two different sources; either heat or light. A process using heat to

polymerize resin is called Thermal-polymerization or Thermal-curing. A light induced chemical practice to instantly cure or dry matrix i.e. coatings or adhesives; is called Photo-polymerization or Photo-curing. All those methods in which high-intensity ultraviolet light is employed are commonly known as ultraviolet curing or UV curing.

2.5. Photopolymerization of Epoxides

Photopolymerization is light stimulated process, which converts a monomer into polymer. Initiation is activated by radiation: the reaction contains a photosensitive species, called photoinitiator, which produces either radicals or ions, upon exposure to light. Then a continues reaction starts which converts monomers into polymers.

Although photocuring of polymers and polymer composites, from epoxy resin based formulations, have been of growing interest over the time, yet colored epoxy composites are limited in application. Due to particular critical issues, colored epoxy composites have primarily been prepared by thermal curing.

2.5.1. Thin Layer Composites

Ultraviolet curing is well established effective method for curing transparent or very thin films. Up till now, colored composites materials with intense colors, are prepared in thin layers due to their effective depth of cure. During last few years, some researchers [94-95] have worked with strongly pigmented or filled coatings and films with limited thickness. Martin-Gallego and coworkers studied the effect of nanofillers on epoxy resin curing, and found that nanofillers delay the curing due to sheilding effect [96].

2.5.2. Thick Layer Composites

In case of thick samples light attenuation is a downside of photopolymerization. Light attenuation is, decrease in the intensity of light because of photon absorption by photoinitiator [97]. This elevated consumption of photons, by photoinitiator near irradiation source, leaves little number of photons to excite photoinitiators in deeper reagions of thick sample. This results in non-uniform and incomplete polymerization in deeper regions.

Different approaches have been implemented to overcome light attenuation problem. These approaches aim to have a certain concentration of excited photoinitiator throughout sample thickness. Most primitive and uneconomal approach is photon bombardment on sample, which is very expensive and does not cure samples completely every time. Another approach was to reduce initiator concentration, keeping in mind that lesser concentration at the top layer will reduce light attenuation. But this approach failed for thick samples [97]. One of the prominent approaches was, use of photobleaching initiator [98]. It did help to make thick photopolymerized samples [99-101]. Great advantage of this approach is reproducability of results but initiation rate profile is very complex. Recently a different approach of dual cure or hybrid photo/thermal polymerization has been struggled, to cure thick samples, in which photopolymerization is followed by thermal cure [102] This method has excellent output but it overthrows main objective of photopolymerization, i.e. removing the heat source.

After light attenuation, second greatest encounter in thick samples curing is colored additives (pigments or fillers). Since their concentration becomes really high due to

sample's volume or thickness, they strongly compete with photoinitiators by absorbing or reflecting photons, which reduces active centers. So uneven cure results in the form of wrinkles on sample surface [97]. For certain applications where additives are compulsary, another approach was applied. And that approach was to use photoinitiators and additives that absorb different wavelengths [103]. But this approach is not practicable for all kinds of additives and fails to work for certain fillers like CB which absorbs all wavelengths or Titanium dioxide which reflects all.

EXPERIMENTAL

In this chapter materials, synthetic procedures and experimental details of the characterization techniques will be discussed, for Carbon Black surface modification and composite preparation.

PART-I: Carbon Black Surface Modification

Carbon Black was surface modified by two different conducts; Heat (thermal modification) and Light (UV modification).

3.1 Thermal Modification of CB

3.1.1 Oxidation of CB

3.1.1.1 Material:

Two different types of Carbon Black have been used for surface modification.

1) Furnace black (Vulcan N-115 from Cabot Chemical), commercially available black powder, with relative density 1.7-1.9 g/cm^3 at 20°C, surface area 123 m^2/g, Iodine absorption value 160 mg/g, Dibutyl phthalate adsorption (DBPA) 113 mL/100 g. It is named in the dissertation as Pristine-VCB.

2) Charcoal activated (glassy carbon, spherical powder from Sigma Aldrich) with particle size in a range of 10-40 μm, relative density 0.25-0.60 g/cm^3, specific surface area (BET) >100 m^2/g, resistivity 1375 μΩ-cm 20°C. It is named in the dissertation as Pristine-Glassy CB.

Concentrated Nitric acid (70% from Sigma Aldrich) has been utilized as oxidizing

agent. Lab grade Hydrochloric acid (37% from Sigma Aldrich) has been utilized as oxidizing agent. All chemicals were used without further purification.

3.1.1.2 Methods:

3.1.1.2.1 CB Oxidation by refluxing in Nitric Acid

5-7 g CB (Pristine-VCB or Pristine-Glassy CB) was oxidized, by refluxing in 30-40 mL Conc. Nitric acid, for 90 minutes. After cooling and dilution with demineralized water, the suspension was filtered, washed with water and dried at 110^0C for 24 hours. The products were named as VCB-Oxi and Glassy CB-Oxi respectively.

3.1.1.2.2 CB Oxidation with Nitric Acid/Acetic anhydride at 5 ^{0}C

3 g Pristine-VCB was oxidized with 30 mL Conc. Nitric acid in presence of Acetic anhydride (120 mL), at 5 ^{0}C, as follows: Pristine-VCB and Acetic anhydride were charged in a round bottom flask (RBF). The RBF was placed in ice bath and HNO_3 was added drop by drop, while stirring and keeping temperature below 5 ^{0}C. After complete addition of HNO_3, reaction was left at room temperature for 5 hours. Then reaction mixture was cooled and diluted with 1 L ice-chilled distilled water, the suspension was filtered, washed with water and dried at 110^0C for 24 hours.

3.1.2 Silanization of Oxidized CB

3.1.2.1 Material:

Structures of materials are presented in Figure 3.1. Pristine-VCB has been described in section 3.1.1.1. Mercaptopropyltrimethoxysilane (MPTS), *purchased from Sigma Aldrich* and Concentrated Nitric acid (70%) have been utilized for CB oxidation. Acetic anhydride (purity ≥98.0%) has been utilized as co-oxidizing agent. Analytical grade ethanol (purity 99.8%) was used as solvent. Distilled water was used as

washing solvent. Sodium hydroxide (pellets, semiconductor grade, 99.99%) was used to provide basic medium for reaction. All chemicals were used without further purification.

3.1.2.2 Method:

3 g Pristine-VCB was oxidized with 30 mL Conc. Nitric acid in presence of Acetic anhydride (120 mL), at 5^0C, as follows: Pristine-VCB and Acetic anhydride were charged in a round bottom flask (RBF). The RBF was placed in ice bath and HNO_3 was added drop by drop, while stirring and keeping temperature below 5^0C. After complete addition of HNO_3, reaction was left at room temperature for 5 hours. Then reaction mixture was cooled and diluted with 1 L ice-chilled distilled water, the suspension was filtered. After filtration, washed again with distilled water until neutral pH was reached. 2.5 g MPTS and 1.56 g NaOH were mixed in 140 mL ethanol. Filtered CB ($\cong$3g) was added into this mixture at 0^oC. It was stirred for 48 hours. Modified Carbon Black (named as MPTS-VCB) was then filtered, washed with distilled water and dried at 100^oC for 24 hours.

3.1.3 Thiolation of CB

3.1.3.1 Material:

Pristine-VCB used for surface modification, has been described in section 3.1.1.1. MPTS, Nitric acid, Acetic anhydride, Sodium hydroxide and solvents have been described in section 3.1.2.1. Thiolation was carried out with different agents including: Mercaptopropyltrimethoxysilane (MPTS), Pentaerythritol-tetrakis-3-mercaptopropionate (PETMP), Trimethylolpropane Tris-3-mercaptopropionate

(TMP3MP), Octadecane- -thiol. All chemicals were used without further purification.

Chemical structures are presented in Fig 3.1.
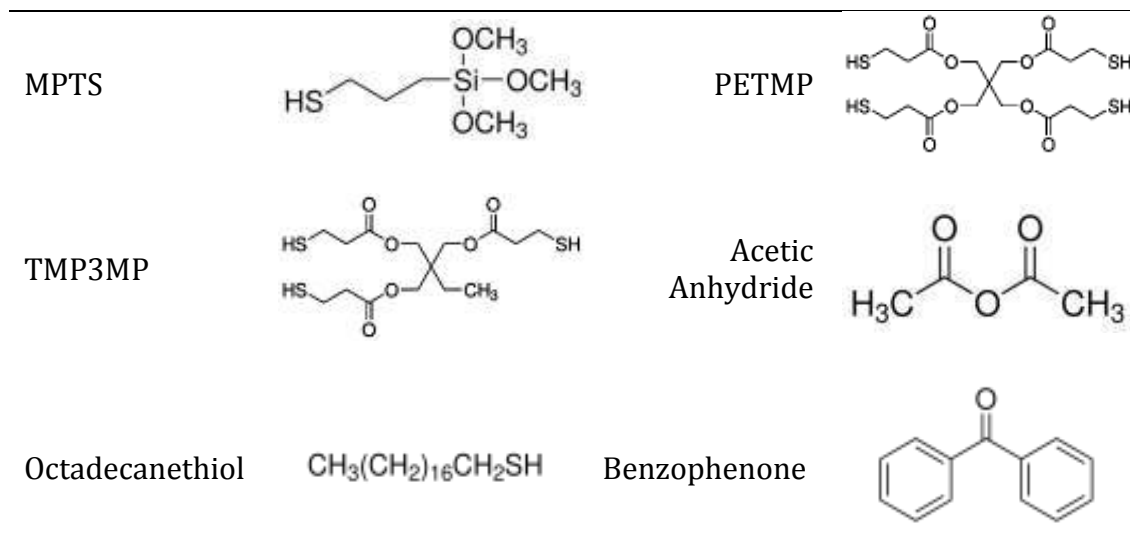
Figure 3.1: Thiolation agents for Carbon Black surface modification

Thiol Used	Pristine-VCB		Thiol		CB:Thiol	NaoH
	(g)	(mol)	(g)	(mol)	(mol)	(g)
MPTS	3	0.25	2.55	0.013	20:1	1.56
PETMP	3	0.25	1.58	0.013	20:1	1.56
TMP3MP	3	0.25	1.72	0.013	20:1	1.56
Octadecanthiol	3	0.25	3.18	0.011	20:1	1.56

Table 3.1: Thiols used for CB modification

3.1.3.2 Method:

Samples were prepared as per quantities mentioned in Table 3.1. 3 g Pristine-VCB

and 120 mL Acetic anhydride were charged in a RBF. The RBF was placed in ice bath

and 30 mL HNO_3 was added drop by drop, while stirring and keeping temperature

below 5^0C. After complete addition of HNO_3, reaction was left at room temperature

for 5 hours. Then reaction mixture was cooled and diluted with 1 L ice-chilled distilled water, the suspension was filtered. After filtration, washed again with distilled water until neutral pH was reached. Specific amount of Thiol and NaOH (1:3 mole ratio) were mixed in 140 mL ethanol. Filtered CB ($\cong$3g; 20:1 mole ratio to Thiol) was added into this mixture at 0°C. It was stirred for 48 hours. Modified Carbon Blacks were then filtered, washed with distilled water and dried at 100°C for 24 hours.

3.2 Ultraviolet modification of CB by Thiolation:

3.2.1 Material

Two types of CBs (described briefly in section 3.1.1.1), MPTS (described in section 3.1.2.1) have been used for UV surface modification of CB. Benzophenone has been used as photoinitiator. Structures are represented in Figure 3.1. Solvents (Acetone, Tetrahydrofuran, Diethyl ether, Cyclohexane and Toluene; purchased from Sigma Aldrich) have been used for experimentation, without further purification.

3.2.2 Methods

Different techniques have been implemented for photochemical modification of CB.

Technique 1: All the ingredients (CB, PI and Modifier) in different weight ratios were added in the flask and irradiated for a specific time period.

Pristine-Glassy CB, MPTS (1:2 molar ratios) and PI (1:150 molar ratios with MPTS) were taken in glass flask. The contents of flask were mixed for 30 minutes, by using mechanical stirrer, and irradiated for 60 seconds, with UV radiation of intensity 33 mW/cm^2. Final products were filtered, washed with Tetrahydrofuran (THF) and dried at 60^{0}C for 30 minutes.

Technique 2: Photoinitiator was taken separately in a flask, irradiated for a specific time period and mixed in CB + Modifier mixture.

Samples were prepared in weighed quantities as per Table 3.2. CB (either Glassy CB-Oxi or Pristine-VCB as mentioned in the Table 3.2) and MPTS in 4:1 molar ratios were taken in glass flask. The contents of flask were mixed for 30 minutes, by using mechanical stirrer. Then weighed amount of Photoinitiator (PI), 1:5 molar ratios with MPTS, was taken separately in a vial, and irradiated with UV radiation of intensity 33 mW/cm². Then irradiated PI was mixed with CB. Final product was then filtered, washed with Tetrahydrofuran (THF) and dried at 60⁰C for 30 minutes, and is named as m60/120/180

Sample description		CB (g)	CB (mol)	MPTS (g)	MPTS (mol)	PI (g)	PI (mol)	Irradiation (Sec)
Glassy CB-Oxi	m-60	0.25	0.021	1	0.005	0.2	0.001	60
	m-120	0.25	0.021	1	0.005	0.2	0.001	120
	m-180	0.25	0.021	1	0.005	0.2	0.001	180
Pristine-VCB	V-120	0.25	0.021	1	0.005	0.2	0.001	120

Table 3.2: Composition of Pristine- & modified Glassy CB

Tailing scheme 2; some samples as per Table 3.3 were prepared with Pristine-VCB, to verify the effect of solvent.

	Solvent (10 mL)	Pristine-VCB (g)	Pristine-VCB (mol)	MPTS (g)	MPTS (mol)	PI (g)	PI (mol)	Irradiation (Sec)
V-CH-3	Cyclohexane	0.5	0.042	1	0.005	0.5	0.003	300
V-CH-4		0.5	0.042	1	0.005	0.5	0.003	999
V-DE-3	Diethylether	0.5	0.042	1	0.005	0.5	0.003	300
V-DE-4		0.5	0.042	1	0.005	0.5	0.003	999
V-Ac-3	Acetone	0.5	0.042	1	0.005	0.5	0.003	300
V-Ac-4		0.5	0.042	1	0.005	0.5	0.003	999

Table 3.3: Composition of Samples prepared to check effect of solvent

Technique 3: PI, while being irradiated, was added drop by drop into CB + Modifier mixture. Pristine-VCB and MPTS (8:1 molar ratios) were taken in glass flask and mixed for 30 minutes, with mechanical stirrer. Weighed amount of PI (1:2 molar ratios with MPTS) in solvent was taken in a burette. UV lamp was adjusted close to burette's tip and flask carrying CB and MPTS mixture, was placed below burette (Figure 3.2 represents apparatus organization). Then UV radiation (intensity 33 mW/cm^2) and burette's tip were opened simultaneously, in such a way that each PI drop gets sufficient irradiation before dropping into CB and MPTS mixture flask, which was fitted with a mechanical stirrer to mix PI drops. Final product was then filtered, washed with Tetrahydrofuran (THF) and dried at 60^{0}C for 30 minutes.

Burette with 50wt.% PI solution in PC

UV radiation source (intensity 33 mW/cm^2)

Flask containing 8:1 molar ratio mixture of Pristine-VCB and MPTS
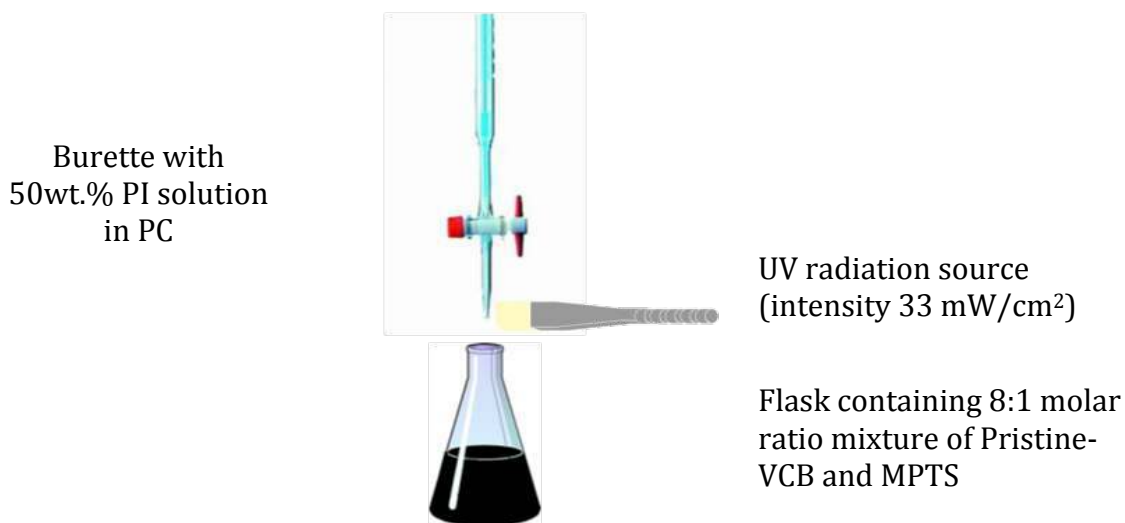
Figure 3.2: Apparatus of Technique 3 for UV surface modification of CB

3.3 Characterization of Modified Carbon Black:

Samples have been characterized using the techniques described here below.

3.3.1 X-ray Photoelectron Spectroscopy (XPS) Analysis:

Versa Probe PHI 5000 instrument was utilized for survey scan and high resolution X-ray Photoelectron Spectroscopy (XPS). The powder carbon black was dried in

oven at 100°C for 24 hours at atmospheric pressure before analysis and thereafter placed in the XPS pre-chamber overnight, in order to avoid anomalous outgassing during the XPS characterization, performed in UHV condition (10 -8 pascal). X-ray source, used for analysis, was a monochromatic 100 μm diameter beam, with Al (1486.6 eV) source, and a power of 25.6 W. Analyses were carried on a square area of 500 μm x 500 μm with the aim to have a good average and better statistics of powder behavior. A double beam (electron and argon ion gun) neutralization system, dedicated to reduce the charging effect on samples, during the data acquisition was also employed.

3.3.2 Real Time Infrared Spectroscopy (RTIR) Analysis:

For FTIR, samples were mixed with KBr in 0.5-1.0% w/w suspensions. Mixed samples were ground and dried for 2 hours at 120°C. Discs (12.7 mm in diameter and 1 mm thick) were obtained by pressing sample powder under 10^4 kg for 5 minutes. Spectra (4000-500 cm^{-1}) were collected on a Nicolet 5700 FTIR.

3.3.3 Thermal Gravimetric Analysis (TGA):

TGA/SDTA851^e METTLER TOLEDO instrument was utilized for TGA of 15-20 mg of each sample. Gas flow was kept at 60 ml/min; temperature increment was 10°C/min from 25 to 800°C. 70 μL Alumina crucible was used to place sample.

3.3.4 Raman Spectroscopy Analysis:

Raman spectroscopy (Renishaw Ramascope, Ar+ laser 514.5 nm excitation) has been used to evaluate the modification in carbon structures before and after functionalization. From the Raman spectra the average size of nano-crystallites can be determined in terms of changes in position, width and intensity ratio of two

Raman peaks observed at 1345 cm^{-1} (the disordered, or D peak) and 1575 cm^{-1} (the graphite, or G peak). The shape of those peaks depends on the crystallite sizes. When the crystallites become larger, the peaks become narrower, their maxima move to higher frequencies and the intensity of the G peak systematically increases in comparison with the d peak. Lateral size of the crystallites (L_a) was calculated by using "Tuinstra and Koenig" formula.

$$L_a = 4.35 \ (I_g/I_d) \ \ (nm) \hspace{3cm} (3.1)$$

3.3.5 Field Emission Scanning Electron Microscopy (FE-SEM) Analysis:

Field Emission Scanning Electron Microscopy; FE-SEM (Model Zeiss Supra 40) has been used to evaluate the structural changes in samples before and after functionalization treatments.

3.3.6 Energy Dispersive Spectroscopy (EDX) Analysis:

Energy Dispersive Spectroscopy (*EDX, Oxford Inca Energy 450*) has been used to recognize elements present on samples surface before and after chemical treatments.

3.3.7 Elemental Analysis:

The compositions of samples were determined by vario EL cube (Elementar Analysen system, Germany), equipped with Mettler-Toledo XP6 (Mettler-Toledo GmbH, Germany).

3.3.8 Brunauer–Emmett–Teller (BET) Analysis:

The Brunauer–Emmett–Teller (BET) specific surface area (SBET), pore volume (PV), average pore diameter (APD) and isotherms were measured by means of N2 sorption at 77 K on a Micromeritics TriStar II, USA (surface area and porosity)

instrument on samples that had previously been outgassed at 150 °C using Micromeritics FlowPrep 060, USA (sample degas system).

3.3.9 Dynamic Light Scattering (DLS) Analysis:

Zeta potential measurements were carried out by using Dynamic Light Scattering (DLS, Nanosizer ZS90, Malvern) using 1% w/v suspensions of Pristine-CB and m-CB, prepared as follows: 1mg Carbon was dispersed in 100mL of deionized water and sonicated for 10 minutes.

PART-II: UV-cured Epoxy Composites

UV-cured epoxy composite were prepared in thin layer (100μ) as well as in thick dimensions (cm).

3.4. Material

Neopentyl glycol diglycidyl ether (colorless liquid with relative density 1.04 g/cm^3 at 25 °C; purchased from Sigma Aldrich) has been used as Bi-functional Epoxy monomer. Triarylsulfonium Hexafluoroantimonate (purchased from Sigma Aldrich as 50 wt.% solution in Propylene Carbonate) has been used as photoinitiators. Structures are presented in Figure 3.3. Pristine-VCB used as filler in composite, is described briefly in section 3.1.1.1. Other commercial fillers were used as reference, listed below: Silica (essay 99.8%, purchased from sigma aldrich), Alumina (essay ≥98%, purchased from sigma aldrich), Azo-Yellow pigment (N4090399, Nan-Tong DIC color company, china) and Phthalocyanin green pigment (9627, Yi-Xing Pigment factory, China).

Neopentyl glycol diglycidyl ether
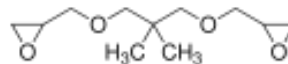
Triaryl Sulfonium Hexafluoroantimonate
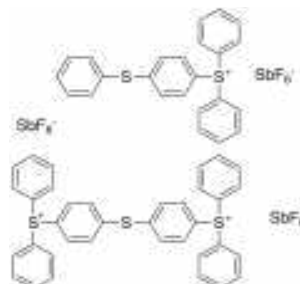
Figure 3.3: Monomer and Photoinitiator used for Composite samples

3.5 Method

3.5.1 Thin Layer Composites

Filler (1-10wt%) and photoinitiator (1mol%) were mixed in epoxy. Thin layers of mixture were prepared on Aluminum, Glass and Polypropylene (PP) sheets. These thin-layer composites were irradiated partially (Figure 3.4) or completely (Figure 3.5) with UV radiation of intensity 33mW/cm^2, for different time intervals. Thin layer composite samples, after irradiation, were checked for tentative gel time and Gel contents.
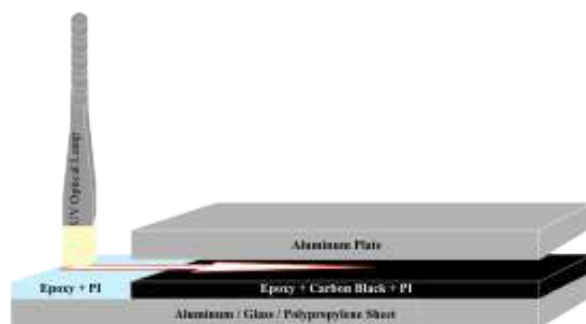
Figure 3.4: Partial irradiation of Thin Layer Composite samples
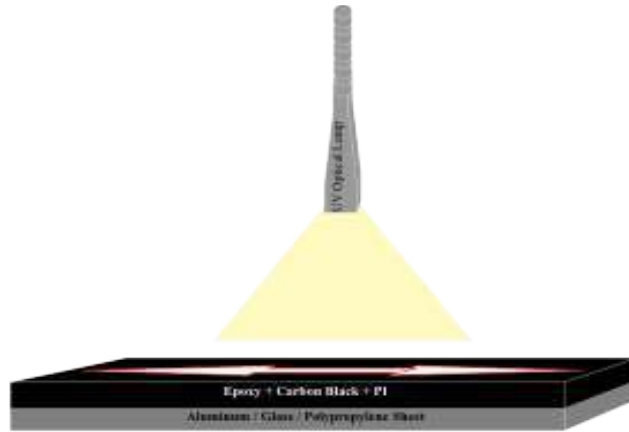
Figure 3.5: Complete irradiation of Thin Layer Composite samples

3.5.2 Thick Layer Composites

Two different methods have been used for Thick Layer Composite samples; named Conventional method and Smart Approach. A brief is as follows:

a) CONVENTIONAL METHOD: Filler and photo-initiator were mixed in epoxy. Mixture was irradiated for different time intervals (10sec-10min), with UV radiation of intensity 33mW/cm^2. Schematic representation is presented in Figure 3.6.
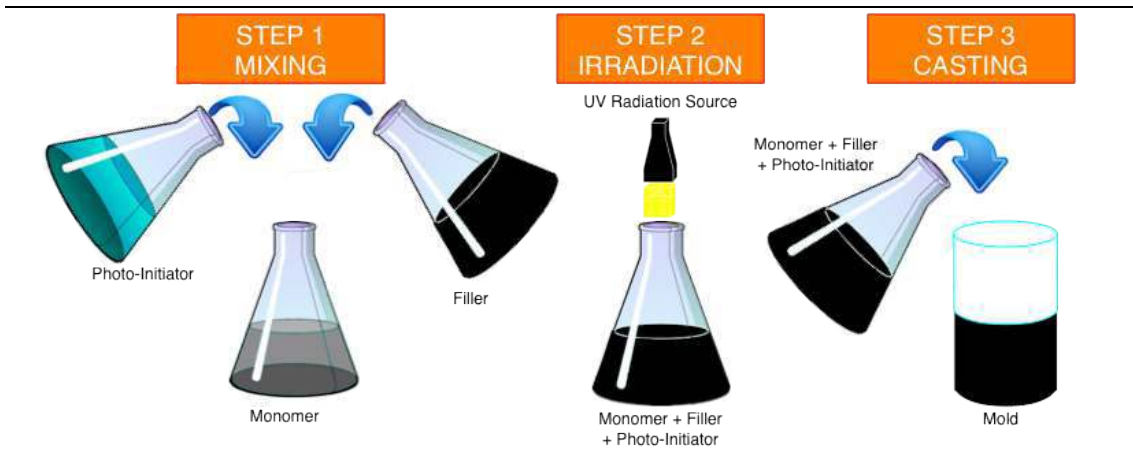
Figure 3.6: Scheme of Conventional Method for Thick Composite samples

b) SMART APPROACH: Filler particles were mixed in epoxy. In a separate vial, photo-initiator was irradiated for 90 sec, with UV radiation of intensity 33mW/cm^2, and was mixed with filler-epoxy mixture. Schematic representation is presented in

Figure 3.7.
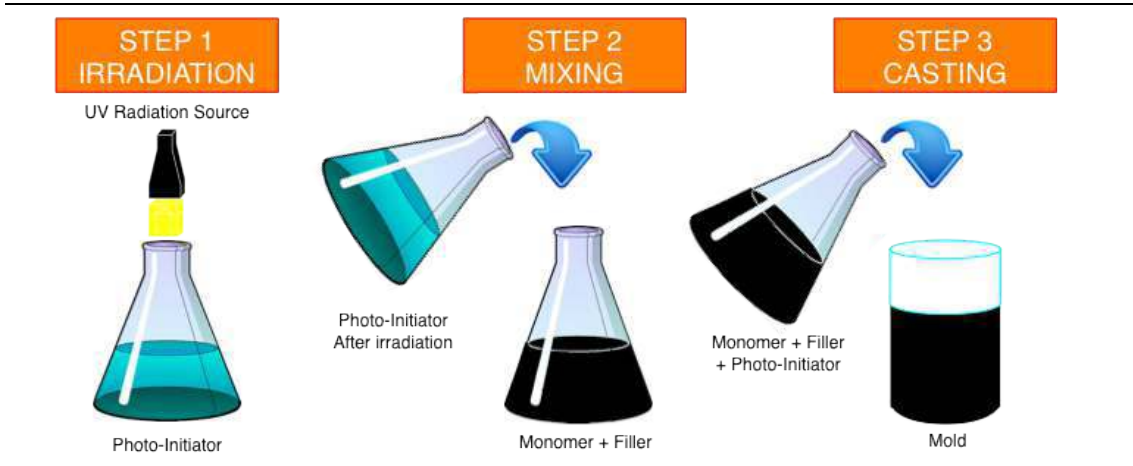
Figure 3.7: Scheme of Smart Approach for Thick Composite samples

3.6 Characterization of Nanocomposites:

In this segment, Epoxy-nanocomposites characterization techniques, used in the study, are described. Characterization has a crucial part in interpreting the structure and property relationship between nanocomposites. The techniques used are; scanning electron microscopy (SEM) for microstructural characterization, differential scanning calorimetry (DSC), thermogravimetric analysis (TGA), dynamic mechanical analysis (DMA) for thermal property characterization, Real Time Fourier Transform Infrared (RT-FTIR) spectroscopic analysis and Gel time measurements for kinetic description of polymerization rate.

3.6.1 Thermal Differential Scanning Calorimetry (Thermal DSC):

Thermal analysis was performed by a TA DSC2000 differential scanning calorimeter (DSC) with UV-curing accessory, using irradiation intensity of 33mW/cm². A radiometer (Honle UV technology, Germany) was manipulated to adjust the intensity. Since protocol was not feasible for Smart samples, so conventional

samples formulations were tested for Degree of cure ($DC_{PHOTO-DSC}$) by using equation (3.2). Where ($H_{PHOTO-DSC}$) was obtained by integrating the peak area; and (H_{tot}) was found from literature.

$$\% \ DC_{PHOTO-DSC} = \frac{H_{Photo-DSC}}{H_{tot}} \ X \ 100 \qquad (3.2)$$

2.6.2 Photo Differential Scanning Calorimetry (Photo-DSC):

Degree of cure was studied through DSC analysis as well, by estimating the residual heat of polymerization for uv-cured samples. A DSC scan was performed on each sample using a TA DSC2000 differential scanning calorimeter (DSC) at a heating rate of 10°C/min, in temperature range from -80°C to 500°C. Area integration of the exothermic DSC peak after baseline subtraction was utilized to calculate enthalpy of reaction (H_{DSC}). To obtain the extent of reaction, H_{DSC} for each sample was compared to the total enthalpy of polymerization (H_{tot}), found in literature, by using following Equation.

$$\% \ DC_{DSC} = (\ 1 - \frac{H_{DSC}}{H_{tot}} \ ) \ X \ 100 \qquad (3.3)$$

3.6.3 Dynamic Mechanical Analysis (DMA):

Storage modulus and glass transition (Tg) measurements of nanocomposites were performed on DMA (Model 242C, NETZSCH, Germany) in Tensile Configuration. Experiments were carried out in the temperature range of -100 to 50 °C under nitrogen flow. Heating rate was 3°C/min. Scans were conducted at a frequency of 1 Hz. The specimen dimension was 50(L) × 5(W) × 1(H) mm.

3.6.4 Thermal Gravimetric Analysis (TGA):

TGA/SDTA851^e METTLER TOLEDO instrument was utilized for TGA analysis of 10-15mg of each sample. Airflow was kept at 60 mL/min; temperature increment was 10 ^{o}C/min from 25 to 800°C. 70 μL Alumina crucible was used to place sample.

3.6.5 Gel content:

Gel contents were measured for all composite samples, by gauging composite weight loss in chloroform for 24 hours, according to ASTM D2765-84. Gel contents were calculated using the following equations:

$$\% \text{ Extract} = \frac{W_s - W_d}{W_s} \text{ X } 100 \qquad (3.4)$$

$$\% \text{ Gel content} = 100 - \% \text{ Extract} \qquad (3.5)$$

Where, W_s is weight of the specimen being tested, W_d is weight of dried gel.

3.6.6 Attenuated Total Reflectance (ATR) Analysis:

The degree of conversion was studied by near-IR (Nicolet 5700) spectrometer equipped with an attenuated total reflectance (ATR) attachment. Degree of conversion (DC_{ATR}) was determined by Eq. (3.6); taking into account the decrease in epoxy peak area at 926 cm^{-1}, after UV curing.

$$DC_{ATR} = \frac{A_0 - A_t}{A_0} \text{ X } 100 \qquad (3.6)$$

A_0 and A_t represents respectively, peak area of uncured epoxy and peak area of cured epoxy composite samples.

3.6.7 Gelation Time:

Gelation time was checked tentatively. For thin films, it was done by touching the surface time to time till there was no feeling of tackiness. For thick composite samples, the purpose was solved either by shaking or turning the sample vial upside down till no flow was observed.

3.7 Kinetics of Polymerization:

Real time polymerization kinetics has been studied by Fourier Transform-Infra Red (FTIR; Nicolet 5700) spectrometer with UV optical lamp attached as accessory having 33mW/cm^2 irradiation intensity. Approximately 15µm thick composite films, with different weight ratios (0.5-10wt%) of different fillers (CB, Silica, Alumina) were scanned for their degree of cure while being irradiated with UV radiation. Degree of polymerization varied with time of irradiation, and was calculated by monitoring the rate of decrease in epoxy peak area (at 926 cm^{-1}) with time. Percent conversion is calculated by equation 3.7:

$$\% \text{ Conversion} = (1 - \frac{\text{Peak ratio at time t}}{\text{Peak ratio at t=0}}) \times 100 \qquad (3.7)$$

In this chapter results of the experimentation for CB surface modification and composite preparation, are presented.

PART-I: Carbon Black Surface Modification

CB surface modification, either thermally or photochemically, has generated appreciable results.

4.1 Thermal Modification of CB

4.1.1 Oxidation of CB

Keeping in mind that oxygen contents of CB affect its properties, oxidation of Pristine-CBs has been carried out. Two types of CBs; Glassy CB and Vulcan CB (VCB), has been oxidized through nitric acidic treatment, ensuing similar protocol of acidic reflux for 90 minutes [104]. This part of dissertation presents an investigation of oxygen contents of CB, before and after oxidation treatment. A comparative study has also been conducted for oxidation protocol, by using different types of Pristine-CBs. When CBs are treated with acid, a significant increase of oxygen contents on CBs has been observed.

Figure 4.1 & 4.2; represent FTIR spectra of Pristine & oxidized Glassy CB & VCB respectively. Regarding the spectra of the Oxidized-CBs, clearly visible peaks near 3200-3700 cm^{-1}, 1600-1700 cm^{-1} and 600 cm^{-1}, due to oxidized groups (hydroxyl,

carbonyl and metal oxide groups respectively [105-108]), which were either weak or absent in Pristine CBs.
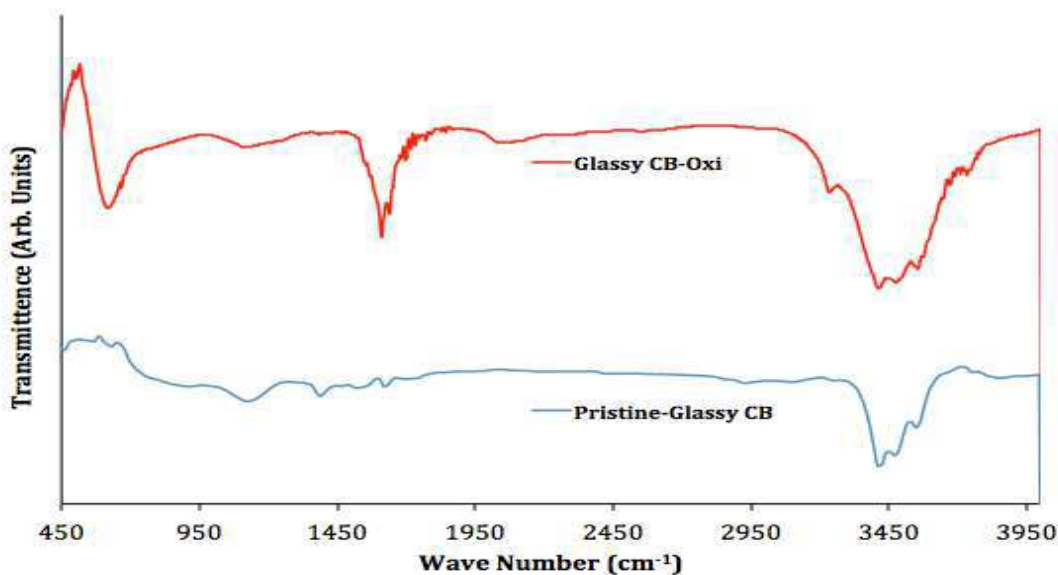
Figure 4.1: FTIR spectra of Pristine & Oxidized Glassy CB
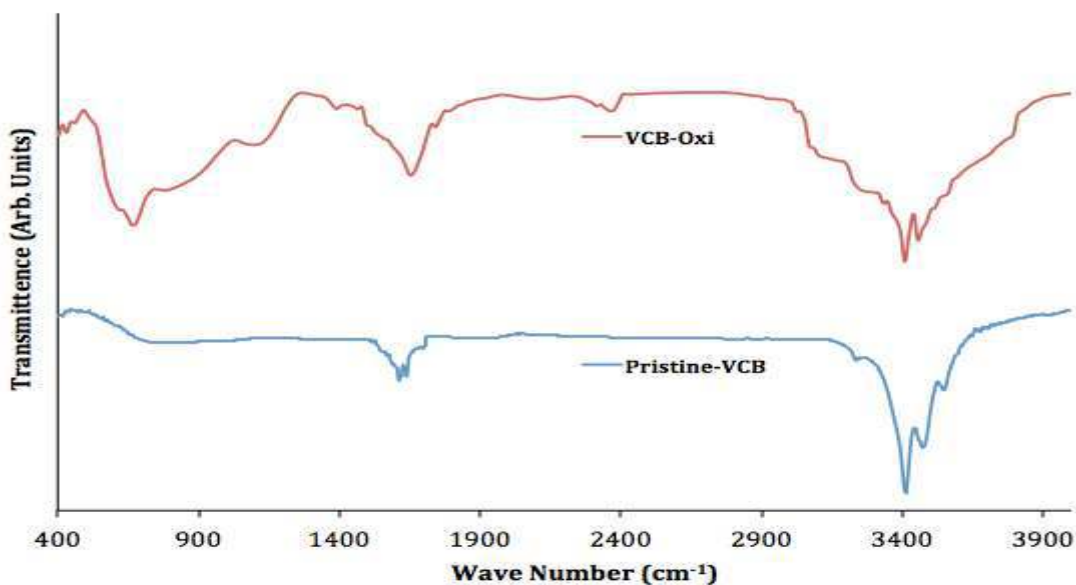
Figure 4.2: FTIR spectra of Pristine & Oxidized VCB

Figure 4.3 contains XPS Survey Scan spectra of Pristine & oxidized Glassy CB. Noteworthy rise in oxygen contents can be observed clearly, from O1s peak at 532 eV; values mentioned in Table 4.1 and compared with EDX data (detailed discussion

below Table 4.1). Same oxidation procedure was followed by Pristine-VCB; XPS Survey Scan spectra of VCB before and after oxidation treatment are presented in Figure 4.4. Oxygen peak at 532 eV, assigned to O1s shows an increase of % area from 6.9 to 17 as per XPS analysis (Table 4.1).
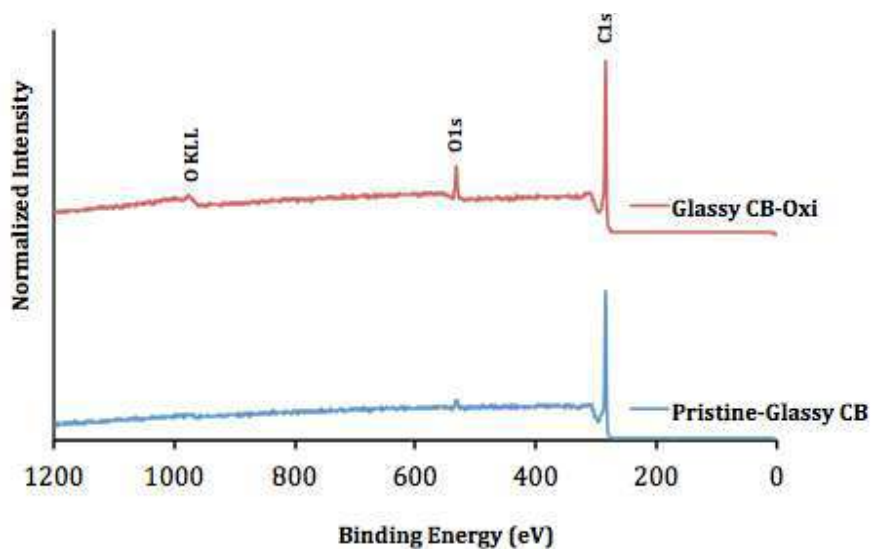
Figure 4.3: XPS Survey Scan spectra of Pristine & Oxidized Glassy CB
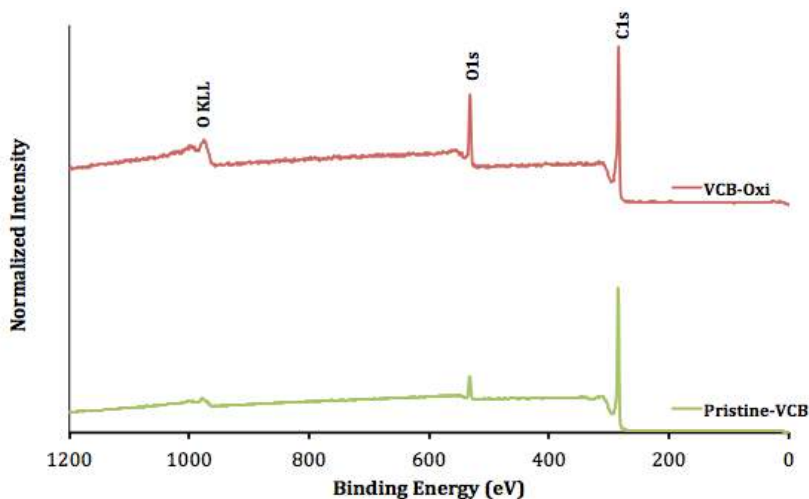
4.4: XPS Survey Scan spectra of Pristine & Oxidized VCB

Table 4.1 contains data of Pristine and oxidized, Glassy CB and VCB, obtained through different techniques. For Glassy CB-Oxi, XPS shows 5% increase in oxygen

contents while EDX shows 0.6% increase. This can be justified by the fact that Glassy CB-Oxi has micron sized spherical shape; intense acidic modification has changed the structure of Glassy CB below its upper layer, moreover instrumental competencies to analyze samples thickness are not the same, so both instruments have given different results. On the other side, for VCB, XPS results are almost in accordance to EDX data. This is due to fine powder like structure of VCB. Although both instruments analyze different thickness of sample, yet similar results prove homogeneity of modification procedure.

| | XPS data | | EDX data | | ζ (mV) | pH |
	% [C]	% [O]	% [C]	% [O]		
Pristine-Glassy CB	96.4	3.6	100.0	0.0	-7.5	5.58
Glassy CB-Oxi	91.5	8.5	99.4	0.6	-11.0	5.05
Pristine-VCB	93.1	6.9	97.0	2.5	-9.5	5.06
VCB-Oxi	83	17	82.9	15.7	-16.0	4.87

Table 4.1: Data of instrumental analysis of Pristine and Oxidized samples

After modification, zeta potential of modified samples has decreased (see Table 4.1). This decrease in zeta potential specifies supplementary charged species on their surface, which is in accordance with FTIR, XPS and EDX data. Increase in oxygen functional groups has made samples slightly acidic, as observed from pH (Table 4.1). Deconvolution of XPS signals has given a further insight into the different forms of oxygen contents of CBs. Figure 4.5(a) & (b) displays high-resolution fitted spectra of oxygen (O1s) recorded on Pristine and Oxidized Glassy CB, respectively.

Three main components have been observed in pristine-Glassy CB; 530.96eV (M-O 12%), 532.35eV (Hydroxyl 48%) and 533.52eV (Carbonyl 40%). While components observed in Glassy CB-Oxi are 532.35eV (Hydroxyl 68%), 533.64eV (Carbonyl 23%)

and 534.51eV (adsorbed oxygen 9%). Highest increase in %area after modification has been observed for Hydroxyl group; which is in accordance with FTIR data.
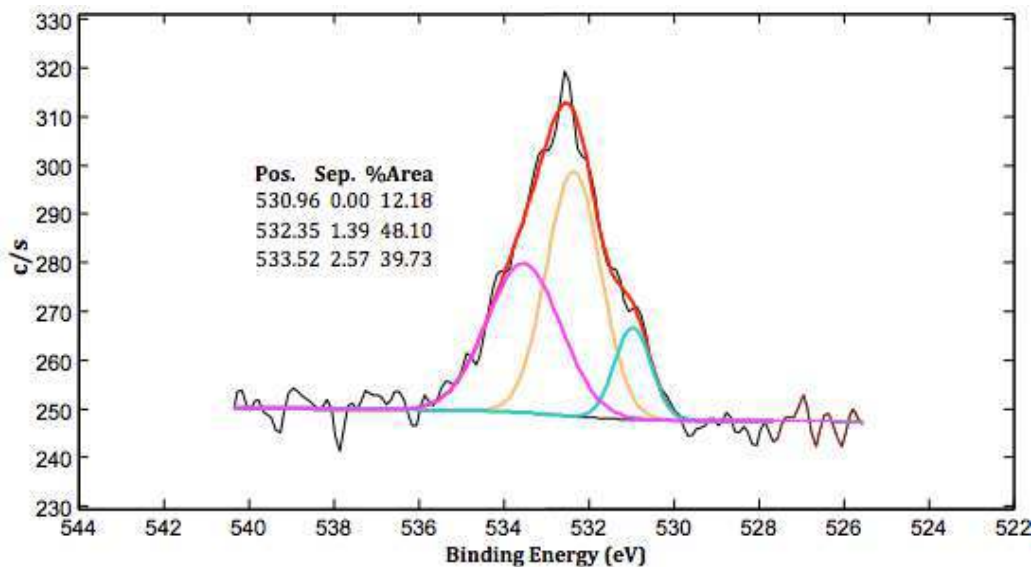
Figure 4.5(a): O1s fitting Spectra of Pristine-Glassy CB
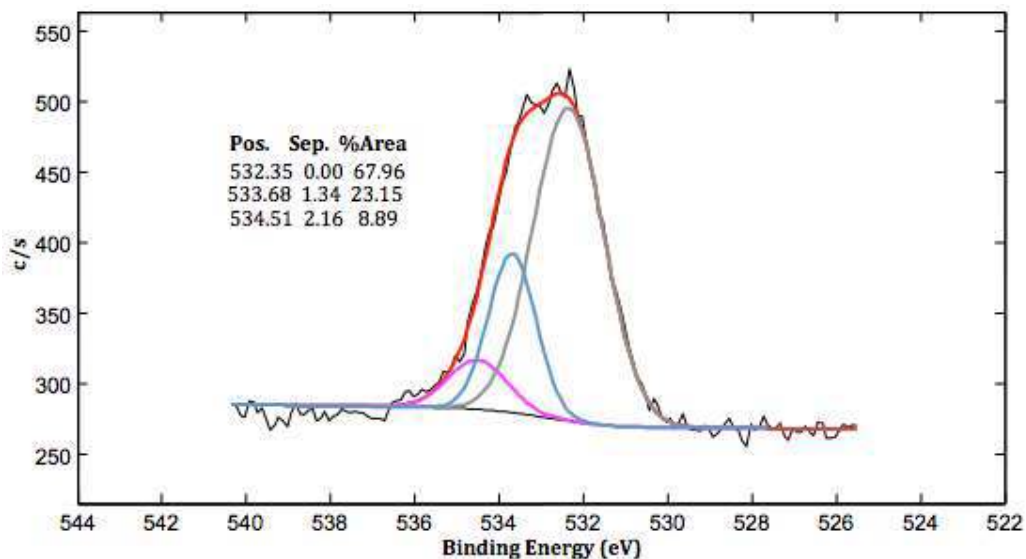
Figure 4.5(b): O1s fitting Spectra of Glassy CB-Oxi

XPS oxygen signals have also been deconvoluted for Pristine and oxidized VCB. After oxidation, a decrease in peak area at 531.75eV, representing M-O bond, has been observed from 18% (Pristine-VCB) to 10% (VCB-Oxi). Along with that an increase in peak area at 532.5eV representing hydroxyl groups, has been noticed from 39%

(Pristine-VCB) to 51% (VCB-Oxi) has been observed. Carbonyl peak (533.74 eV) decreases in area from 43% to 39%. Deconvoluted spectra are presented in Figure 4.6 (a & b). Results are in conformity with other instrumental data.
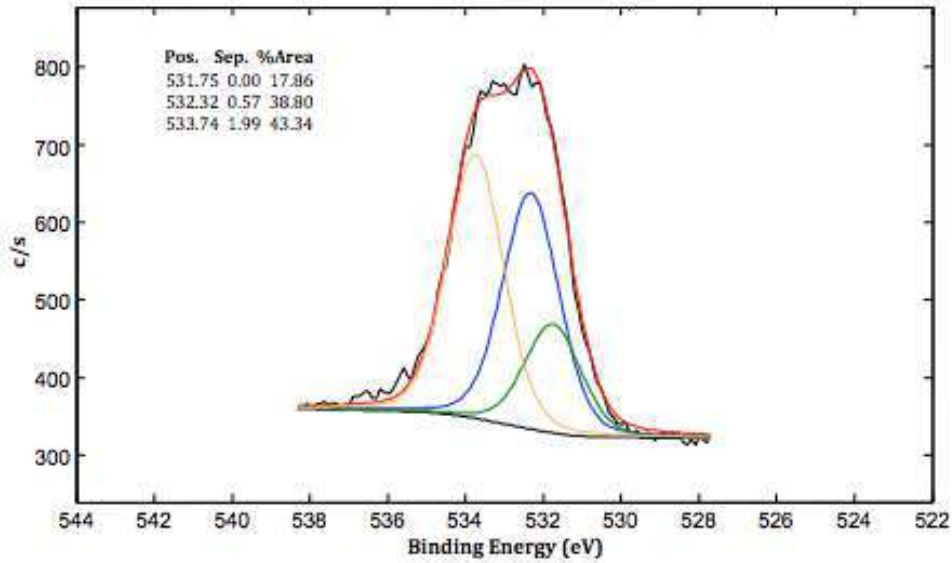
Figure 4.6(a): O1s fitting Spectra of Pristine-VCB
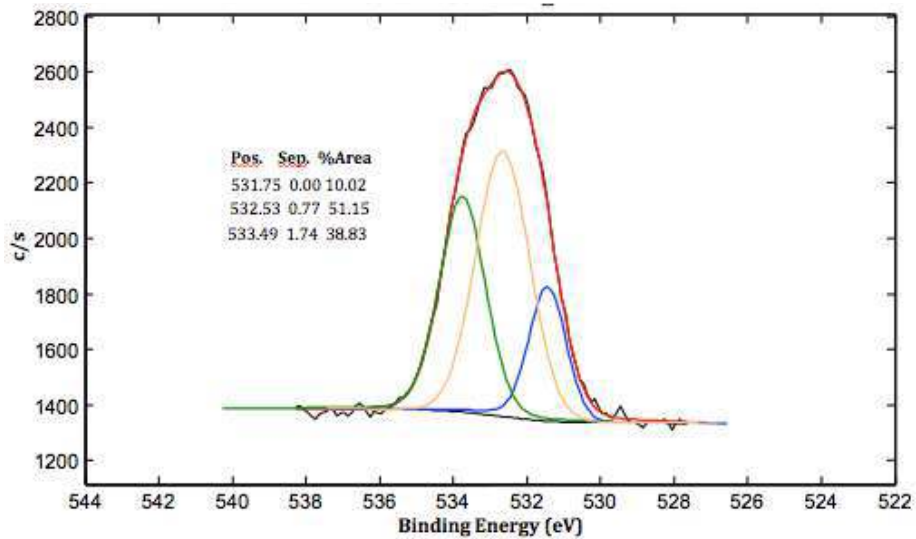
Figure 4.6(b): O1s fitting Spectra of VCB-Oxi

Thermal gravimetric analysis data was collected for starting materials as well as for products by thermal treatment from 25 to 800°C with temperature ramp rate of 10°C/min. TGA spectra are shown in Figure 4.7 (a & b) for Glassy CB and VCB,

respectively. Each figure shows a comparative analysis of respective CB before and after oxidation treatment. Decreased thermal stability after surface modification verifies efficiency of modification procedure. Pristine-Glassy CB on thermal decomposition leaves 90% stuff at 800°C, where as Glassy CB-Oxi leaves 82% at same temperature. For VCB thermal decay shows quite different results, because of its powder like fluffy structure: Pristine-VCB decomposes 95% at 700°C, where as after treatment VCB-Oxi decomposes almost same at 610°C.
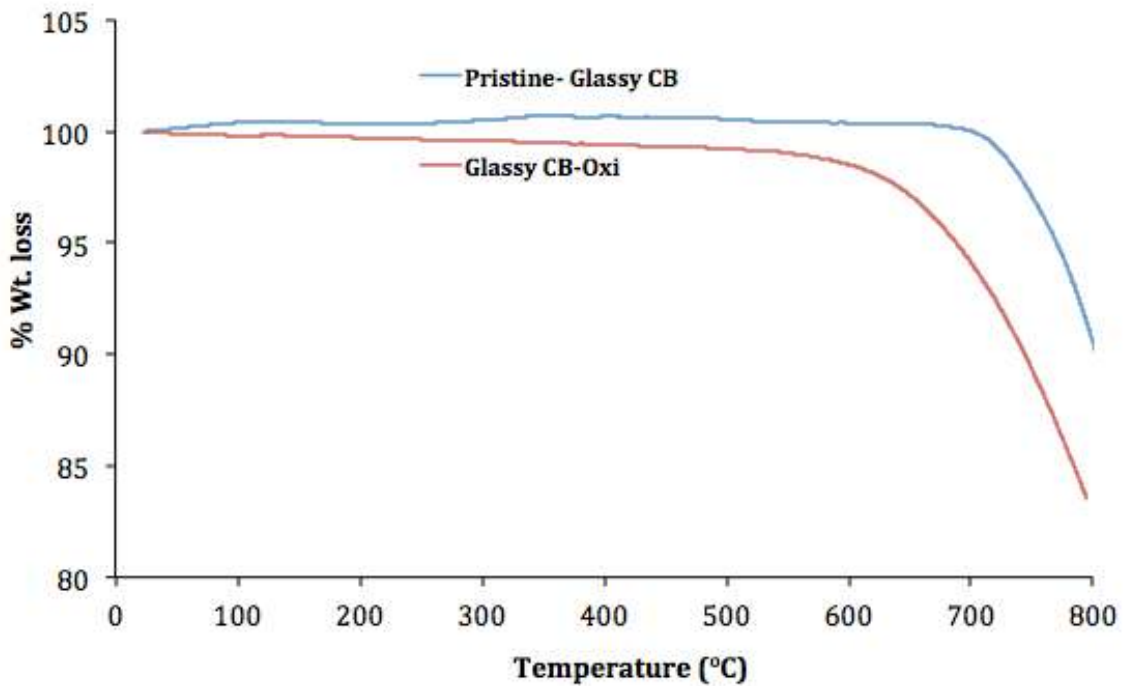
Figure 4.7(a): TGA of Pristine & Oxidized Glassy CB
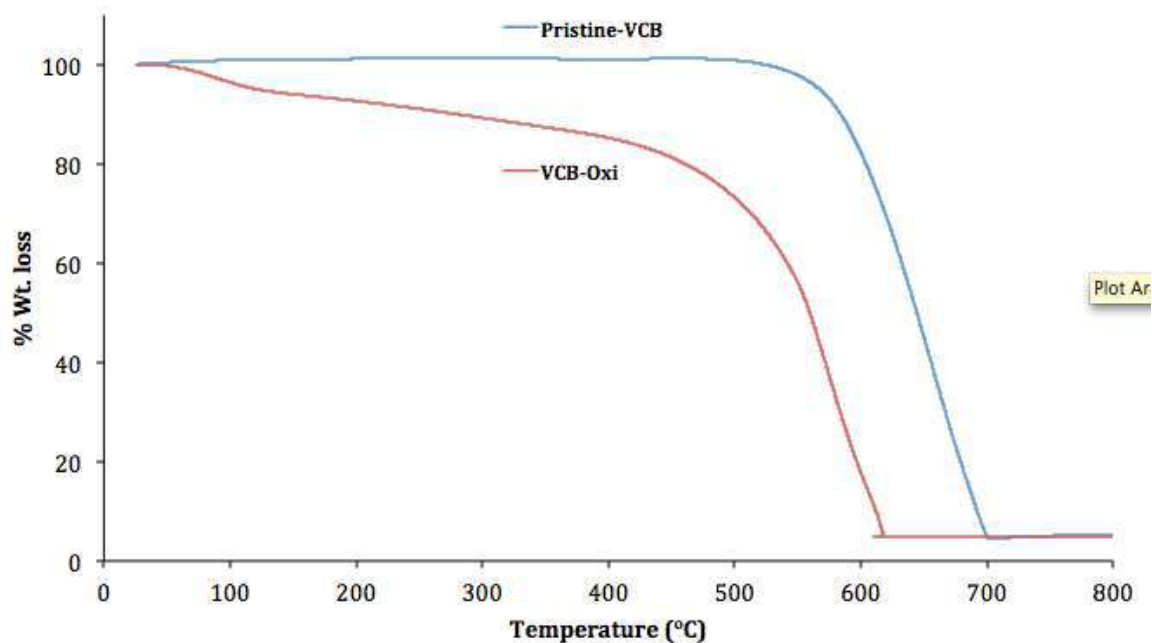
Figure 4.7(b): TGA of Pristine & Oxidized VCB

Thermal disintegration of samples, before and after modification, can be sketched by $T_{2\%}$, $T_{5\%}$ and $T_{10\%}$ estimation i.e. the temperature at which there is a loss of 2, 5 and 10% (Table 4.2). Speedy decomposition of modified samples, in comparison to their pristine counterparts, indicates oxygen incorporation on their surface. Residual masses of CB samples after 800^0C also depends on their configuration; residual mass of Glassy CB, at 800^0C is 82% due to its big compact ball like structure where as residual mass of VCB at 800^0C is 5% which is because of its powder like fluffy structure.

		Pristine-Glassy CB	Glassy CB-Oxi	Pristine-VCB	VCB-Oxi
$T_{2\%}$	(^{0}C)	739	625	549	81
$T_{5\%}$	(^{0}C)	770	688	567	123
$T_{10\%}$	(^{0}C)	800	743	584	281

Table 4.2: Data of thermal disintegration of Pristine and Oxidized samples

In Raman analysis 3 peaks are mainly considered: G peak at ~1580 cm^{-1} also called graphite peak; D peak at ~1360 cm^{-1} also known as disordered carbon peak; G' peak

43

at 2700 and 2735 cm^{-1} representing strongly graphitic and annealed (very ordered) carbons. Raman spectra of Pristine and oxidized glassy CB & VCB are presented in Figure 4.8(a) & (b) respectively. The Pristine-Glassy CB sample is composed only by carbon. Raman spectra (Figure 4.8(a)) show the presence of secondary peaks in the region 2600-3300 cm^{-1} due to the replications of D and G peaks (in particular: G'=2D ($\sim$2689cm^{-1}), D+G ($\sim$2936cm^{-1}), 2G ($\sim$3225cm^{-1})). Glassy Carbon Black after oxidation shows an increase of disorder (D peck increase, G' peak decrease). This means that the structure changed significantly. This could be correlated with FESEM images. Figure 4.8(b) compares Raman spectra of Pristine- and Oxidized VCB. It is clear from comparison that D and G peaks remain at the same intensity. Which means oxidation process has not dented the structure of VCB.
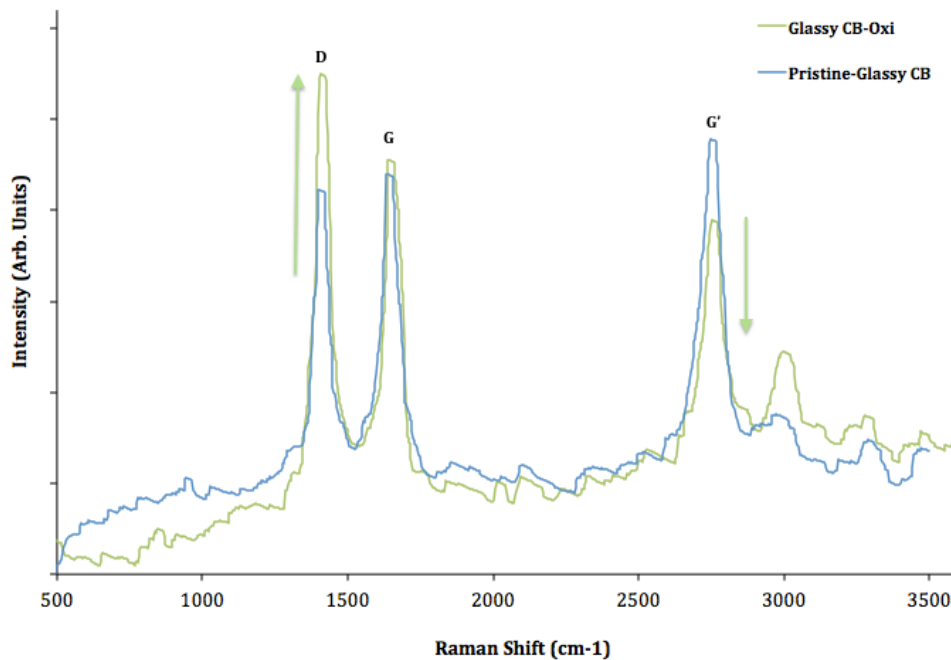
Figure 4.8(a): Raman Spectra of Pristine & Oxidized Glassy CB
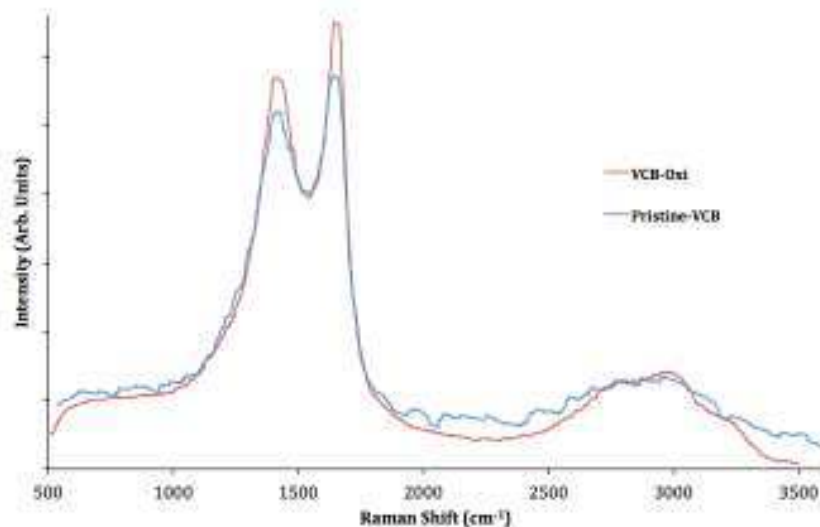
Figure 4.8(b): Raman Spectra of Pristine & Oxidized Glassy CB

SEM images of Glassy CB before and after modification has been presented in Figure 4.9 (a) and (b). EDX analysis of Glassy CB-Oxi shows trace of Oxygen. FESEM images show a deterioration of the external carbon surface of spheres, this contributes to increase the structural disorder (increase of ID peak intensity).
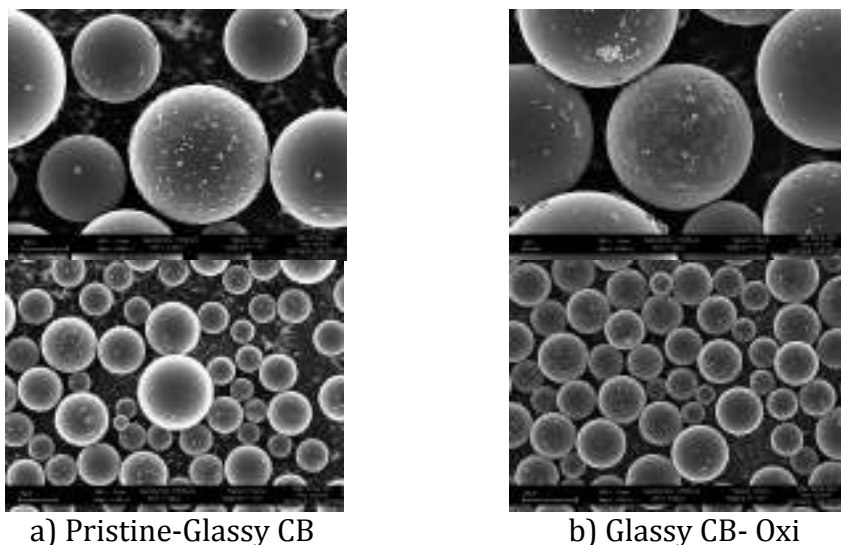
a) Pristine-Glassy CB   b) Glassy CB- Oxi

Figure 4.9(a): SEM images of (a) Pristine-Glassy CB and (b) Glassy CB-Oxi

a) Pristine-VCB   b) VCB- Oxi
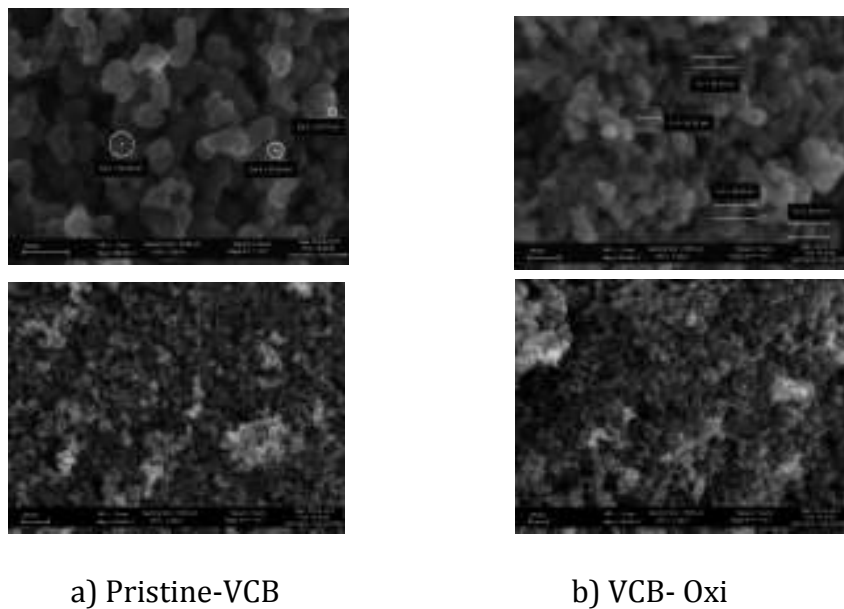
Figure 4.9(b): SEM images of (a) Pristine-VCB and (b) VCB-Oxi

4.1.1 Thiolation / Silanization *(This part has been published in Journal)*

The pristine-CB used in this study is a typical CB obtained by a furnace process, therefore characterized by few reactive surface groups. It was treated with a strong acid, as widely reported in the literature [104]. Then an organoalkoxysilane Mercaptopropyl-triethoxysilane (MPTS) was introduced into the reaction for surface modification. Reaction between the silane coupling agent and a filler such as CB consists of two steps, as widely described in the literature [109]. The first step is hydrolysis of tri-alkoxy groups and formation of silanol groups followed by their condensation reactions with the oxidized groups of Pristine-CB. Under the alkaline conditions adopted in this work strong nucleophiles are formed, enhancing both hydrolysis and condensation reactions.

Figure 4.11 reports the FTIR spectra of (i) the CB subjected to the silanization reaction (MPTS-VCB) and (ii) the Pristine-VCB. The spectrum of MPTS is also plotted

46

for reference. For MPTS, the peaks at 2920 and 2850 cm^{-1} can be assigned to the anti-symmetric and symmetric stretching bands of the methylene groups, while the peak at 820 cm^{-1} is the signal for the rocking of the methyl group of Si-OCH3. The peak at 1191 cm^{-1} is assigned to Si-OCH3 bending, the peak at 1089 cm^{-1} to Si-O stretching. An unambiguous peak for S-H is found at 2550 cm^{-1}.
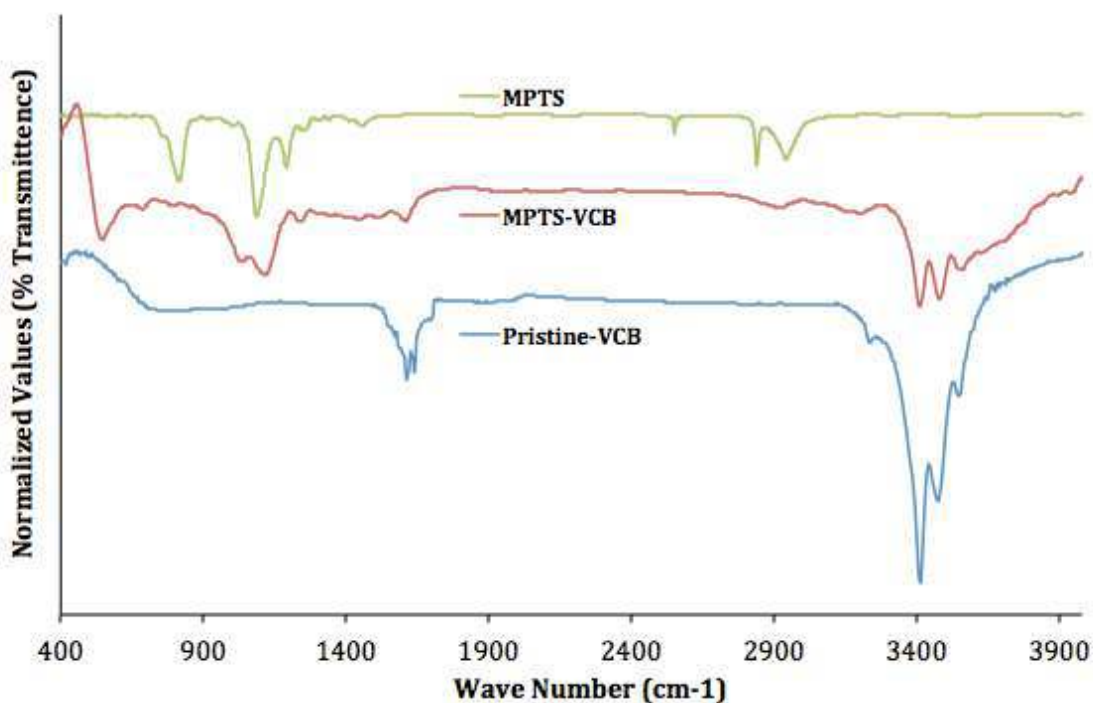
Figure 4.11: FTIR spectra of Pristine-VCB, MPTS and MPTS-VCB

Looking at the main features of the spectrum of the Pristine-VCB, one can point the presence of complex peaks in the region 1680-1700 cm^{-1} and 3410-3530 cm^{-1}, due to oxidized groups (carbonyl and hydroxyl groups respectively) already present in the material before any treatment [105-8]. In MPTS-VCB the carbonyl functional groups at around 1700-1680 cm^{-1} almost completely disappear; there are still oxygen containing groups at around 3400 cm^{-1}: there is likely to be an overlapping

with the 3700 cm^{-1} band related to the Si-OH groups [110]. The breaking of the trimethoxy groups is further suggested by the absence of a band at 820 cm^{-1}.

Further evidence of the silanization comes from the weak bands present at 2920 and 2850 cm^{-1} due to the methylene groups of MPTS. Moreover the appearance of peaks at around 1000 cm^{-1} and their broadening with respect to MPTS indicates Si-O-Si and Si-O-C bond formation. Interestingly the peak at 550 cm^{-1} signposts thioether bond formation. However no S-H signal at 2550 cm^{-1} is present, suggesting utilization of thiol group during reaction, in addition to the hydrolysis and condensation of the alkoxy groups [111].

On the basis of the FTIR analyses, one can propose the following sketch (Scheme 1) to describe the surface functionalization obtained:
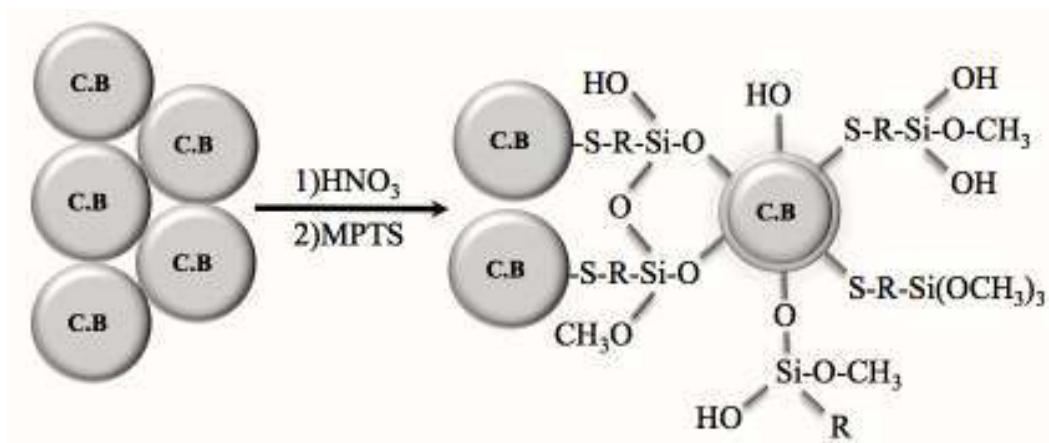
Scheme 4.1: VCB surface modification by MPTS

The XPS analysis of Pristine-VCB and MPTS-VCB has been conducted. The survey spectra of the two samples are overlapped in Figure 4.12 Common peaks are assigned to C1s (284.8 eV), O1s (532 eV) with the related Auger oxygen peak at 978 eV. The main difference between the samples is occurring at low binding energy (100-200 eV): the peaks at 100 and 150 eV are due to Si2p and Si2s respectively, the

48

peaks at 164 and 229 eV can be assigned to S2p and S2s. Therefore the spectra indicate clearly the presence of sulfur and silicon after modification.
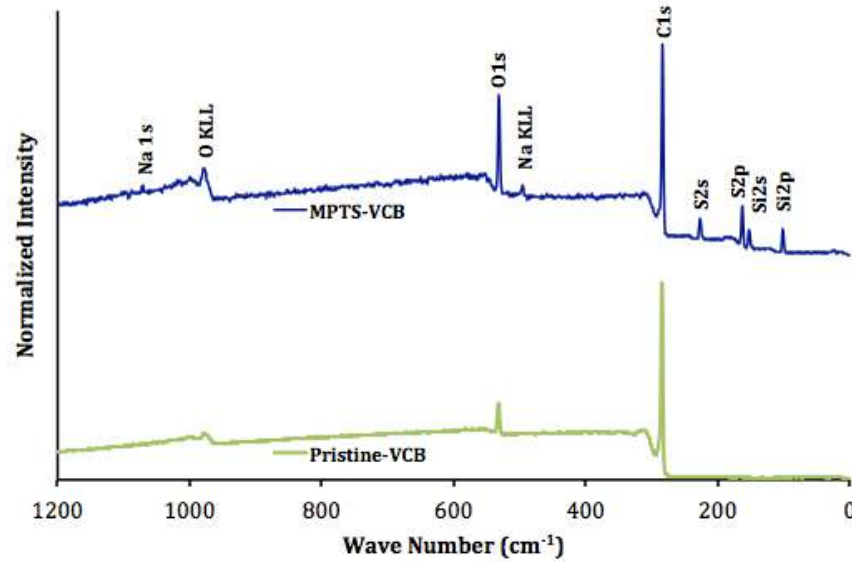
Figure 4.12: XPS Survey Scan spectra of Pristine-VCB & MPTS-VCB

Deconvolution of relevant signals has been done to further insight into the different forms of fixed sulfur and silicon. Figure 4.13 displays high-resolution fitted spectra of sulfur (S2p) recorded on MPTS-VCB.
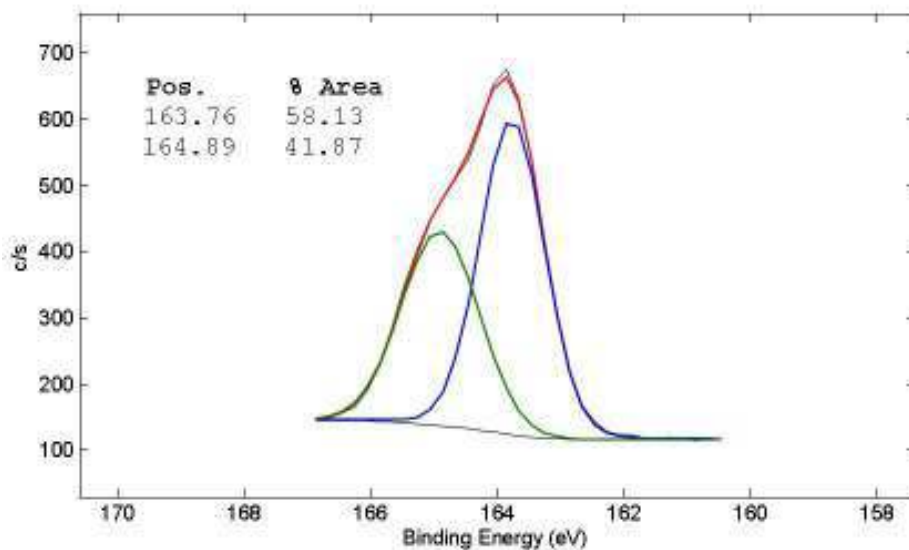
Figure 4.13: Fitting Spectra of MPTS-VCB S2p

As seen in Figure 4.13, two main components are detected. According to E. Papirer [8], the component at 163.8 ± 0.1 eV represents sulfur covalently linked to C atoms at the border of aromatic structures. According to C.H. Chang [112] the component at 164.9 ± 0.2 eV represents sulfur compounds like C-S-C. Therefore the XPS data suggest that MPTS reacted with CB both through the alkoxy groups and the thiol groups. This is in agreement with the data obtained by FTIR spectroscopy.

Concerning the C1s signal, as can be seen in Figure 4.14, the comparison of the samples helps in the interpretation of the modification process. The 284.81 eV component corresponds to sp^2/sp^3 non-functionalized carbons of aromatic ring like structures. After modification it has shifted to 284.52 eV, with a strong reduction of its intensity, which is nearly halved (from 78.5% to 40%). While in the Pristine-VCB there is a component at 286.16 eV representing C-O-R, and a component at 287.71 eV representing carboxylic groups, in the MPTS-VCB we find different deconvolution results. Disappearance of the 287.71 eV component in MPTS-VCB suggests consumption of carboxylic group [113] present on the surface of Pristine-CB. A new component at 285.16 eV appears and represents aliphatic carbons [112]: aliphatic chain is a part of the incorporated silane molecule, therefore this component is missing in Pristine-VCB.

According to E. Papirer [8], 284.52 eV component in MPTS-VCB represents carbon atoms attached directly to sulfur. The 286.16 eV component is perhaps shifted to 286.23 eV.

In both samples the component at 289.3-289.5 eV represents COOR bond and plasmons.
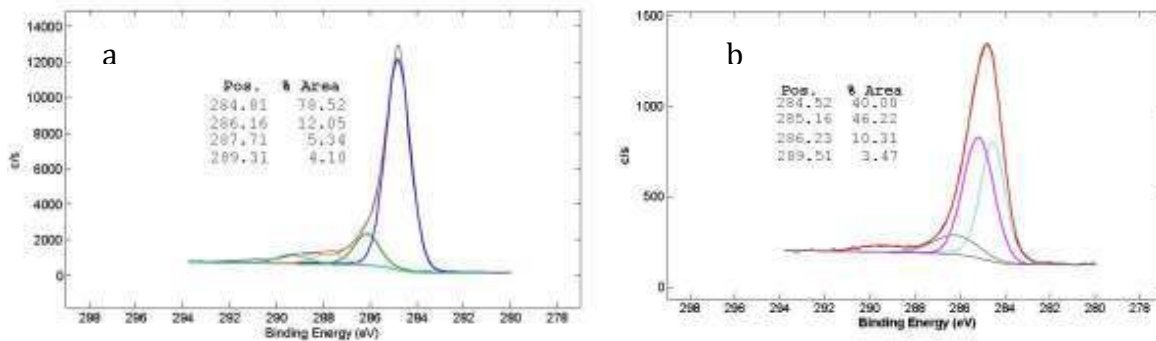
Figure 4.14: Carbon fitting spectra (a) Pristine-VCB and (b) MPTS-VCB

In Figure 4.15 the oxygen peak of the Pristine-VCB and MPTS-VCB samples are deconvoluted. The modified sample exhibits a sharper signal than the pristine sample. Three main components are proposed to fit the signal: (i) component at 531.75 eV corresponds to the system C-O-Na as reported in the literature, [114] (ii) component at 532.32 eV represents oxygen singly bonded to sp3 carbon, i.e hydroxyl in Pristine-CB and methoxy group,[8] and (iii) component at 533.74 eV represents oxygen both singly bonded to sp2 carbon, i.e Ph-O-Ph and having double bond with sp2 carbon, i.e. carboxyl groups [113]. All components are present in both samples, but in different ratios. There is clearly a strong decrease of carboxyl groups and oxygen linked to sp2 carbons, while the main component becomes the one at 532.32 eV representing oxygen singly bonded to sp3 carbon, as present in the methylene chains and the methoxy groups of the MPTS structure. Results are in agreement with analysis of C1s, which indicates a decrease in concentration of carbon doubly bonded to oxygen.
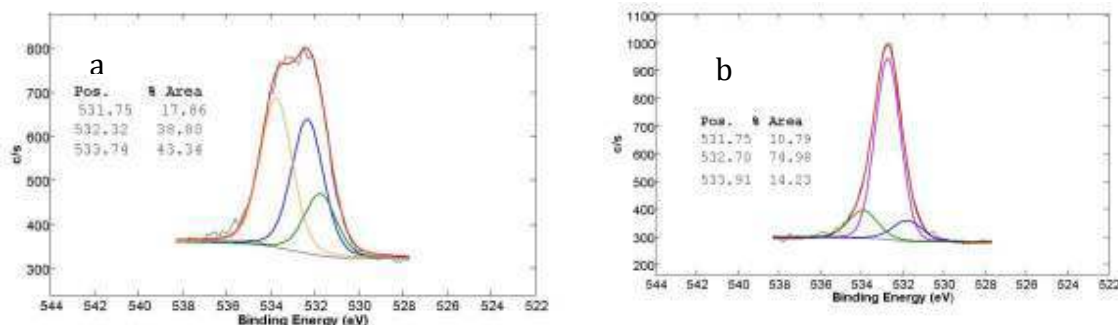
Figure 4.15: Oxygen fitting spectra (a) Pristine-VCB and (b) MPTS-VCB

On the basis of the XPS spectra a chemical analysis can be conducted and the results are compared, in Table 4.3, to those obtained by EDX.

Technique	Sample	C[%]	O[%]	S[%]	Si[%]
XPS Analysis	Pristine-VCB	93.1	6.9	0.0	0.0
	MPTS-VCB	72.0	16.5	4.6	6.2
EDX Analysis	Pristine-VCB	97.0	2.5	0.5	0.0
	MPTS-VCB	70.0	10.2	8.5	9.2

Table 4.3: ESCA and EDX composition of Pristine-VCB and MPTS-VCB

With both techniques it is shown that MPTS-VCB is different than the pristine-VCB, in particular as already discussed above, silicon and sulfur are present only on the sample treated with MPTS. Accordingly there is an increase of oxygen and a decrease of carbon content. Comparing the results obtained by the two methods, they are consistently different. In fact XPS and EDX explore and probe the material through different sampling, therefore differences among the data are usual and indicates heterogeneities in composition.

The samples were also analyzed by Raman spectroscopy. Results are plotted in Figure 4.16. No major effects can be detected: the bands give details of the crystalline structure in which silanization does not take place. There is however an increase in the intensity of the broad G' peak (2800-3000 cm^{-1}). This peak corresponds to an overtone and is due to D+G phonons contribution and its

evidence in MPTS-VCB sample suggest that treatment led to higher order [115].
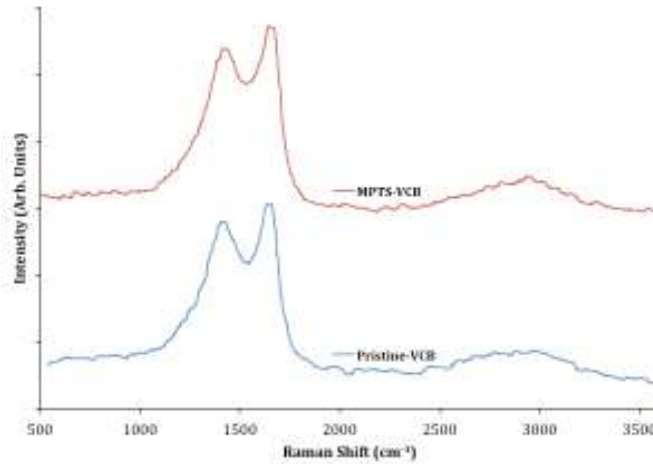
Figure 4.16: Raman spectra of Pristine-VCB and MPTS-VCB

From the Raman spectra the average size of nano-crystallites can be determined in terms of changes in position, width and intensity ratio of two Raman peaks observed at 1345 cm^{-1} (the disordered, or D peak) and 1575 cm^{-1} (the graphite, or G peak). The shape of those peaks depends on the crystallite sizes. When the crystallites become larger, the peaks become narrower, their maxima move to higher frequencies and the intensity of the G peak systematically increases in comparison with the d peak. A first glance at Fig.4.16 shows that there are no big variations in the quoted features. Hence it is not a surprise that, using the empirical formula found by Tuinstra and Koenig [116] to evaluate L_a (lateral size of the crystallites).

$$L_a = 4.35 \ (I_g/I_d) \ (nm)$$

We get similar values for both samples: 5.3 nm for Pristine-CB and 5.5 nm for m-CB. These data refers to primary particles. Usually primary particles are invariably fused into larger aggregates having size in the range of 200–1000 nm and further to

micro-sized agglomerates.

In Figure 4.17(a) FE-SEM image for Pristine-VCB is presented. The shape of the primary aggregates (shown by circles) is quasi spherical as expected, ranging from 20 up to 50 nm. After modification, Figure 4.18(a), primary aggregates are less defined with smaller size, around 30 nm but still spherical.

Accordingly, when BET measurement was performed, it resulted that the specific surface area of the MPTS-VCB has increased significantly as reported in Table 4.3. It is interesting to report that a conventional modification such as oxidation is not able to increase the surface area so significantly: the VCB-Oxi has a specific surface area of 86 m^2/g, i.e. slightly higher than Pristine-VCB.

Secondary aggregates are evidenced in Figures 4.17(b) and 4.18(b). They are bigger after modification, at the same time the aspect has changed. Before modification they are elongated, after modification they appear globular with some holes in the structure.

By correlating above structural information we can conclude that CB has a multi scale structure. The lower size (sensed by Raman) is barely modified, while relevant changes both in term of agglomerate size and porosity occur upon modification.
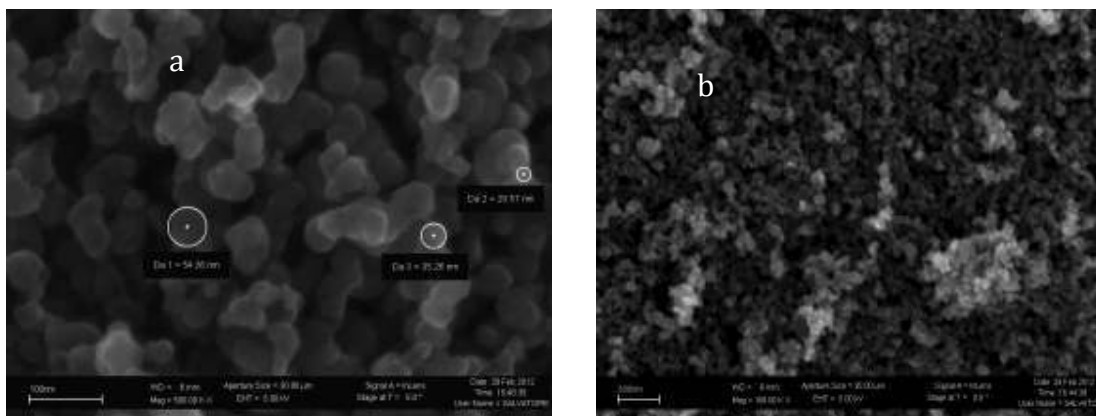
Figure 4.17 (a) & (b): FESEM IMAGE of Pristine-VCB
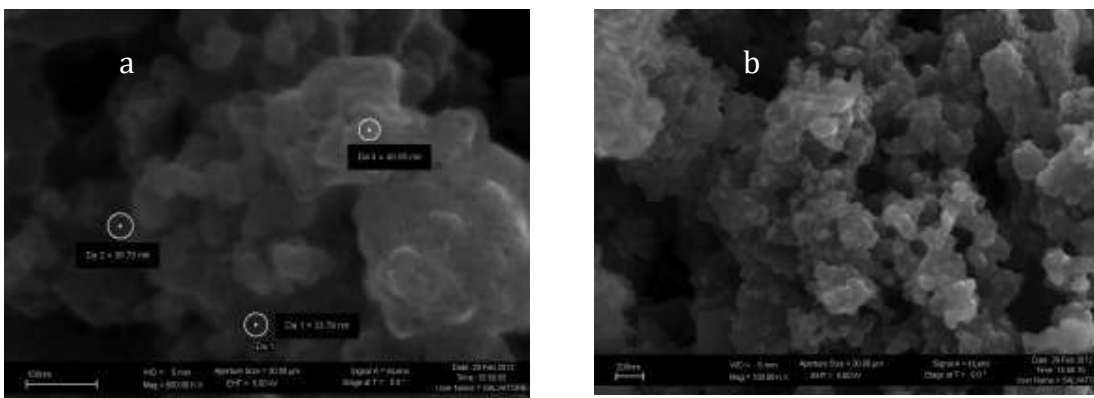
Figure 4.18 (a) & (b): FESEM IMAGE of MPTS-VCB

Sample	ζ (mV)	Surface Area (BET) m²/g
Pristine-VCB	-9.5	70
MPTS-VCB	-36.5	126

Table 4.4: Properties of Pristine- & MPTS-VCB through different Techniques

Another interesting remark on the particle comes from DLS measurements (in water) is that: after modification, there is a strong decrease in Zeta potential value ζ indicating effective change on the surface of the MPTS-VCB (Table 4.4). This highly negative value, which depends on the functional groups at the surface, can be interpreted in relationship with the ESCA data of Table 4.3 (which showed higher amount of oxygen at the very surface than in the deeper layer probed by EDX) as represented in scheme 1. Hydrolysable oxygenated silanol groups originated by the hydrolysis of MPTS, and thiol groups present in the MPTS structure can contribute to the surface potential of the particles.

Thermal gravimetric analysis on the reaction products, MPTS-VCB, and on the starting material, Pristine-VCB, went through the same thermal treatment (from 25 to 1600°C with temperature ramp rate of 10°C/min). Results of TGA analysis are shown in Figure 4.19.

We can identify two regions: (i) T < 500 °C (ii) T > 500 °C (on the thermogram a line

55

indicates the two regions). In the first region, while pristine-VCB does not show weight loss, MPTS-VCB has a significant weight loss. We attribute this behavior to the effect of increased surface area and increase amount of oxygen, incorporated during the modification by MPTS. Over 500°C, while pristine-VCB completely degrades at 700 °C leaving a residue of about 5%, CB treated with MPTS shows a much slower degradation pace. This confirms the presence of silica structures protecting CB from combustion; literature also reports that carbon sulfur compounds that can't be removed until 450°C and later are covalently bonded stable complex carbon sulfur surface compounds [8]. TGA residual at T=1600°C of MPTS-VCB samples were analyzed by elemental analyzer. Sulfur and silicon contents of 2.3 wt.% and 50 wt% respectively were found.
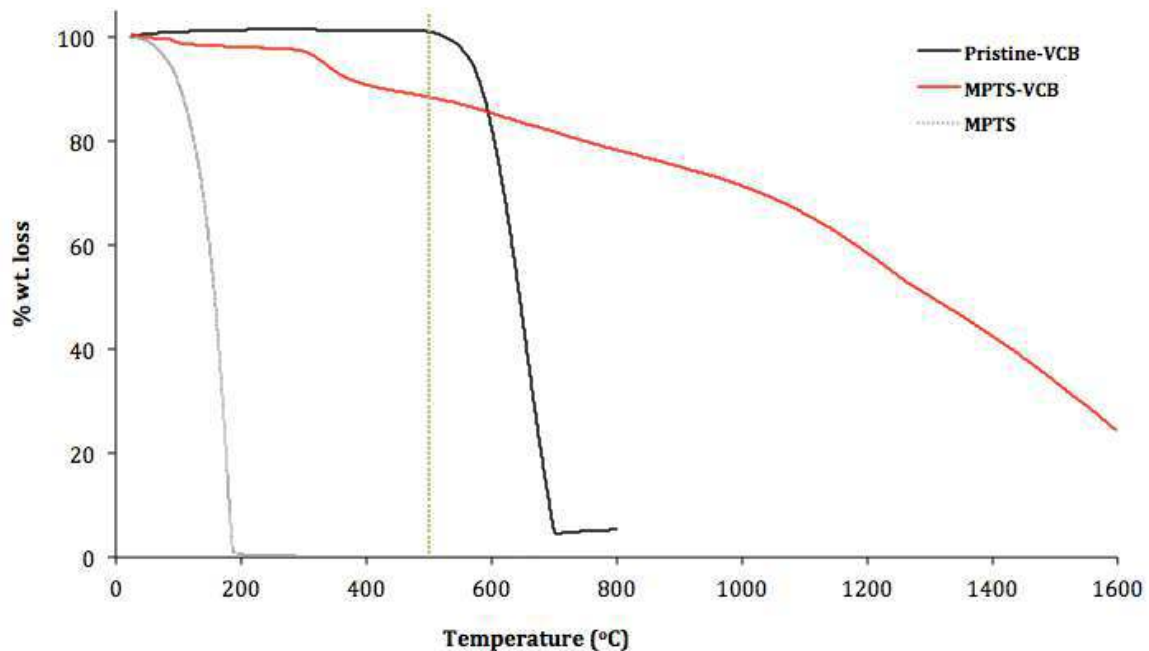
Figure 4.19: TGA of Pristine-VCB, MPTS and MPTS-VCB.

The modification deeply changes the surface of the particles, as indicated by different spectroscopic analyses, the values of zeta potential and the morphological

analyses. The modification makes MPTS-VCB easily dispersible in a variety of solvents. as one can appreciate in Figure 4.20 where it is compared with pristine-VCB. A comparison with a CB modified by a conventional method reported in the literature [117] was also performed. VCB-Oxi is a sample that was subjected to a strong oxidation: after treatment with nitric acid its zeta potential was around -47 mV. The photograph shows the dispersions after 30 minute from preparation during which they were left to stand at room temperature. While pristine-VCB is not dispersible, MPTS-VCB was found to be dispersible in all solvents. VCB-Oxi was efficiently dispersed in polar solvents such as water and propylene carbonate. It is evident that the systems containing MPTS-VCB are much more versatile than those based on Pristine-VCB or VCB-Oxi. MPTS-VCB is universally dispersible in polar and nonpolar solvents; only in water and propylene carbonate VCB-Oxi and MPTS-VCB have similar behavior.
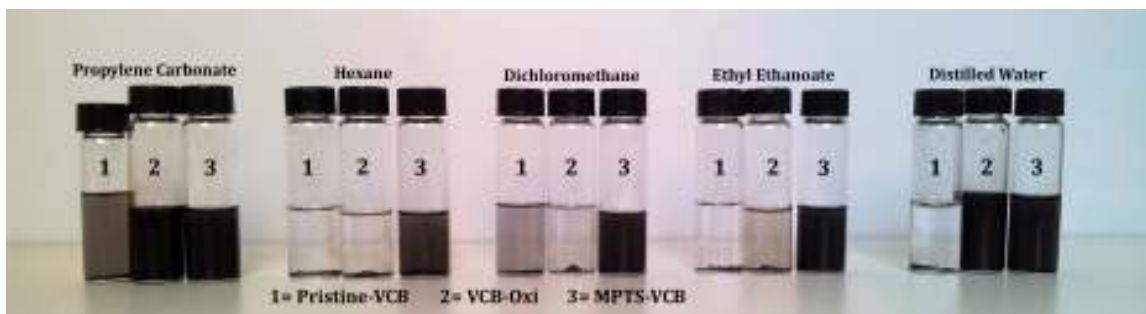
Figure 4.20: Pristine-VCB, VCB-Oxi & MPTS-VCB dispersion (10mg/5mL) in different solvents

Astounding dispersion of MPTS-VCB has been observed also in epoxy monomer. In this case shaking was done manually over 5 seconds, the resulting dispersions as they appear just after preparation (Figure 4.21 a) and after 48 hours (Figure 4.21 b) are compared with VCB-Oxi and Pristine-VCB. Over longer times, it is evident that

the dispersion with pristine-VCB is unstable; also VCB-Oxi after 48 h starts settling. The stability can be a consequence of the high surface potential and larger surface area of the MPTS-VCB.
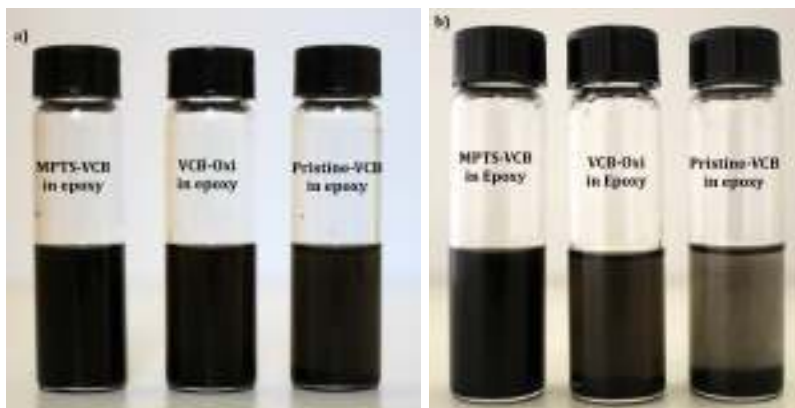
Figure 4.21: Dispersion of 1wt% Pristine-VCB, VCB-Oxi & MPTS-VCB in Epoxy
(a) Immediately after preparation (b) after 48 hours.

4.2 Ultraviolet Thiolation of CB

In this part of dissertation, photochemical Thiolation of CB has been demonstrated, that produces covalent attachment of thiol moiety onto CB surface. This part contains some unique photochemical approaches for CB surface functionalization.

For scheme 1, UV radiation was implemented to cause surface modification while all the ingredients were available together, where as for scheme 2; PI was irradiated for a specific time period and was mixed into CB & modifier mixture. For scheme 3; PI was irradiated while being added into the mixture of CB & modifier.

Results obtained from scheme 1 samples are discussed below.

Figure 4.22 is FTIR spectra of Pristine and modified Glassy CB, along with MPTS spectra as reference. For MPTS spectrum, 2920 and 2850 cm^{-1} peaks represent methylene groups, while 820 cm^{-1} peak represents methyl group in Si-OCH$_3$. The 1191 and 1089 cm^{-1} peaks are assigned to Si-O. An unambiguous peak for S-H is

found at 2550 cm^{-1}.

Modified CB shows bunch of peaks below 1700cm^{-1} (due to oxygen containing functional groups); along with that, it shows peaks at 2800-2960 cm^{-1} (representing methylene groups) and 3400-3700 cm^{-1} (hydroxyl groups). Reaction was estimated by consumption of thiol groups (peak in MPTS at 2550 cm^{-1} disappeared) and formation of thio-ether bond (peak in MPTS-Glassy CB arrived at 550 cm^{-1}). Methoxy peak is also absent in modified sample, which is assumed to be converted in hydroxyl groups; Raman spectra (Figure 4.24) confirms the assumption by showing a peak at 3475 cm^{-1}, due to hydroxyl groups.
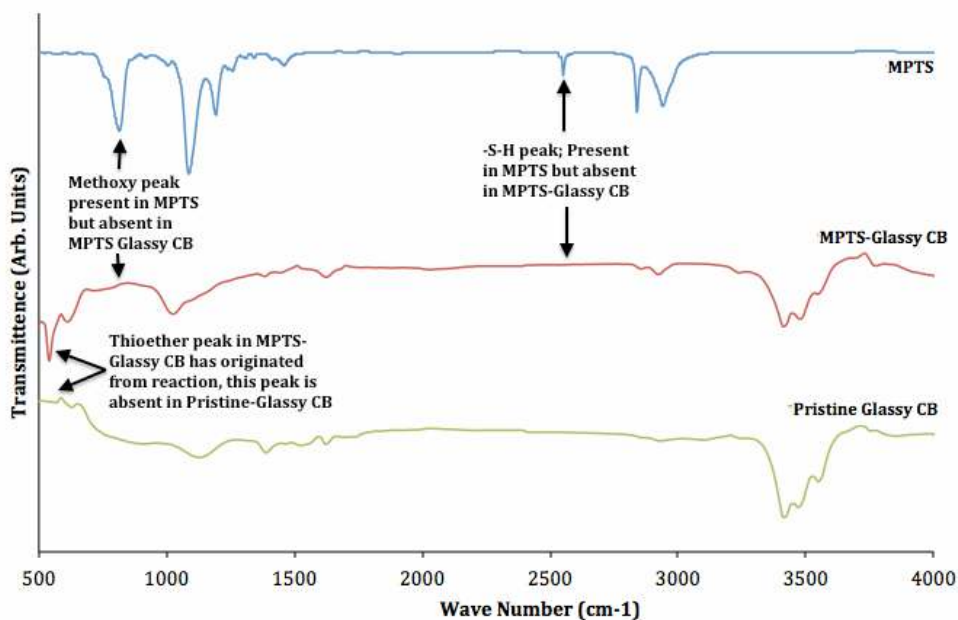
Figure 4.22: FTIR spectra of Pristine-Glassy CB, MPTS and MPTS-Glassy CB

Figure 4.23 contains XPS survey spectra of CB before and after functionalization, named respectively as Pristine-Glassy CB and MPTS-Glassy CB. Along with common peaks of C1s (284.8 eV) and O1s (532 eV): the peaks at 100 and 150 eV (due to Si2p and Si2s respectively) and at 164 and 229 eV (assigned to S2p and S2s) are present

only in modified sample. Therefore spectra indicate clearly the presence of sulfur and silicon after modification.
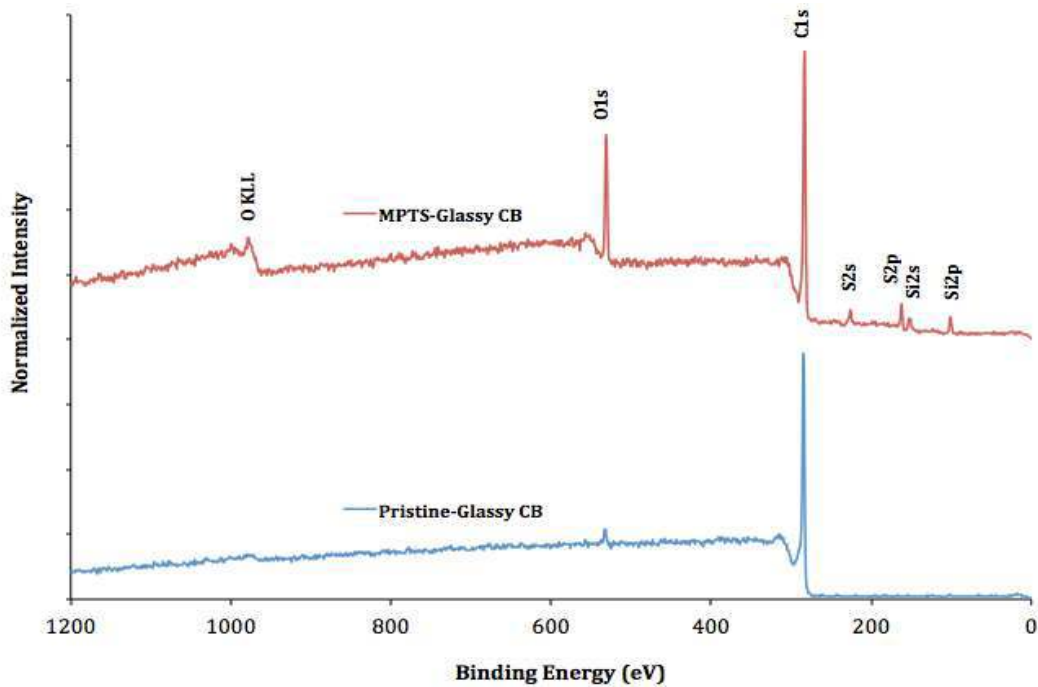
Figure 4.23: XPS spectra of Pristine-Glassy CB and MPTS-Glassy CB

Raman spectrum of modified sample "MPTS-Glassy CB" (Figure 4.24) displays a slight increase in G and G' peaks with reference to D peak; which indicates a disorder decrease in material after functionalization. A new peak, at 3475 cm^{-1}, has appeared in the spectra of functionalized sample, which represents hydroxyl groups[118]. Diminutive signals of surface modifications are reasonable if we think that glassy CB balls are over 10 micrometers in diameter; functionalization alters only surface and Raman is a bulk technique.
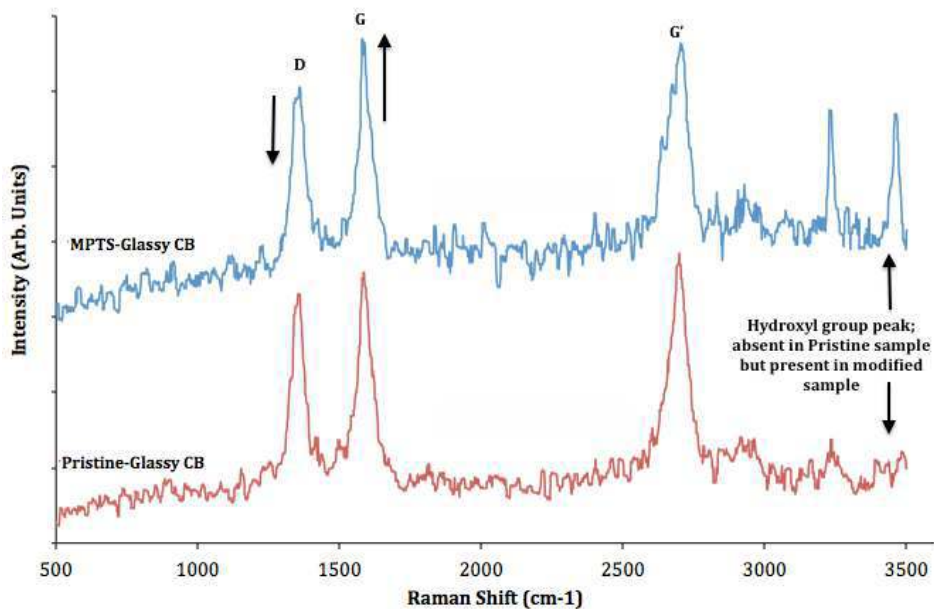
Figure 4.24: Raman spectra of Pristine-Glassy CB and MPTS-Glassy CB

FESEM images of Pristine- Glassy CB and MPTS-Glassy CB are presented in figure 4.25(a & b) and 4.26(a & b) respectively. Images indicate that glassy CB shells are modified after functionalization treatment. Focusing on the brightness of CB surface, concerning electrical properties, an increase in dark regions, after functionalization, has been widely observed. Moreover, the lower figures show that the surface of the magnified CB after functionalization is rougher. So, we might hypothesize that the functionalization brings about a large-scale alteration of the CB surface.
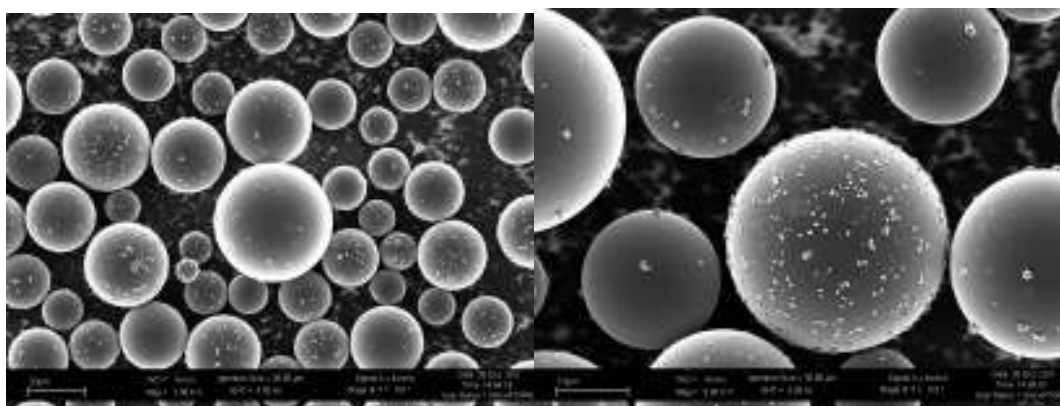
Figure 4.25 (a) and (b): FESEM images of Pristine-Glassy CB
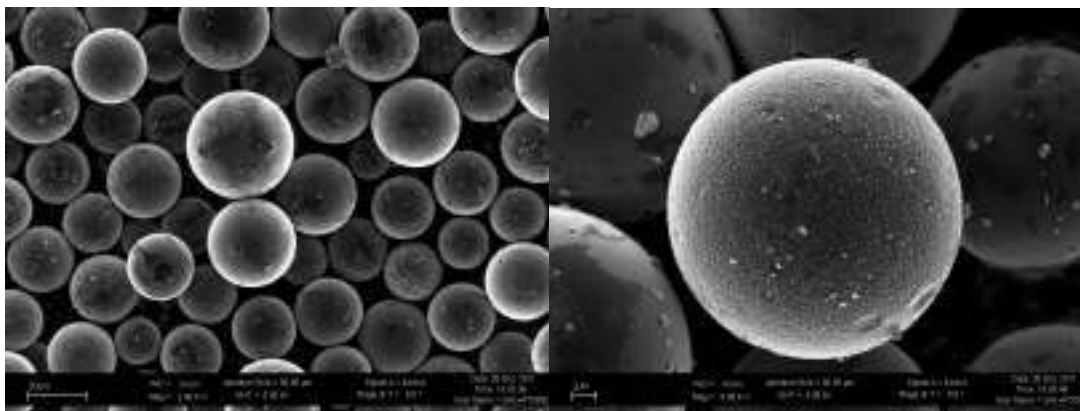
Figure 4.26 (a) and (b): FESEM images of MPTS-Glassy CB

Thermal gravimetric analysis, of Pristine and modified glassy CB, followed same thermal treatment (from 25 to 800°C with temperature ramp rate of 10°C/min). Results of TGA analysis are shown in Figure 4.27. TGA of starting material Pristine-glassy CB shows thermal stability till almost 700°C and afterwards it starts decomposing. On the contrary modified sample MPTS-glassy CB shows slight degradation at around 250°C and afterwards it shows thermal stability till 800°C. Modified sample's degradation at 250°C can be justified by the effect of increased surface area (due to surface roughness) and increase amount of oxygen (incorporated during the modification by MPTS).
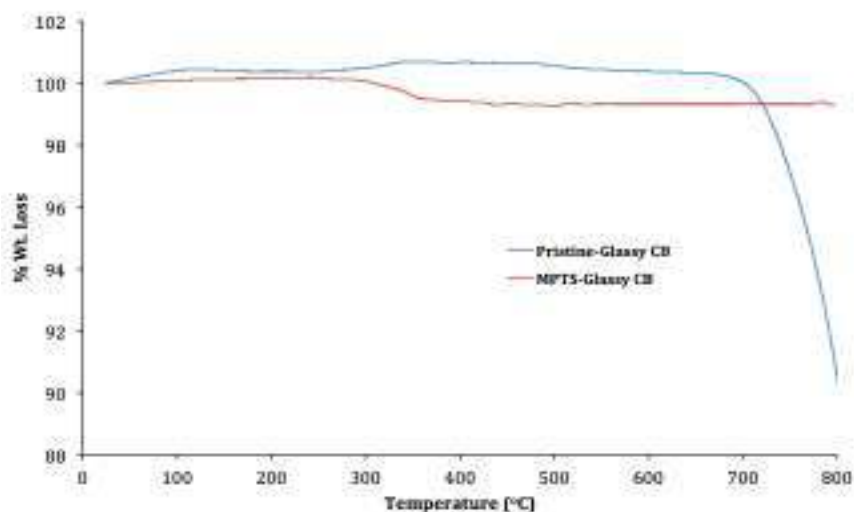
Figure 4.27: TGA of Pristine- and MPTS-Glassy CB

At the same time of sample preparation through scheme 1, miscellaneous aspects were studied on samples, including: effect of irradiation time and thermal treatment during UV modification. Under scheme 1, increase in irradiation time was not considerably effective to modify Glassy CB, even if it was raised from 60 Sec to 600 Sec. Reason is obvious that CB masks PI to block UV radiation, so time factor in this case becomes impractical. On the contrary thermal treatment, in scheme 1, has initiated a noticeable effect, in modified samples.

MPTS-Glassy CB sample was re-performed but at raised temperature, i.e. 50°C and was named as MPTS-T-Glassy CB. It was found to have 3 folds higher sulfur contents than the sample prepared at room temperature. Table 4.5 contains XPS and EDX data of starting material (Pristine-Glassy CB) and modified samples; one prepared at room temperature (MPTS-Glassy CB) other with thermal treatment (MPTS-T-Glassy CB). XPS and EDX data is not in accordance with each other; reason of this disagreement in data, as explained earlier, is due to the structure of Glassy CB and lopsided competencies of both instruments to analyze same thickness of Glassy CB balls. Hence as a conclusion, as per XPS data, thermal treatment was found effective during UV modification. But this thermal treatment has generated another situation, which was observed through FESEM.

Technique	Sample	C[%]	O[%]	S[%]	Si[%]
XPS Analysis	Pristine-Glassy CB	96.4	3.6	0.0	0.0
	MPTS-Glassy CB	78.9	15.2	2.5	3.3
	MPTS-T-Glassy CB	59.5	22.7	7.1	10.8
EDX Analysis	Pristine-Glassy CB	100.0	0.0	0.0	0.0
	MPTS-Glassy CB	99.8	0.0	0.1	0.1
	MPTS-T-Glassy CB	99.9	0.0	0.0	0.1

Table 4.5: XPS and EDX data of Pristine and modified Glassy CB

FESEM images of "MPTS-T-Glassy CB" present a thin layer of modifier on the surface of CB balls. Images of starting material (Pristine-Glassy CB) and modified sample (MPTS-T-Glassy CB) are presented in Figure 4.28 (a & b).

a)
b)
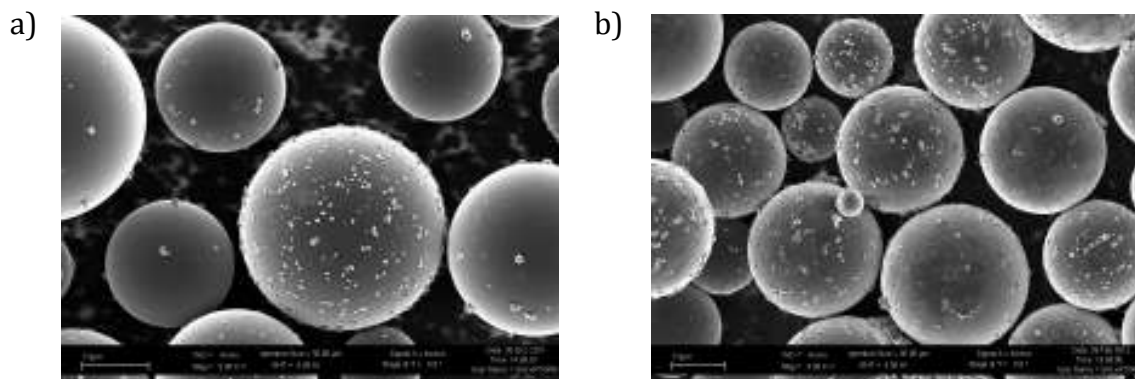
Figure 4.28: SEM images of (a) Pristine-Glassy CB (b) MPTS-T-Glassy CB

Accompanied by thin covering on CB surface, some bulge like structures were also observed (Figure 4.29). These bulge like structures looked like modifier deposition due to raised temperature. High temperature treatment converted methoxy groups into hydroxyl groups; evidenced from Raman spectrum (figure 4.30) that presents a sharp peak at 3475 cm^{-1}, assigned to OH stretching vibrations; which was absent in Pristine sample [118].
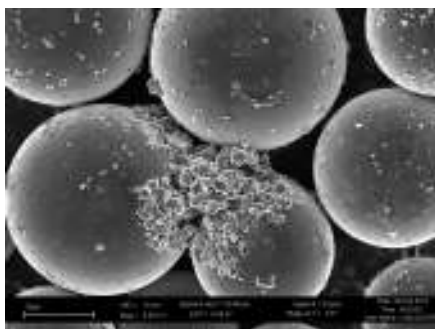
Figure 4.29: SEM image MPTS-T-Glassy CB

Raman spectra of Pristine and modified samples are presented in Figure 4.30. Upon comparison amongst modified samples, one prepared at room temperature (MPTS-Glassy CB) shows a decrease in disorder evidenced by increase in G peak; in contrast

the sample prepared with thermal treatment (MPTS-T-Glassy CB) shows increase in disorder evidenced by decrease in G peak. Moreover the later shows an intense Raman shift peak at 3475 cm^{-1} representing conversion of methoxy groups of modifier molecule into hydroxyl groups. Sample prepared at room temperature shows same peak but relatively less intense.
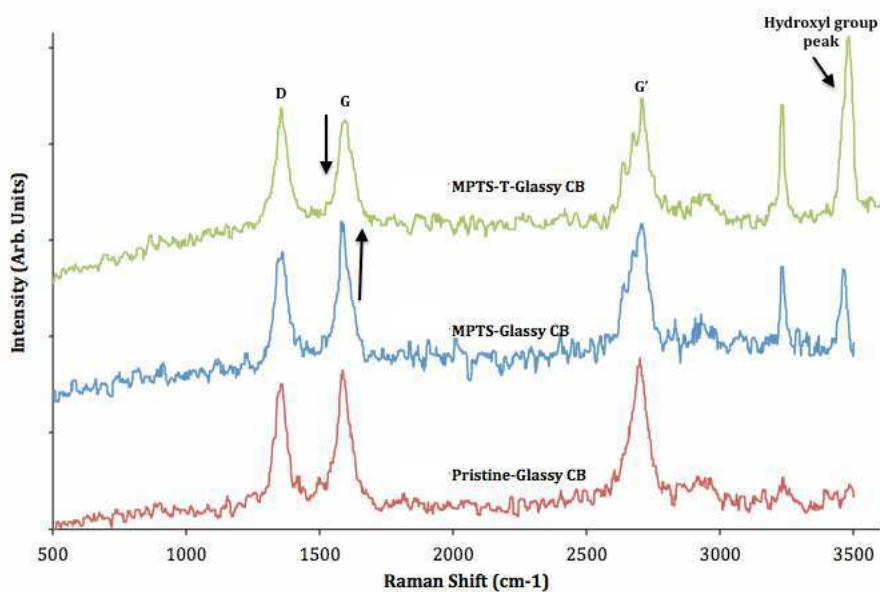
Figure 4.30: Raman Spectra of Pristine and modified Glassy CB

Scheme 1 entertained a major drawback; it did not work satisfactory for huge CB samples. Since CB, due to its higher concentration tints the sample strongly, forbidding PI to absorb sufficient UV radiation. This drawback bred the need of an alternative approach. So scheme 2 was designed to increase photon availability to PI so that massive amounts of pristine-CB could be modified through UV radiations. Samples prepared through scheme 2 are discussed below:

Starting material for scheme 2 was Glassy CB-Oxi, (described in section 3.1.1.2.1). Glassy CB-Oxi was reacted photochemically with thiol containing alkoxysilane, for

different time intervals to see the effect of irradiation time variation, as PI for the said technique was irradiated separately.

FTIR spectra of Glassy CB-Oxi and UV treated CB (m-60, m-120, m-180), along with MPTS spectrum (for reference), are plotted in Figure 4.31. MPTS spectrum shows peaks at 2920 and 2850 cm^{-1} that characterize methylene groups, while 820 cm^{-1} peak represents methyl group in Si-OCH$_3$. The 1191 and 1089 cm^{-1} peaks are assigned to Si-O. An unambiguous peak for S-H is found at 2550 cm^{-1}.

Spectrum of Glassy CB-Oxi, prior UV treatment, portrays compound peaks at 1600-1680 cm^{-1} and 3225-3699 cm^{-1}, originated from oxygen containing groups (carbonyl and hydroxyl respectively) and a strong peak at 600 cm^{-1} [108]. Upon photochemical treatment, these peaks have reduced intensity. This gradual reduction in peak size, from m-60 to m-180, can be inversely related to increase in treatment time. Absence of 820 cm^{-1} peak suggests methoxy group consumption; Raman spectra of samples do not show any hydroxyl peak, like other photochemical Glassy CB samples; this situation suggests a possibility of condensation reaction between MPTS and Glassy CB-Oxi. Tiny peaks at 2920 and 2850cm^{-1} indicate methylene groups coming from MPTS. Consumption of thiol groups consequently resulting in thio-ether bond formation are evidenced, respectively by vanishing of 2550 cm^{-1} peak and arrival of 550 cm^{-1} peak.
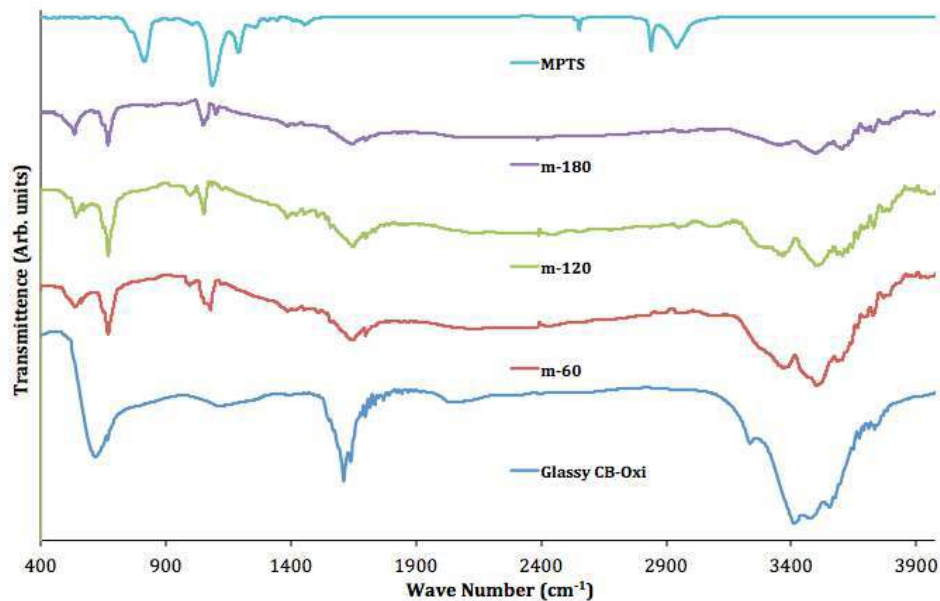
Figure 4.31: FTIR spectra of Pristine & modified Glassy CB-Oxi and MPTS (0.05-0.1 wt% in KBr)

XPS survey scan spectra of Glassy CB-Oxi and modified samples are presented in figure 4.32. Significant modification is observable from peaks of sulfur (164 and 229 eV) and silicon (100 and 150 eV).
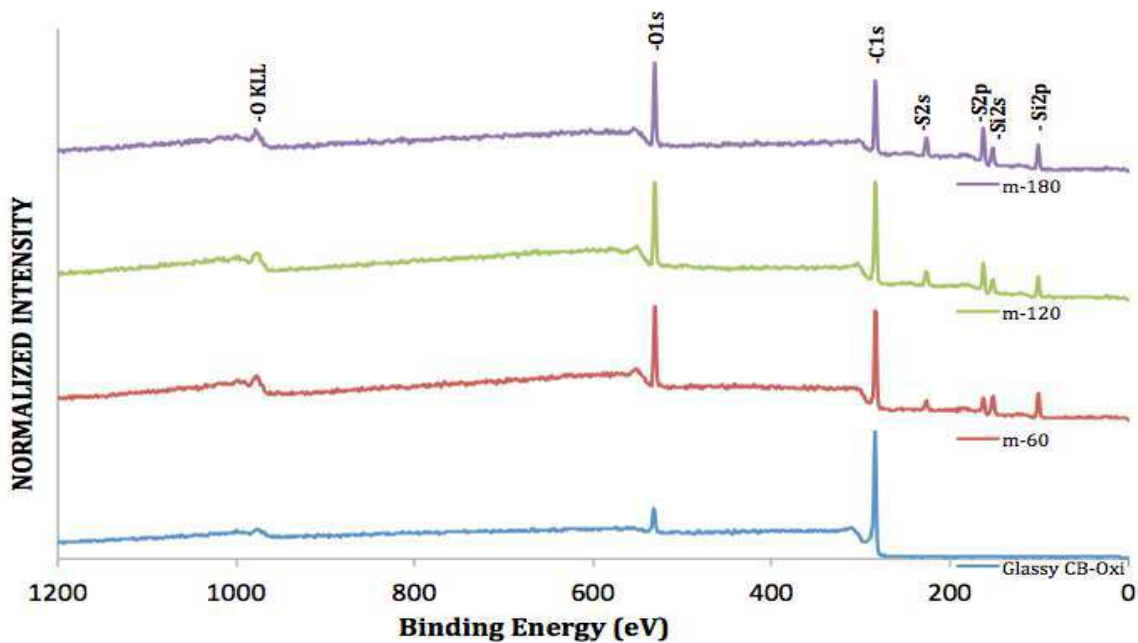
Figure 4.32: XPS Survey scan spectra of Glassy CB-Oxi and modified samples

Sulfur signals of modified samples have been deconvoluted for detailed information on different forms of fixed element. Figure 4.33 displays high-resolution fitted spectra of sulfur (S2p) recorded on modified glassy CB samples.

a)

b)

c)

d)
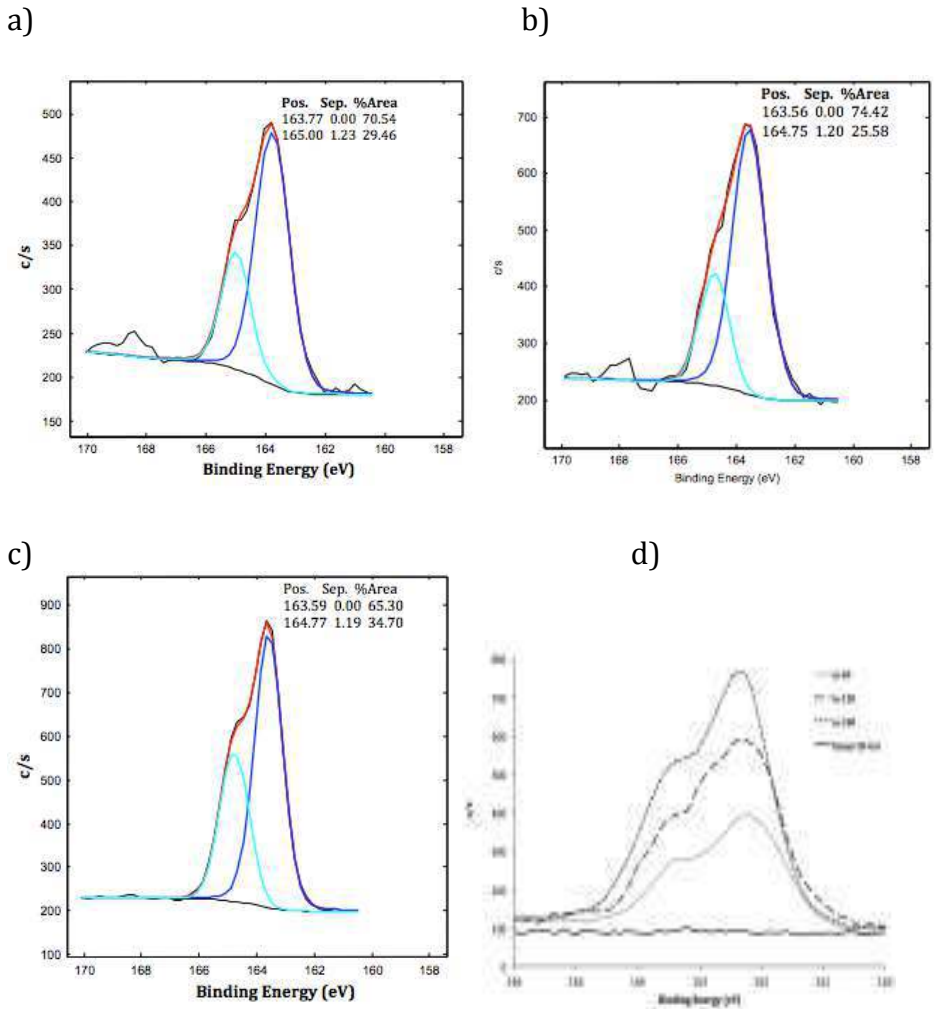
Figure 4.33: XPS HR spectra S2p of (a)m-60, (b)m-120 and (c)m-180; (d) Comparative analysis of S2p peak of Glassy CB-Oxi and modified samples

Figures 4.33(a), (b) & (c) clearly indicate two main components, at 163.8 ± 0.1 eV and 164.9 ± 0.2 eV. Where the first component represents sulfur covalently linked to C atoms at the border of aromatic structures [8], and second component represents sulfur compounds like C-S-C [112]. Figure 4.33 (d) contains XPS sulfur peak of modified samples (m-60, m-120, m-180) comparatively analyzed with each other as

well as with starting material (Glassy CB-Oxi). Comparative study indicates a gradual increase in both components of XPS sulfur peak, keeping their ratio almost constant (70% : 30%).
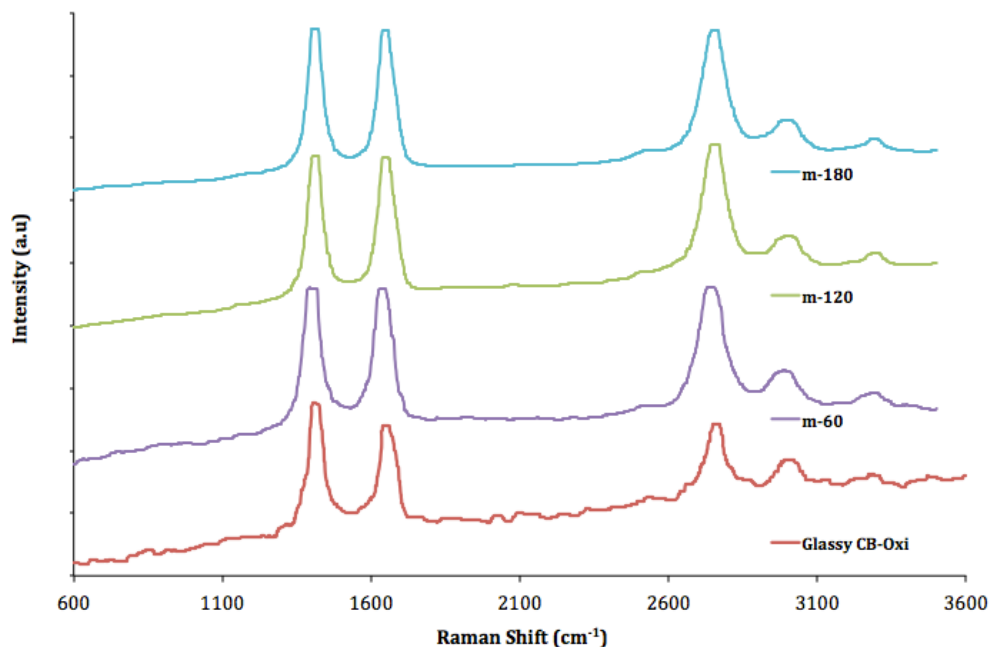
Figure 4.34: Raman spectra of Glassy CB-Oxi and modified samples

From Raman spectra of modified samples (Figure 4.34) an intensification of G and G' peaks is distinctly noticeable, which indicates a decrease in disorder after treatment with respect to the starting material "Glassy CB-Oxi".

FESEM images of starting material (Glassy CB-Oxi) and modified samples (m-60, m-120, m-180) are presented in figure 4.35. Starting material has apparently noticeable rough surface (Figure 4.35(a)). On the contrary, surfaces of all modified samples are smooth due to the covering of modifier layer. (Figure 4.35(b) (c) (d))

a

b

c

d
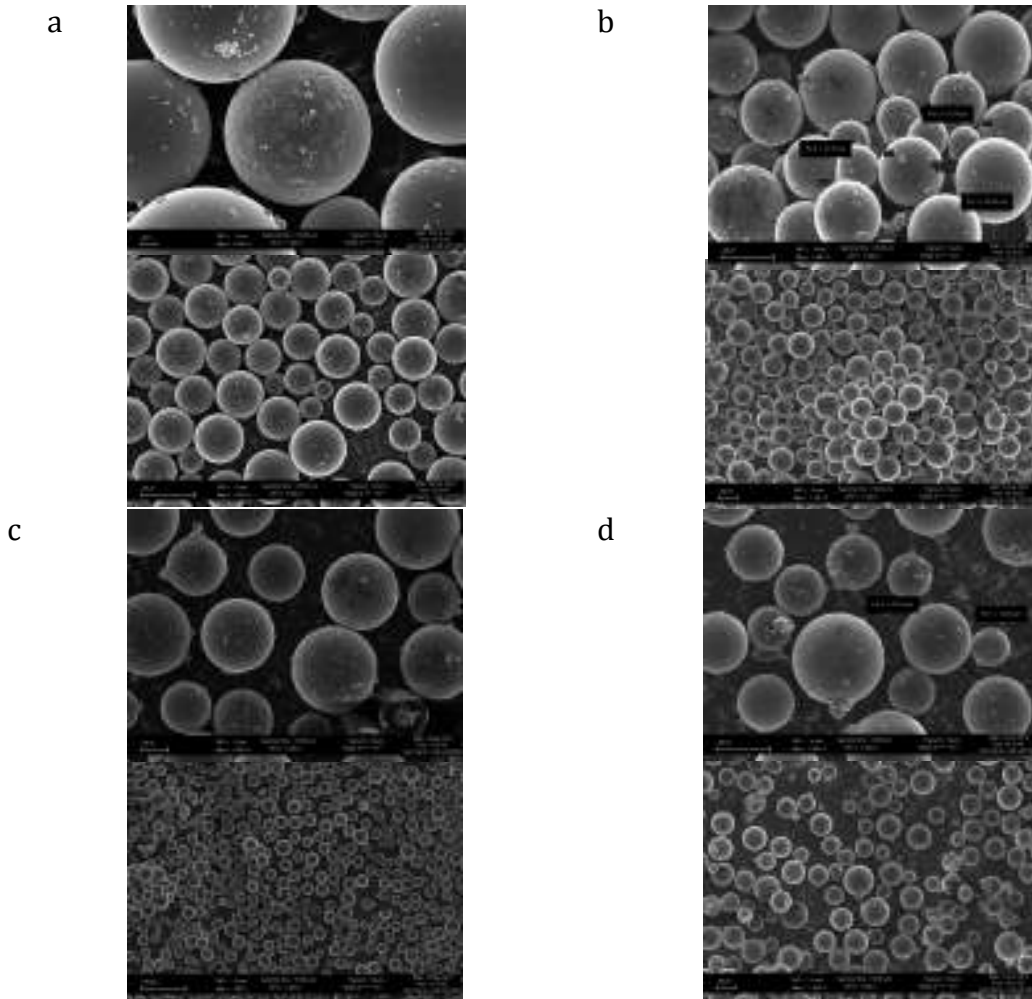
Figure 4.35: FESEM Images (a)Glassy CB-Oxi, (b)m-60, (c)m-120, (c)m-180

Figure 4.36 shows a FESEM image of modified sample m-180. A clearly visible thin

coating of modifier material on CB surface is present. The layer on the surface is

damaged from some points that can be attributed to abrasive movements of ball like

structures.
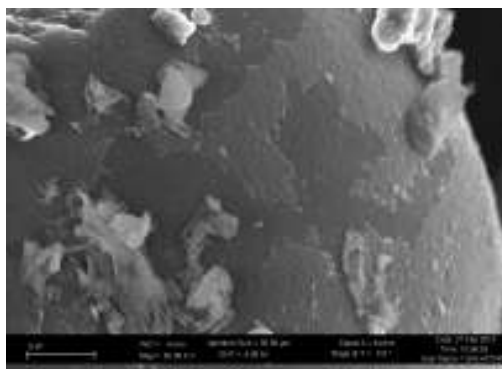
Figure 4.36: FESEM Image of m-180

Figure 4.37 contains TGA curves of starting material (Glassy CB-Oxi) and modified samples. Pristine-Glassy CB has also been plotted as reference. All the samples were thermally treated alike, from 25 to 800°C with temperature ramp rate of 10°C/min. Starting material (Glassy CB-Oxi) shows rapid weight loss, due to the oxidized functional groups on its surface that support its thermal decay. In comparison, modified samples have shown better thermal stability, even better than Pristine-Glassy CB (Commercial product). This better thermal stability suggests that modification process has created a significant change in CB structure.
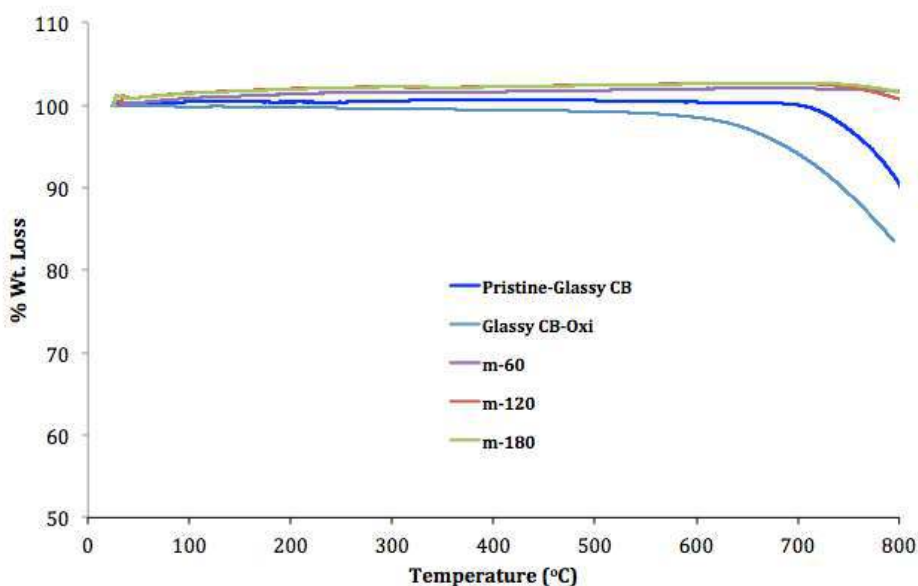
Figure 4.37: TGA of Glassy CB-Oxi, Pristine and modified Glassy CB samples

Procedure of sample m-120, with same conditions, was repeated with Pristine-VCB instead of Glassy CB-Oxi, and sample was named as V-120. Efficacy of procedure was analyzed for these samples, as of the dissimilarity in starting materials. XPS analysis showed that sulfur incorporation reduced from 5.8% (m-120) to 2.2% (V-120). XPS survey scan spectra are presented in Figure 4.38.
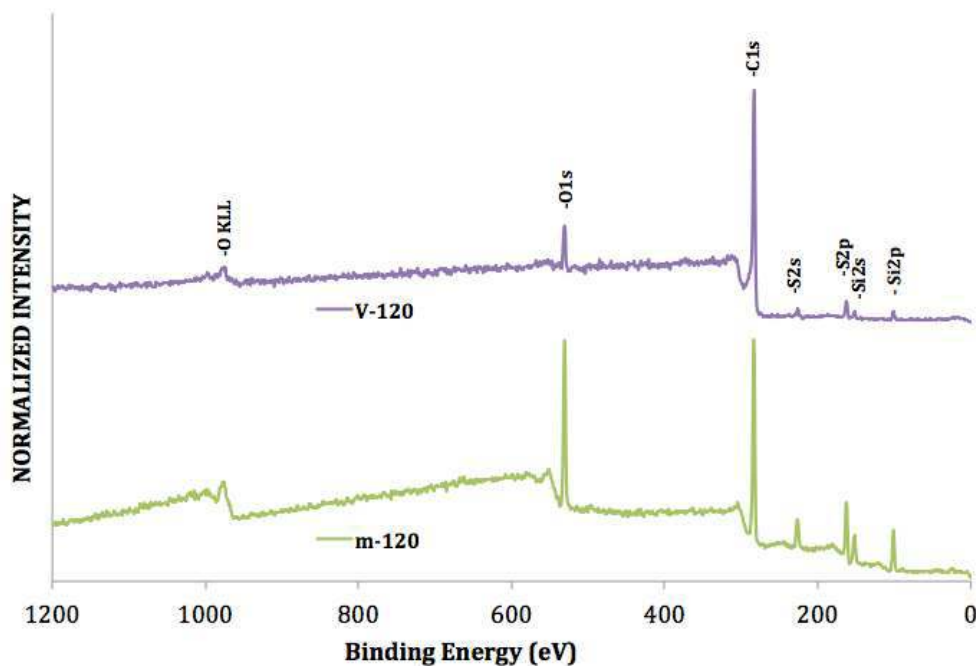
Figure 4.38: XPS survey scan spectra of m-120 and V-120

Oxygen contents were almost same in both starting materials, but differ a lot in modified samples (values in Table 4.6). Since modifier molecule MPTS carries 3 oxygen atoms inside its structure, so increase in sulfur should be accompanied by increase in oxygen. Increase in oxygen contents of modified sample m-120 confirms effective sulfur incorporation on its surface in comparison to V-120. Hence we can assume that configuration of CB particles play important role in photochemical modification.

Technique	Sample	C[%]	O[%]	S[%]	Si[%]
XPS Analysis	Glassy CB-Oxi	91.7	8.3	0.0	0.0
	m-120	62.4	22.4	5.8	9.4
	Pristine-VCB	93.1	6.9	0.0	0.0
	V-120	87.4	8.0	2.2	2.4

Table 4.6: XPS data of m-120 and V-120

Utilizing VCB, sets of experiments were conducted under scheme 2, to verify the effect of solvent on UV modification. XPS analysis for sulfur contents of these samples showed almost same effect of different solvents used (Figure 4.39; Table 4.7).
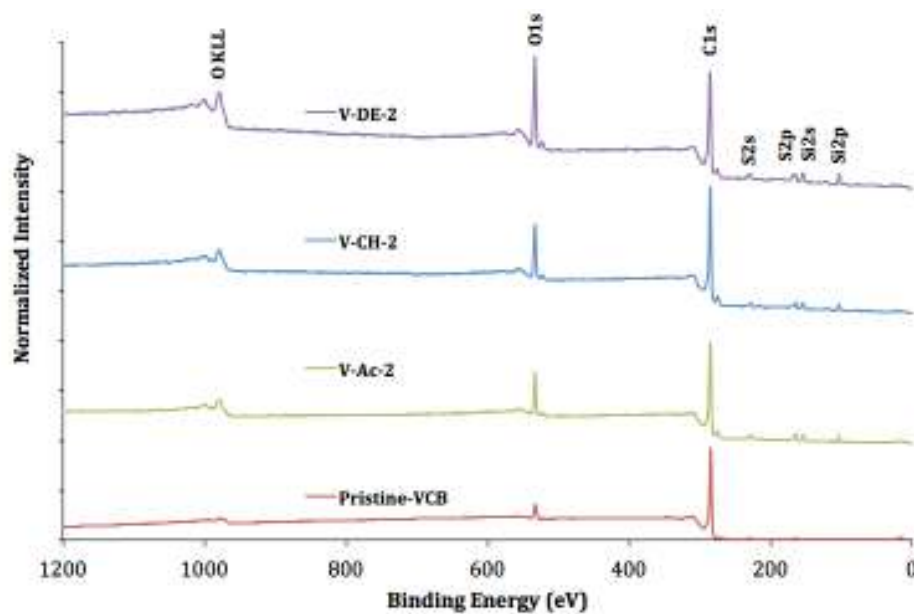
Figure 4.39: XPS survey scan spectra of Pristine and modified VCB samples prepared in different solvents.

Technique	Sample	C[%]	O[%]	S[%]	Si[%]
XPS Analysis	Pristine-VCB	93.1	6.9	0.0	0.0
	V-Ac-2	77.4	11.9	4.9	5.8
	V-CH-2	76.1	13.2	4.5	6.2
	V-DE-2	67.9	20.8	4.7	6.6

Table 4.7: XPS data of Pristine and modified –VCB, with different solvents.

For sulfur incorporation, same tendency has been observed for different solvents used, however oxygen contents of modified samples has shown quite different scenario. Cyclohexane (V-CH-2) and Acetone (V-Ac-2) samples have shown almost double oxygen contents to that of Silicon contents, but an increase have been observed in oxygen contents of sample with Diethylether solvent. Hence different solvents result in equal incorporation of sulfur on CB but they play important role in altering the oxygen contents.

An alternative approach (scheme 3) was exploited not only to increase the efficacy of UV modification but also to minimize energy dissipation during the modification. Actually scheme 3 was an effort to improve scheme 2, with similar tactic to irradiate PI without CB. Till now results are not as per consideration. Reason might be the extended time period of irradiating PI in open air. Each drop of PI was kept hanging from burette's tip for a few seconds, in front of UV source for ample irradiation.

PART-II: UV-cured Epoxy Composites

This part of dissertation contains data and discussion about UV-cured Epoxy composites. Samples were prepared in thin films of micron sized dimensions with a variety of fillers to investigate their effect on epoxy polymerization kinetics; apart from that, samples with thickness in centimeters have also been prepared with different pigments / fillers in diverse weight percentages, through different photo-curing techniques. These techniques were comparatively analyzed for their efficiency to photo-polymerize the composites.

4.1 Thin Layer Composites

Epoxy composites were prepared in thin layers of micron dimensions. Initial experiments were conducted, on pristine epoxy, to check tentative tack free time with different PI concentrations. 1mol% of PI was found best to cure epoxy film of 100μm thickness while irradiation intensity was 33mW/cm^2 and irradiation time was 90 sec. In second phase, CB-Epoxy composites were prepared with both types of commercial CBs in different wt.% i.e. 1%, 3% 5% and 10%. These composite samples were kinetically studied through RT-FTIR. Figures 4.40 (a, b & c) show kinetic study of different wt.% of CB-Epoxy composites (irradiation intensity 33mW/cm^2, irradiation time 300sec). Comparative study has revealed following trends quite observable:

1) Composites with filler particles (CB) show speedy polymerization and higher conversion than Pristine-epoxy. In fact CB particles augment epoxy conversion because of hydroxyl functionalities at their surface. Pristine epoxy obeys Activated Chain End (ACE) mechanism, where each monomer leaves an activated end for next monomer to attack. While CB–Epoxy composites follows an additional conversion mechanism, i.e. Activated Monomer (AM) mechanism, where hydroxyl groups on the surface of CB also help to initiate epoxy polymerization.

2) Composites with Pristine-VCB show elevated polymerization kinetics than composites with Glassy CB. The reason is that VCB disperses well in epoxy due to its smaller particle size and higher surface area. Better dispersion

allows sufficient room for the epoxy to polymerize more over surface functionalities also boost up the reaction.

3) Composites with higher wt.% of filler (CB) show reduced polymerization kinetics. The reason could be; overcrowding weakens the effect of surface functionalities of filler particles, or reduced dispersion per unit volume.
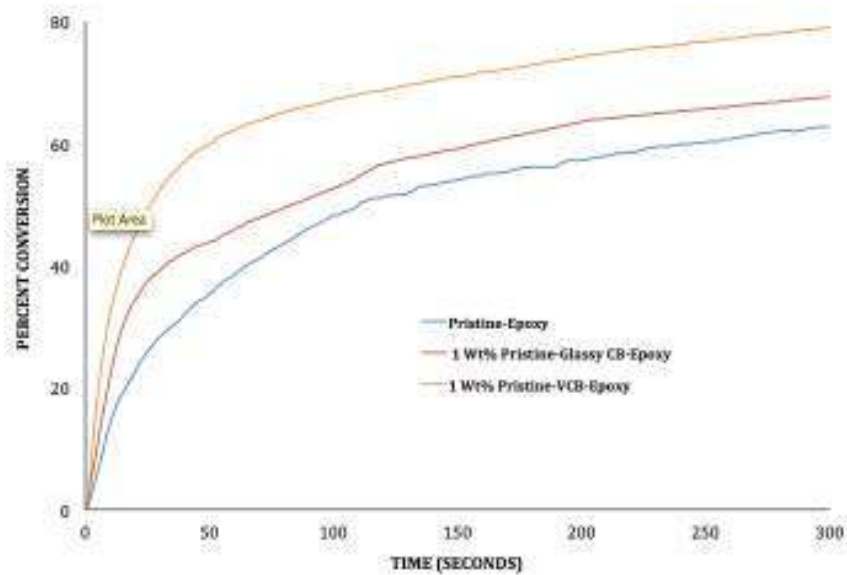
Figure 4.40(a): Effect of 1 wt.% fillers on epoxy polymerization kinetics
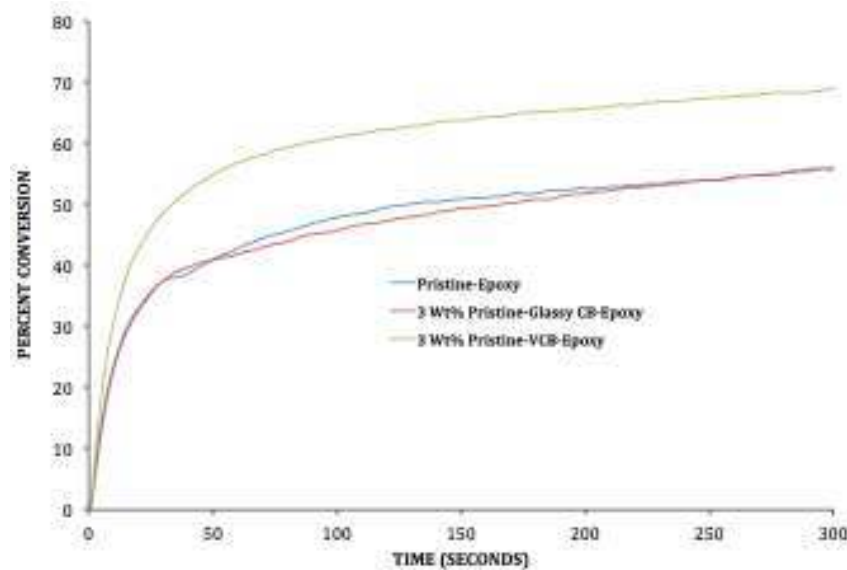
Figure 4.40(b): Effect of 3 wt.% fillers on epoxy polymerization kinetics
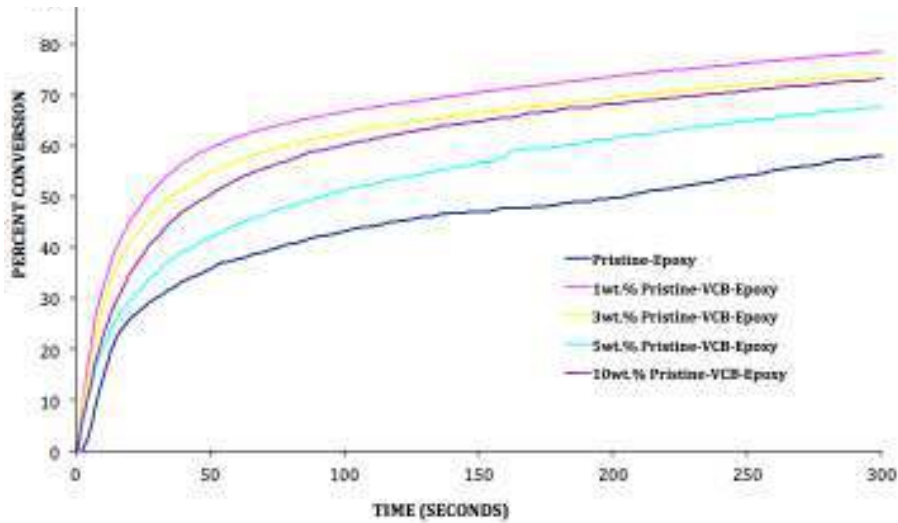
Figure 4.40(c): Effect of 1-10 wt.% fillers on epoxy polymerization kinetics

As per above-mentioned kinetic study of CB-epoxy curing, effect of filler has been found constructive. In this array of experiments modified CB was also checked for its effect on epoxy curing rate. A relative dispersion analysis and kinetic study, between Pristine-VCB and MPTS-VCB was made and it was found that modified sample is not only easy to disperse in epoxy (see Figure 4.21 a & b) but also it helps effectively to photo-polymerize epoxy (Figure 4.41).
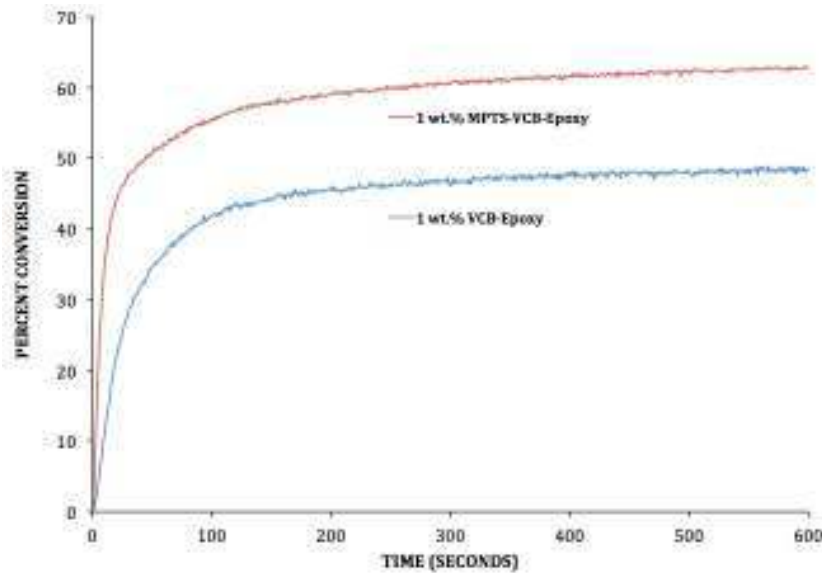
Figure 4.41: Effect of Pristine and modified VCB on epoxy curing

Some other fillers, like Alumina and Silica were also checked for their effect on epoxy curing; pristine- epoxy was taken as standard. For comparative analysis Pristine and MPTS-VCB were also analyzed. All fillers were used in 1wt.% of epoxy. Data is presented in figure 4.42.
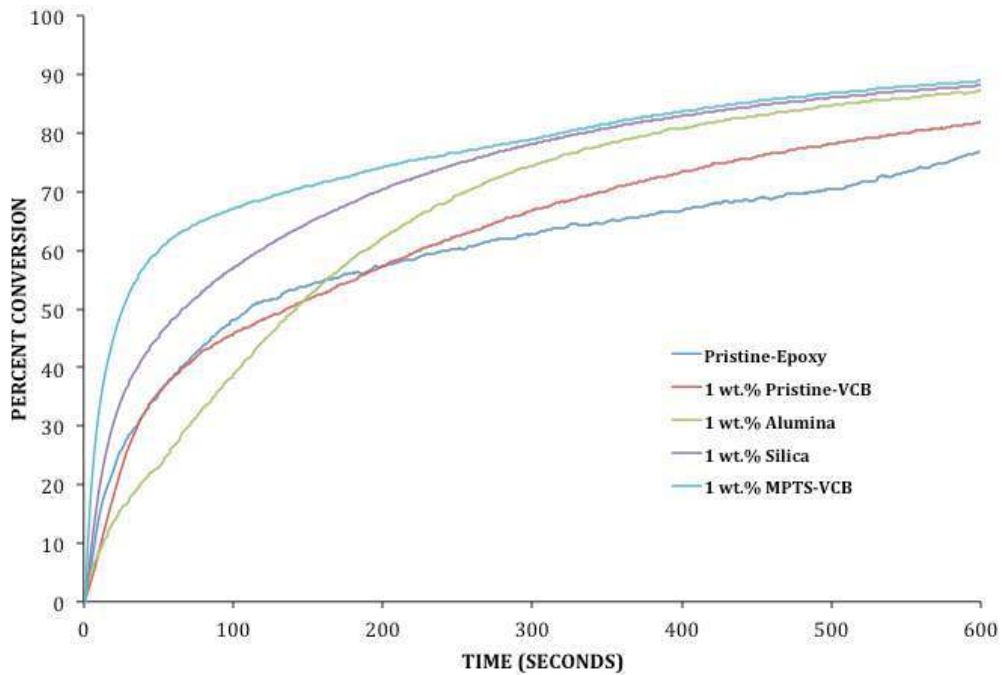
Figure 4.42: Effect of 1wt.% CB and other fillers on epoxy curing

Figure 4.42 specifies evidently that modified sample "MPTS-VCB" shows better kinetics and high percent conversion, in comparison with commercial filers.

CB-epoxy composites were prepared in thin films of 100-microns, on surfaces of different materials, including: Polypropylene sheets, Glass slides and Metal plates. Diverse curing conducts were witnessed (Figure 4.43); composites on Polypropylene sheets were cured easily in short time, while as it composition on metal plate took very long time to cure.
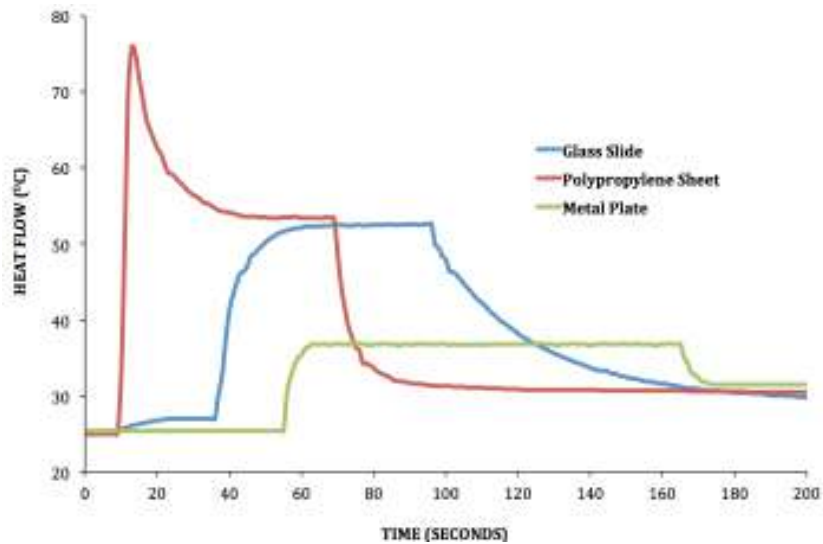
Figure 4.43: Temperature curves of VCB-epoxy composites on different substrates

4.2 Thick Layer Composites

As the UV-curing processes rely on the absorption of radiation passing through the matter, the thickness of the material is usually limited: for this reason nowadays main applications of UV-curing are commonly in the field of varnishes, paints, printing inks, adhesives, printing plates, microcircuits and other devices in the form of thin polymer films. Moreover, curing is also difficult when samples are colored as pigments and dyes compete with the photoinitiator to absorb energy from the light.

In the case of epoxides the mechanism of curing is cationic and the reactive species are long living and active even after switching the light off. Ficek *et. al.,* [119] characterized the diffusion of the cationic active centers in photo-polymerizations of cycloaliphatic epoxides, and demonstrated that the cure can continue for several hours to extend deep below the illuminated surface in unfilled systems. In this work was investigated the cure of epoxides in the presence of carbon black: the propagation rate equation coupled with the active center concentration profiles yielded theoretical cure times for the carbon black nanocomposite coatings. The

79

illumination time determines the number of active centers produced, and therefore available for diffusion and cure. The post-illumination curing time decreases with increasing illumination time, especially at short illumination times. As the coating thickness is increased, the required cure time increases significantly at a given illumination time. For 30 mm thick samples curing time one can estimate is very long, since time calculated, as per model proposed in [119] for 0.8 mm thick samples, is 4 hours. With reference to the previous studies, we tried an alternative method to cure epoxides in 1 mm and 30 mm thickness, containing dyes like carbon black or colorants. The technique consists of irradiating the photoinitiator and then mixing it with the monomer containing the colored additive, while usually the reactive mixtures are prepared first and then irradiated. Initially 1 mm thick samples, obtained by conventional and alternative method (called smart method) were examined; afterwards these two methods were used to prepare thick samples. 1 mm samples obtained by these methods are shown in Figure 4.44 (a & b).

A typical difunctional epoxy monomer, 1,4-butandioldiglycidilether, was used in this study. In the epoxy monomer different fillers were added, i.e. carbon black and organic dyes at a concentration of 1wt.%.

Figure 4.44: 1mm thick colored epoxy samples

For 1 mm thick samples we monitored the degree of curing by turning the sample upside down, every 30 sec, after stopping the irradiation (irradiation time = 90 s): when no flow was observed, the corresponding time was considered the gel time. The values are reported in Table 4.8 to compare the preparation methods.

CONVENTIONAL METHOD		SMART METHOD	
Sample	Gel-Time (min)	Sample	Gel Time (min)
Pristine-Conventional	≅8	Pristine-Smart	6
Black-Conventional	*	Black-Smart	4
Green-Conventional	*	Green-Smart	3
Yellow-Conventional	*	Yellow-Smart	2

Table 4.8: Epoxy composite sample gelation time

* No Gel formation observed within 12 hours, after sample preparation and irradiation

The data show a clear difference in the curing. For conventional method, without filler, gelation time was 8 minutes after interrupting the irradiation; while with the same formulation through the 'smart method' 6 minutes were enough to obtain a solid sample. Striking difference was observed with samples containing the colored additives: through the conventional method, none was gelled within 12 hours from the end of the irradiation where smart method samples were gelled in just 2-4 minutes, i.e. in a shorter time than the neat sample. This decrease in gel time of the colored samples with respect to the neat one is interesting. In the case of carbon black an acceleration of the polymerization kinetics can be related to the presence of acid groups on the filler surface [120]. For the yellow dye, which is an azo compound with OH functionalities [121] a beneficial influence on the kinetics can be related to the OH groups. In the case of the green dye, the reason of a faster gelation is not so clear.

Epoxy bond conversion of 1 mm thick samples is calculated by photo-DSC, DSC, ATR and gel contents. The results are listed in Table 4.9. With the exception of photo-DSC data, results refer to samples obtained by a 90 sec irradiation followed by 12 hours storage.

Sample	CONVENTIONAL				SMART			
	Photo - DSC[0]	DSC	ATR[*]	Gel Content	Photo -DSC[1]	DSC	ATR[*]	Gel Content
Pristine-	80	83	88	88	NA	90	90	100
Black-	38	41	31	39	NA	88	92	100
Green-	52	50	48	48	NA	97	97	100
Yellow-	53	55	51	54	NA	99	99	100

Table 4.9: Conversion values and gel content of the composites with 1wt.% additive.

[0] irradiation time : 15 min, light intensity of 33 mW/cm^2
[1] Photo-DSC analyses were not feasible for the Smart method
[*] ATR conversion data is calculated by using equation [5]

Photo-DSC analysis was feasible only for conventional samples. As expected, they evidenced that reaction conversion is strongly reduced in the presence of a dye like carbon black or other colorant.

DSC data shows that when the conventional method is used conversions are always reduced in the presence of a colorful additive. Accordingly the gel content is fairly low when an additive is present.

In the case of samples prepared by the smart method the curing conversion by DSC, calculated by equation [3.2], is always higher than for the homologous conventional samples. Gel content data confirm the previous results: the values indicate formation of a firm cross-linked network and nonexistence of extractable monomers even in the presence of a colored additive, when the smart method is adopted.

Figure 4.45 shows ATR absorption spectra of monomer (as reference) and cured

composite samples. Epoxy conversion data was calculated through ATR by using equation [3.6] and the results are in agreement with the previous finding.
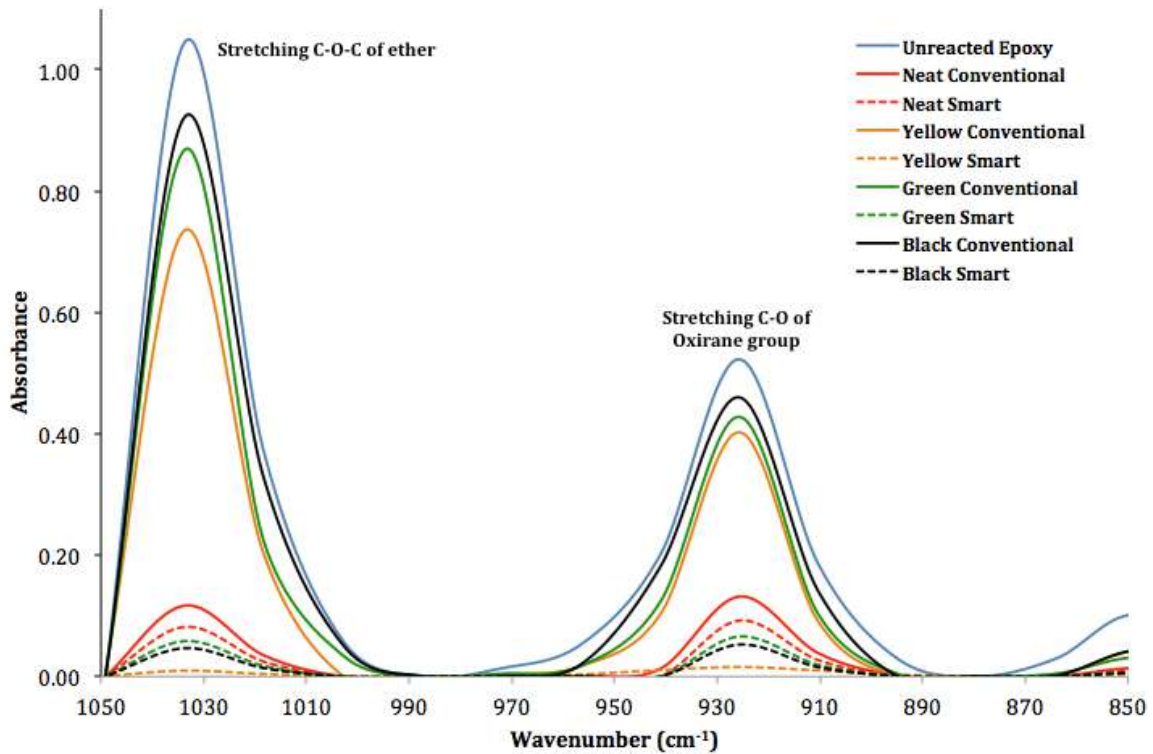
Figure 4.45: ATR spectra of 1mm thick epoxy samples

1 mm thick samples were subjected to DMA analyses in tensile configuration. Figure 4.46 compares the dynamo-mechanical properties of the samples prepared with either method. In 4.46(a) the storage modulus E' of the samples without additive is plotted: in agreement with its higher conversion and its higher gel content the Pristine-smart sample is stiffer than the pristine-conventional sample both in the glassy and in the rubbery region. The tan δ curves reported in Figure 4.46(b) evidence the difference of the samples: for the Pristine-smart polymer the curve is less broad and the maximum is bigger. The maximum is reached at a higher temperature meaning that there is an increase in the Tg for Pristine Smart (-24°C), in comparison to Pristine-conventional (-28°C).
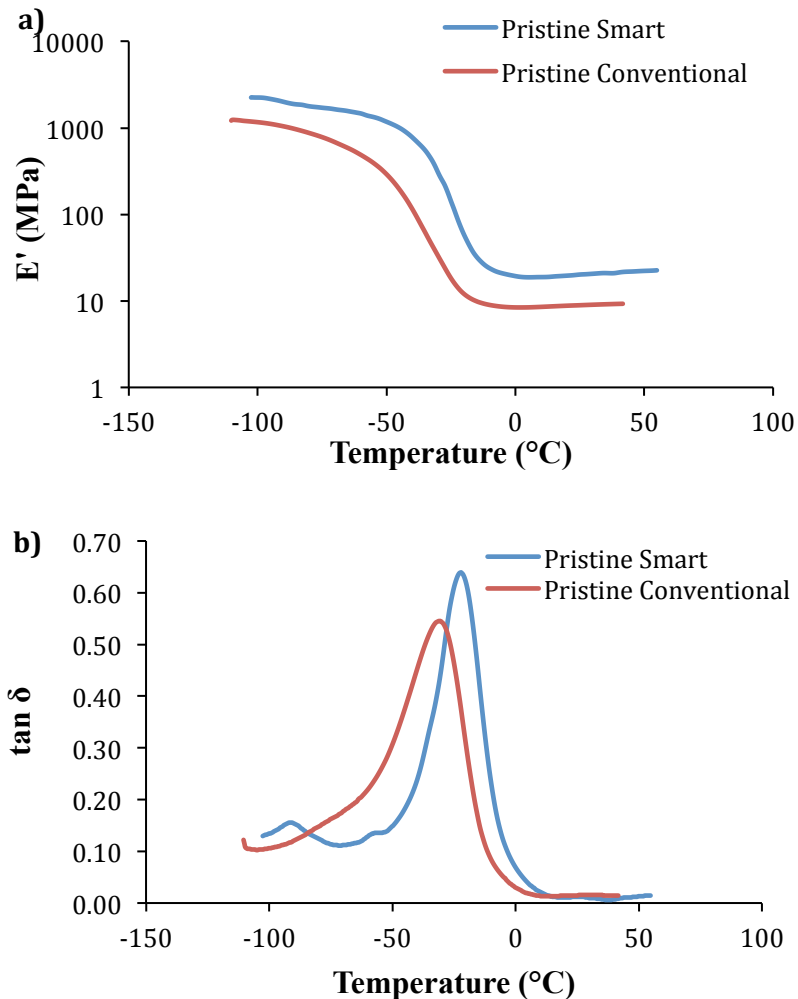
Figure 4.46: a) Elasticity Modulus b) tan delta of Pristine Conventional & Pristine-Smart composites

In Figures 4.47(a) and 4.47(b) a comparison of the colored Smart samples with Pristine Smart is reported. It was not possible to do DMA analyses of colored samples obtained by the conventional method, as they were not fully cured and could not be clamped.

For the Smart samples a meaningful increase in Tg as well in storage modulus is observable (Table 4). This increase is after incorporation of 1% of additive with respect to the monomer, which can be indorsed to the higher conversion obtained in the presence of the additives. In addition, interfacial interactions between polymer

and filler can contribute, especially in case of CB where surface functionalities can assure interaction with the matrix.

The main E' values before and after the glass–rubbery transition and the T*g* of the samples obtained by the smart methods are collected in Table 3: the values are higher if the additive is present, in agreement with the T*g* increase. T*g* values obtained by DMTA are compared with those measured by DSC; a very good agreement is found.
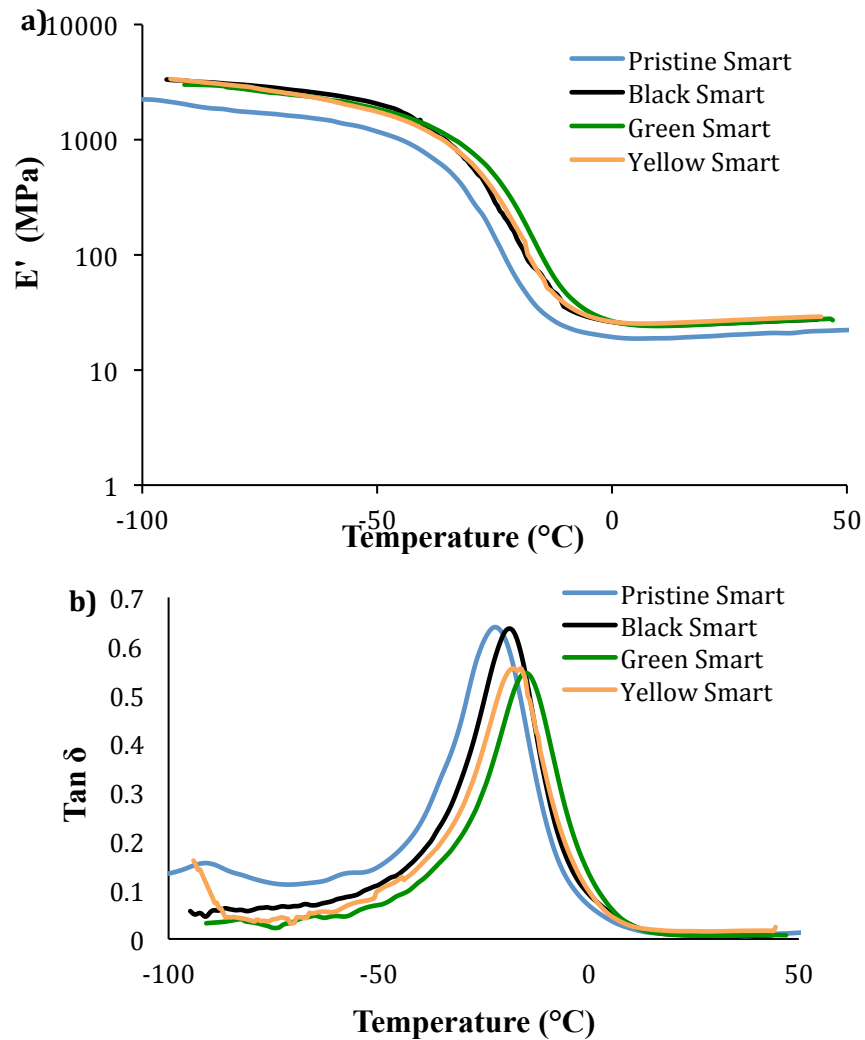
Figure 4.47 a) Elasticity modulus, b) tan δ of Pristine-Smart & (1wt%)Filler-Epoxy Composites prepared by Smart Approach

Sample	E′ (MPa)		$T_g{}^1$	$T_g{}^2$
	-80⁰C	40⁰C		
Pristine Conventional	879	9	-31	-30
Pristine Smart	1782	21	-23	-22
Black Smart	3040	27	-19	-19
Green Smart	2813	27	-15	-12
Yellow Smart	2955	29	-16	-14

Table 4.10: $E′$ and T_g of different composite samples

$T_g{}^1$ Data from DMA
$T_g{}^2$ Data from DSC

Smart and Conventional samples, stored under same conditions for comparative analysis, were subjected to thermo-gravimetric analysis (TGA) in air. The results are shown in Figures 4.49 comparing Smart samples and Conventional samples.
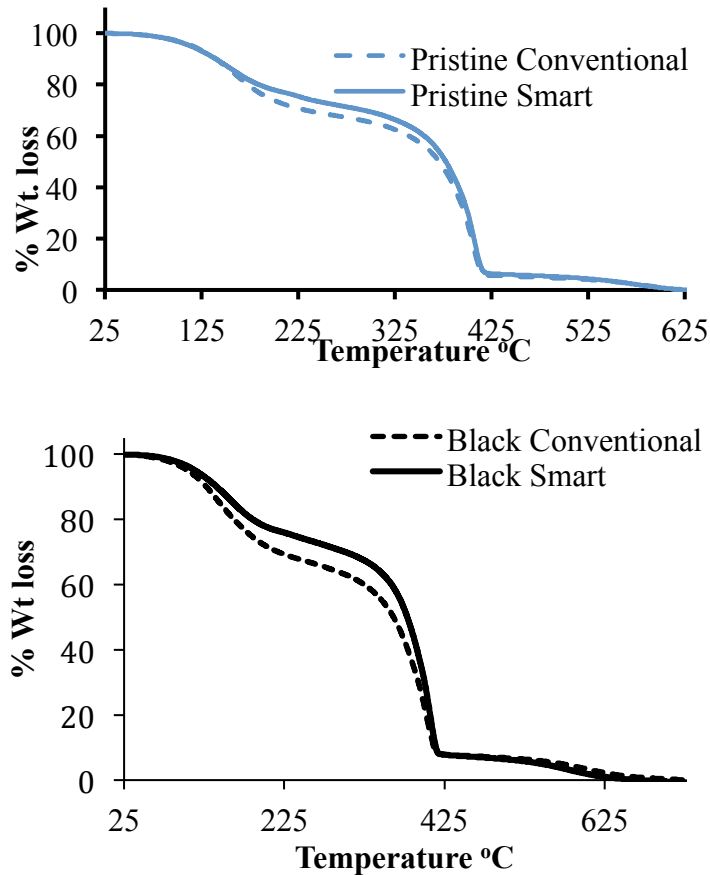
Figure 4.48: TGA of (a) Conventional and Smart Pristine and (b) Conventional and Smart Black

Difference in weight loss patterns is attributed to different synthetic procedures, assuming that these samples have different crosslinking arrangements of polymeric network. T_{50} data (Table 4.11) indicates the temperature at which composite sample loss 50% weight; is fairly different for both techniques. Colored samples prepared by Smart method show a better stability in thermal oxidative degradation with respect to the Conventional samples.

	T_{50} (°C) 50% wt. loss	T_{75} (°C) 75% wt. loss	T_{100} (°C) 100% wt. loss
Pristine Conventional	370	400	618
Pristine Smart	377	403	628
Black Conventional	360	397	728
Black Smart	378	404	670
Green Conventional	363	399	779
Green Smart	372	400	799
Yellow Conventional	377	403	654
Yellow Smart	385	405	662

Table 4.11: Temperature for specific Percentage weight loss of Conventional and Smart Composites

Most of the characterization reported evidences that the Smart Method used to cure 1 mm thick samples, helps to have a better crosslinking and networking structure, even in the presence of colored additives. Therefore the method was adopted to prepare 30 mm thick samples. As described before, the photoinitiator was irradiated for 90 s in a separate beaker, then mixed with the monomer containing the colored additive; the formulation was then poured in cylindrical vials to have a thickness of around 30 mm. Samples obtained are shown in Figure 4.49.

Figure 4.49: 30mm Thick Pristine and Colored Samples

Black-Smart composite sample was characterized after storage for 12 hours at room temperature. To check the difference in characteristics; sample was sliced from three parts named as top layer (one exposed to light source), mid-layer (15-16mm below top layer) and bottom layer (one at the lowest side of sample). Table 6 contains comparative analysis data for different layers of composite sample, not only with each other but also with neat epoxy sample (Pristine-Smart) of same thickness. Exothermic DSC peak area has been utilized to calculate degree of cure (% DC_{DSC}) with equation [3.2]. Degree of cure for neat epoxy and CB-epoxy composite samples is practically equal except for top layer. Top layer of composites show a decrease in %DC_{DSC}, this decrease can be attributed to solvent molecules in this layer, which resulted in decreased conversion. Gel contents of different layers have also confirmed DSC results. Comparable data, of neat

sample and composite, signifies that incorporation of filler does not affect much on the efficacy of the smart approach even for massive thick samples.

Sample title	Layer	%DC$_{DSC}$	Gel Contents
Pristine-Smart	Top	94	99
	Mid	98	99
	Bottom	98	100
Black Smart	Top	78	90
	Mid	94	97
	Bottom	93	97

Table 4.12: Conversion values and gel content of the composites with 1wt.% filler.

PART-I: Carbon Black Surface Modification

In this part of research thermal and UV approaches were used, for CB surface modification, mainly by MPTS. On the basis of spectroscopic measurements and instrumental analyses, one can propose that CB modification conducted in this work takes place both by the alkoxy groups of MPTS and by the thiol functionality and leads to the formation of a surface decorated by sulfur and silicon functionalities. The modification deeply changes the surface composition of the particles. As a consequence particles after modification assume a higher negative surface charge and show a larger surface area. The surface modification dramatically helps to disperse modified samples in any kind of solvent, while particles simply treated by an oxidation process are not dispersible in apolar media. Dispersability of modified samples is also efficient in a reference epoxy monomer: This finding opens the way to the making of composite materials.

PART-II: UV-cured Epoxy Composite

Photo-polymerization of thick systems is much more complex than polymerization of thin films. The presence of colored additives is a further limit to the curing of thick samples. In this work, it was shown that with a simple modification of the method adopted for the preparation of epoxides via a cationic route, 1 mm colored specimens could be obtained, and 30 mm thick samples were also successfully prepared in the same

conditions. The technique was comparatively analyzed against conventional curing method, and it was found to be efficient for maintaining the curing conversion of the colored samples as high as for neat system, while the thermal and mechanical properties were the same.

REFERNCES

1) G. J. Perrott and R. Thiessen. Carbon Black-Properties and uses. The journal of industrial and engineering chemistry 12, (1920) 324-31.

2) J. B. Donnet and A. Voet. Carbon Black; Physics, chemistry and elastomeric reinforcement. Dekker, New York, 1976.

3) E. Enríquez, J. F. Fernández and M. A. Rubia. Highly conductive coating of Carbon black/Silica composites obtained by a sol gel process. Carbon 50 (2012) 4409-17.

4) E. M Dannenberg, L. Paquin and H. Gwinnell. Carbon black. In: J. I. Kroschwitz, M. H. Grant and Kirk-Othmer. Encyclopedia of Chemical Technology, 4th Ed, New York, John Wiley & Sons, 1992.

5) K. Gardiner, W. N. Trethowan, J. M. Harrington, *et.al.* Occupational exposure to carbon black in its manufacture. Ann. Occup. Hyg. (1992) 477-496.

6) T. A. Kuhlbusch, S. Neumann and H. Fissan. Number size distribution, mass concentration, and particle composition of PM1, PM2.5, and PM10 in bag filling areas of carbon black production. J. Occup. Environ. Hyg. (2004) 660–671.

7) Kirk-Othmer. Encyclopedia of Chemical Technology, 5th Ed. New York, John Wiley & Sons, 2005.

8) E. Papirer, R. Lacroix, J. B. Donnet, G. Nanst and P. Fioux. XPS Study of the halogenation of carbon black-part 1. Bromination. Carbon 32 (1994) 1341-58.

9) L. Karásek and M. Sumita. Characterization of dispersion state of filler and

polymer-filler interactions in rubber-carbon black composites. Journal of Materials Science 31 (1996) 281-289.

10) A. W. Nienow, M. F. Edwards, N. Harnby, Dispersion of fine particles in liquid media. Mixing in the Process Industries: Second Edition. Butterwoth Heinemann Publisher, 1997.

11) T. R. Briggs. The tinting strength of pigments. J. Phys. Chem. 22 (1917) 216.

12) E. P. W. Kearsley and G. L. Roberts. Influence of Physical Properties of Carbon Black on Its Tinting Strength. Industrial & Engineering Chemistry 23 (1931) 835-37.

13) F. Li, L. Qi, J. Yang, M. Xu, X. Luo and D. Ma. Polyurethane/conducting carbon black composites: Structure, electric conductivity, strain recovery behavior, and their relationships. Journal of Applied Polymer Science 75 (2000) 68–77.

14) J. B. Donnet, R. C. Bansal and M. J. Wang. Carbon Black; Science and Technology. Second ed. Dekker, New York. 1993.

15) S. Wolff and M. J. Wang. In Carbon Black, Second ed. Dekker, New York. 1993.

16) J. F. Auchter. Chemical Economics Handbook: Carbon Black, Menlo Park, CA, SRI Consulting, 2005.

17) M. Inagaki. Carbon coatings for enhancing the functionalities of materials. Carbon 50 (2012) 3247-66.

18) J. Belmont and C. Adams. Non-aqueous inks and coatings containing modified carbon products. US 5713988 (1998).

19) J. Belmont, J. Johnson and C. Adams. Ink-jet ink formulations containing modified carbon products. US 5630868 (1998).

20) J. H. Lin. Identification of the surface characteristic of carbon black by pyrolysis GC-MASS. Carbon 40 (2002) 183-7.

21) E. Kovács and Z. Wolkober, The effect of the chemical and physical properties of carbon black on the thermal and photo-oxidation of polyethylene, Journal of Polymer Science: Polymer Symposia 57 (1976) 171–180.

22) M. Sumita, K. Sakata, S. Asai, K. Miyasaka and H. Nakagawa. Dispersion of fillers and the electrical conductivity of polymer blends filled with carbon black. Polymer Bulletin 25 (1991) 265-271.

23) J. Janzen. On the critical conductive filler loading in antistatic composites. J. Appl. Phys. 46 (1975) 966.

24) W. Li, Z. Xie and Z. Li. Synthesis and characterization of polyacrylate-g-Carbon Black and its application to soap-free waterborne coating. Journal of Applied Polymer Science 81 (2001) 1100–6.

25) J. Panchompoo, L. Aldous, C. Downing, A. Crossley and R. G. Compton. Facile Synthesis of Pd Nanoparticle Modified Carbon Black for Electroanalysis: Application to the Detection of Hydrazine. Electroanalysis 23 (2011) 1568–78.

26) M. L. Studebaker. Oxygen containing groups on the surface of carbon black. Industrial and Engineering chemistry 48 (1956) 162-6.

27) J. V. Hallum and H. V. Drush. The Organic Nature of Carbon Black Surfaces. II. Quinones and Hydroquinones by Coulometry at Controlled Potential. J. Phys. Chem. 62 (1958) 1502–5.

28) H. P. Boehm. Chemical Identification of Surface Groups. Advances in Catalysis 16 (1966) 179–274.

29) B. Grzyb, J. G. Aguilar, L. Fulcheri and N. Probst. Oxidative Treatment and Characterization of Plasma Carbon Blacks. Fullerenes, Nanotubes and Carbon Nanostructures 19 (2011) 210-24.

30) E. Papirer, R. Lacroix and J. B. Donnet. Chemical modifications and surface properties of carbon blacks. Carbon 34 (1996) 1521-29.

31) T. Takada, *et. al.* Surface modification of and characterization of carbon black with oxygen plasma. Carbon 34 (1996) 1087-91.

32) A. Schröder, M. Klüppel, R. H. Schuster and J. Heidberg. Surface energy distribution of carbon black measured by static gas adsorption. Carbon 40 (2002) 207‑210.

33) S. W. Kenneth. Physisorption of gases by carbon blacks. Carbon 32 (1994) 1311-17.

34) S. W. Kenneth. The use of physisorption for the characterization of microporous carbons. Carbon 27 (1989) 5-11.

35) W. Yuji, O. Sentaro and O. Yoshisada. Physical adsorption of gases at high pressure: V. An Extension of a Generalized Adsorption Equation to Systems with Polar Adsorbents. Journal of Colloid and Interface Science 79 (1981) 399–409.

36) N. Tsubokawa. *et.al.* Grafting of hyperbranched poly(amidoamine) onto carbon black surface using dendrimer synthesis Methodology. Polymer for Advanced Technologies 12 (2001) 596-602.

37) N. Tsubokawa, M. Hosoya and J. Kurumada. Grafting Reaction of Surface Carboxyl Groups on carbon black with polymers having terminal hydroxyl or

amino groups using N,N'-dicyclohexylcarbodiimide as a condensing agent. Reactive and Functional Polymers 27 (1995) 75-81.

38) E. Papirer, V. T. Nguyen and J. B. Donnet. Introduction of sulfur groups onto the surface of carbon black. Carbon 16 (1978) 141-4.

39) L. Qiuying, *et. al.* Grafting modification of carbon black by trapping macro-radicals formed by chemical degradation. Carbon 45 (2007) 2411–16.

40) S. Hayashi, *et. al.* Grafting of polymers onto a carbon black surface by the trapping of polymer radicals. Appl. Organomet. Chem. 12 (1998) 743-8.

41) J. B. Donnet, E. Papirer and A. Vidal. In Chemistry and Physics of carbon. Marcel Dekker, New York. 1975.

42) K. Fujiki, N. Tsubokawa and Y. Sone. Radical grafting from carbon black, graft Polymerization of Vinyl monomers initiated by Azo groups introduced onto carbon black surface. Polymer journal 22 (1990) 661.

43) N. Tsubokawa, K. Fujiki and Y. Sone. Radical Grafting from Carbon Black. Graft Polymerization of Vinyl Monomers Initiated by Peroxyester Groups Introduced onto Carbon Black Surface. Polymer journal 20 (1988) 213.

44) N. Tsubokawa and A. Kogure. Cationic Graft Polymerization from ultrafine silica initiated by Acylium Perchlorate groups introduced onto the surface. J. Polym. Sci. Polym. Chem. Ed. 22 (1984) 1515.

45) N. Tsubokawa, A. Yamada and Y. Sone. Grafting of Polyesters on Carbon Black V. Preparation of Polyester-Grafted Carbon Black with a Higher Grafting Ratio by the Copolymerization of Epoxide with Cyclic Acid Anhydrides Using COOK Groups on Carbon Black as the Initiator. Polymer Journal 16 (1984) 333-40.

46) R. Kroker, M. Schneider and K. Hamann. Polymer reactions on powder surfaces. Progress in Orgnic Coatings 1 (1972) 23-44.

47) R. Laible and K. Hamann. Formation of chemically bound polymer layers on oxide surfaces and their role in colloidal stability. Advances in Colloid and Interface Science 13 (1980) 65-99.

48) K. Ohkita. Grafting of Carbon Black. Rubber Digest: Tokyo 1983.

49) N. Tsubokawa. Functionalization of carbon black by surface grafting of polymers. Progress in Polymer Science 17 (1992) 417-70

50) P. E. Fanning and M. A. Vannice. A DRIFTS study of the formation of surface groups on carbon by Oxidation. Carbon 31 (1993) 721-730.

51) Y. Otake and R. G. Jenkins. Examination of oxygen functional groups on carbonaceous solids by linear temperature desorption techniques. ACS Prepr. Division Fuel Chemistry 32 (1987) 310-17.

52) M. A. Vannice, P. L. Walker, Jr. H. J. Jung, C. M. Castilla and O. P. Mahajan. The catalytic behavior of Carbon-Supported Iron in the Co hydrogenation reaction. Proceeding of 7th International Congress on Catalysis (1981) 460-74.

53) R. C. Bansal, J. B. Donnet and H. F. Stoeckli. In Active Carbons. Marcel Dekker, New York. 1989.

54) M. Janssen. In Organo-sulfur chemistry. Intersciences, New York. 1976.

55) S. Oae. In the organic chemistry of Sulfur. Plenum press, New York. 1977.

56) S. Nakatani, J. I. Yoshida and S. Isoe. Radical carbonylation of alkynes in the presence of thiols. Journal Chemical Society, Chemical Communication 12 (1992) 880-1.

57) G. Colucci *et. al.,* Modification of Silica by Liquid Polybutadienes Containing Alkoxysilane Groups. Macromolecular Symposia 296 (2010) 550–556.

58) J. P. Wibaut. The conduct of sulfur to carbonaceous materials at high temperatures. Rec. Trav. Chim. 38 (1919) 159.

59) R. Juza and W. Blanke. Densitometric studies of the behavior of some carbon to sulfur. Z. Anorg. Allgem. Chem. 210 (1933) 81.

60) B. R. Puri. In Chemistry and Physics of Carbon. Marcel Dekker, New York. 1970.

61) B. R. Puri and R. S. Hazra. Carbon-sulphur surface complexes on charcoal. Carbon 9 (1971) 123-34.

62) E. Papirer, S. Li and A. Vidal. Formation of Carbon black-Sulfur surface derivatives by reaction with P_2S_5. Carbon 29 (1991) 963-68.

63) X. Yanjun, *et. al.,* Silane coupling agents used for natural fiber/polymer composites. Composites Part A: Applied Science and Manufacturing 41 (2010) 806–19.

64) M. Sabzi, *et. al.,* Surface modification of TiO2 nano-particles with silane coupling agent and investigation of its effect on the properties of polyurethane composite coating. Progress in Organic Coatings 65 (2009) 222–8.

65) N. N. Herrera, *et. al.,* Aqueous Dispersions of Silane-Functionalized Laponite Clay Platelets. A First Step toward the Elaboration of Water-Based Polymer/Clay Nanocomposites. Langmuir 20 (2004) 1564–71.

66) A. Nistal, *et. al.,* Analysis of the interaction of vinyl and carbonyl silanes with carbon nanofiber surfaces. Carbon 49 (2011) 1635-45.

67) M. P. Cheng, K. K. Jang and T. B. Zhong. Functionalization of carbon nano-tubes

using a silane coupling agent. Carbon 44 (2006) 3232-38.

68) C. V. Santos, *et. al.,* Chemical functionalization of carbon nanotubes through an organosilane. Nanotechnology 13 (2002) 495-8.

69) Q. He, Y. Xu, C. Wang, S. She, S. Zhou and R. Wang. Silane modification and characterization of activated carbon. Adsorption 18 (2012) 23-29.

70) L. Bokobza and O. Rapoport. Silica and carbon black reinforcement of natural rubber. Macromolecular Symposia, Special Issue: Fillers for the New Millennium 194 (2003) 125–134.

71) N. Nugay and B. Erman. Property optimization in nitrile rubber composites via hybrid filler systems. Journal of Applied Polymer Science 79 (2001) 366–74.

72) W. Zhou, J. Xu and W. Shi. Surface modification of multi-wall carbon nanotubes with ultraviolet curable hyper branched polymer. Thin Solid Films 516 (2008) 4076-82.

73) H. L. Hsu, *et. al.,* Flexible UV-Ozone-Modified Carbon Nanotube Electrodes for Neuronal Recording. Advanced Materials 22 (2010) 2177–81.

74) B. Li, *et. al.,* Photochemical Chlorination of Graphene. ACS Nano 5 (2011) 5957–61.

75) T. Roch, E. Beyer and A. Lasagni. Surface modification of thin tetrahedral amorphous carbon films by means of UV direct laser interference patterning. Diamond and related Materials 19 (2010) 1472-77.

76) P. Woointranont and W. Pecharapa. Effects of Surface Modification of Carbon Nanotubes on the Deposition of NiO/CNTs Nanocomposites. Journal of the Microscopy Society of Thailand 4 (2011) 116-119.

77) M. Levy and M. Szwaz. Methyl affinities of aromatic hydrocarbons. Journal of Chemical Physics 22 (1954) 1621–2.

78) Q. Li, G. Wu, Y. Ma and C. Wu. Grafting modification of carbon black by trapping macroradicals formed by sonochemical degradation. Carbon 45 (2007) 2411–16.

79) S. Oae. Khimiya organicheskikh soedinenii sery (Chemistry of Organic Sulfur Compounds). Moscow: Khimiya (1975) 78.

80) P. M. Rao and A. R. Knight. Reactions of thiyl radicals. Canadian journal of Chemistry 46 (1968) 2462-4.

81) F. Akutsu, M. Inoki, N. Daicho, Y. Kasashima, N. Shiraishi and K. Marushima. Curing behavior and properties of epoxy resins cured with the diamine having the quinoxaline or triazine structure. J. Appl. Polym. Sci. 69 (1998) 1737-41.

82) I. Hamerton, J. N. Hay, B. J. Howlin, P. Jepson and S. Mortimer. The development of controllable complex curing agents for epoxy resins. I. Preparation, characterization, and storage behavior of transition metal–diamine complexes. J. Appl. Polym. Sci. 80 (2001) 1489-1503.

83) I. N. Jan, T. M. Lee, K. C. Chiou and J. J. Lin. Comparisons of Physical Properties of Intercalated and Exfoliated Clay/Epoxy Nanocomposites. Ind. Eng. Chem. Res. 44 (2005) 2086-90.

84) V. Nigam, D. K. Setua, G. N. Mathur and K. K. Kar. Epoxy-montmorillonite clay nanocomposites: Synthesis and characterization. J. Appl. Polym. Sci. 93 (2004) 2201-10.

85) D. Ratna, N. R. Manoj, R. Varley, R. R. K. Singh and G. P. Simon. Clay-reinforced

epoxy nanocomposites. Polym. Int. 52 (2003) 1403-07.

86) F. Bondioli, V. Cannillo, E. Fabbri and M. Messori. Epoxy-silica nanocomposites: Preparation, experimental characterization and modeling. J. Appl. Polym. Sci. 97 (2005) 2382-86.

87) Y. L. Liu and S. H. Li. Using silica nanoparticles as curing reagents for epoxy resins to form epoxy–silica nanocomposites. J. Appl. Polym. Sci. 95 (2005) 1237-45.

88) J. D. Fidelus, E. Wiesel, F. H. Gojny, K. Schulte and H. D. Wagner. Thermo-mechanical properties of randomly oriented carbon/epoxy nanocomposites. Composites A 36 (2005) 1555-61.

89) Y. S. Song and J. R. Youn. Influence of dispersion states of carbon nanotubes on physical properties of epoxy nanocomposites. Carbon 43 (2005) 1378-85.

90) J. K. W. Sandler, J. E. Kirk, I. A. Kinloch, M. S. P. Shaffer and A. H. Windle. Ultra-low electrical percolation threshold in carbon-nanotube-epoxy composites. Polymer 44 (2003) 5893-99.

91) J. M. Park, D. S. Kim, J. R. Lee and T. W. Kim. Nondestructive damage sensitivity and reinforcing effect of carbon nanotube/epoxy composites using electro-micromechanical technique. Mater. Sci. Eng. C 23 (2003) 971-75.

92) H. Miyagawa and L. T. Drzal. Thermo-physical and impact properties of epoxy nanocomposites reinforced by single-wall carbon nanotubes. Polymer 45 (2004) 5163-70.

93) Zhang *et. al.,* Effect of cure cycle on curing process and hardness for epoxy resin. Express Polymer Letters 3 (2009) 534–41.

94) C. Cindy *et. al.,* Cationic photopolymerization of epoxides containing carbon black nanoparticles. Polymer 51 (2010) 6151-60.

95) M. Sangermano, B. Voit, F. Sordo, K. J. Eichhorn, G. Rizza. High refractive index transparent coatings obtained via UV/thermal dual-cure process. Polymer 49 (2008) 2018-22.

96) M. Martin-Gallego, M. Hernandez, V. Lorenzo, R. Verdejo, M. A. Lopez-Manchado and M. Sangermano. Cationic photocured epoxy nanocomposites filled with different carbon fillers. Polymer 53 (2012) 1831-38.

97) Z. W. Wicks, F. N. Jones and S. P. Pappas. Organic Coatings, 2nd ed., John Wiley & Son Inc., New York, 1994.

98) G. Odian. Principles of Polymerization, 3rd ed., John Wiley & Son Inc., New York, 1991.

99) K. K. Baikerikar and A. B. Scranton. Photopolymerizable liquid encapsulants for microelectronic devices. Polymer 42 (2001) 431-41.

100) K. K. Baikerikar and A. B. Scranton. Photopolymerizable liquid encapsulants for microelectronic devices: Thermal and mechanical properties of systems with reduced in-mold cure times. J. Appl. Polym. Sci. 81 (2001) 3449-61.

101) N. Stephenson, D. Kriks, M. El-Maazawi and A. B. Scranton. Spatial and temporal evolution of the photo initiation rate for thick polymer systems illuminated on both sides. Polymer Inter. 54 (2005) 1429-39.

102) J. V. Koleske. Radiation Curing of Coatings. ASTM International, West Conshohocken, PA 2002.

103) K. D. Weiss. Paint and coatings: A mature industry in transition. Prog. Polymer

Sci. 22 (1997) 203-45.

104) N. Tsubokawa, *et. al.,* Grafting of hyperbranched poly(amidoamine) onto Carbon black surface using dendrimer synthesis, methodology. Polymer for Advanced Technologies 12 (2001) 596–602.

105) J. M. O'Reilly and R. A. Mosher. Functional group in carbon black by FTIR spectroscopy. Carbon 21 (1983) 47–51.

106) F. Rositani, *et. al.,* Infrared analysis of carbon blacks. Carbon 25 (1987) 325–32.

107) V. G. Serrano, *et al.,* Formation of oxygen structures by air activation: a study by FT-IR spectroscopy. Carbon 37 (1999) 1517–28.

108) J. P. Coates. Interpretation of infrared spectra: a practical approach. In: Encyclopedia of Analytical Chemistry: Applications, Theory and Instrumentation, John Wiley & Sons, New York, 2000.

109) E. P. Plueddemann. Silane Coupling Agents, Plenum Press, New York, 1991.

110) G. Socrates. Infrared And Raman Characteristic Group Frequencies: Tables and Charts, Third ed., John Wiley & Sons, New York, 2001.

111) C. Flego and L. Dalloro. Beckmann rearrangement of cyclohexanone oxime over silicalite-1: an FT-IR spectroscopic study. Microporous and Mesoporous Materials 60 (2003) 263–271.

112) C. H. Chang. Preparation and characterization of carbon–sulfur surface compounds. Carbon 19 (1981) 175–186.

113) G.J. Ehlert, Y. Lin, H.A. Sodano, Carboxyl functionalization of carbon fibers through a grafting reaction that preserves fiber tensile strength, Carbon 49 (2011) 4246–4255.

114) C.D. Wagner, D.A. Zatko, R.H. Raymond, Use of the oxygen KLL Auger lines in identification of surface chemical states by electron spectroscopy for chemical analysis, Analytical Chemistry 52 (1980) 1445–1451.

115) A.C. Ferrari and J. Robertson. Raman spectroscopy of amorphous nanostructured diamond-like carbon and nanodiamond. Philosophical Transactions of the Royal Society of London, Series A 362 (2004) 2477–2512.

116) F. Tuinstra and J. L. Koenig. Raman spectrum of graphite. Journal of Chemical Physics 53 (1970) 1126–30.

117) R.D. Smith and P.G. Pickup. Voltammetric quantification of the spontaneous chemical modification of carbon black by diazonium coupling. Electrochimica Acta 54 (2009) 2305–11.

118) R. L. Foster, Y. Xi and R. E. Pogson. Raman spectroscopic study of the mineral arsenogorceixite. Spectrochim Acta A Mol Biomol Spectrosc. 91 (2012) 301-6.

119) B. A. Ficek, A. M. Thiesen and A. B. Scranton. Cationic photopolymerizations of thick polymer systems: Active center lifetime and mobility. European Polymer Journal 44 (2008) 98-105.

120) N. Hauptman, A. Vesel, V. Ivanovski and G. K. Marta. Electrical conductivity of carbon black pigments. Dyes and Pigments 95 (2012) 1-7.

121) H. Zollinger. Color Chemistry; Synthesis, properties and application of Organic Dyes and Pigments, 2nd ed, VCH Publisher, 2000.